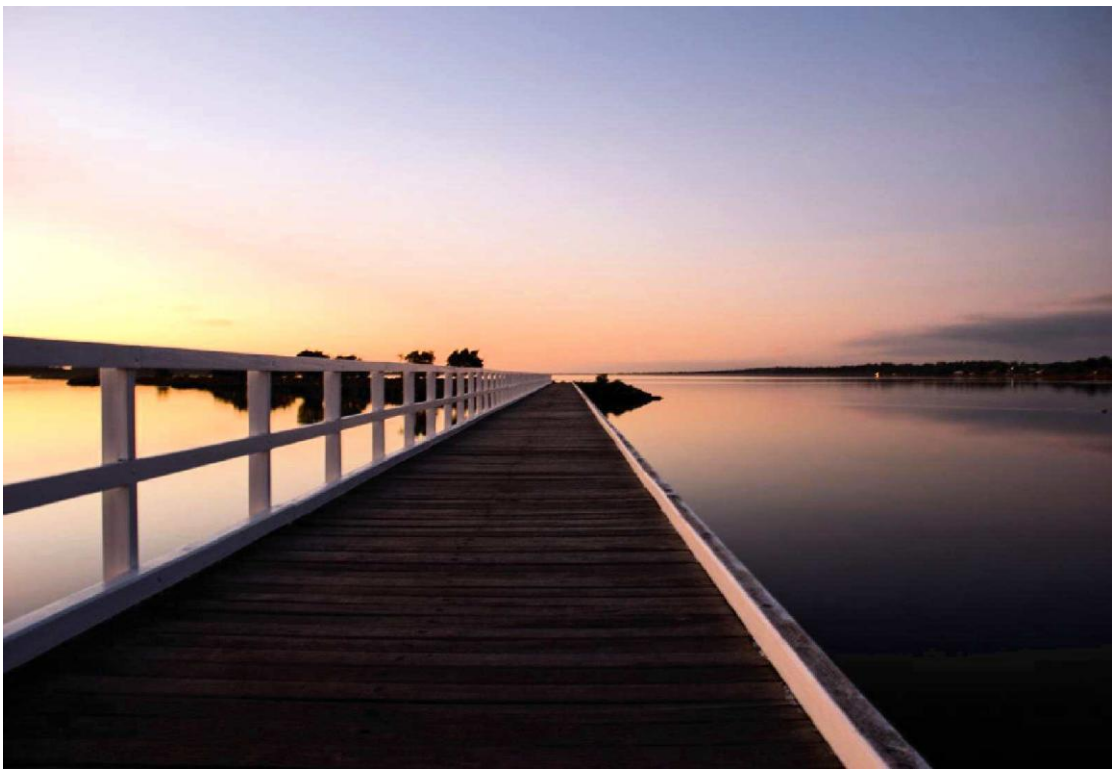

Numerical Hydrodynamic Modelling of the Leschenault Estuary

P. A. Gillibrand
J.R. Andrewartha
M. Herzfeld

October, 2012

Table of Contents

Executive Summary

A 3D primitive equation model was applied to the Leschenault Estuary to examine the hydrodynamics of the region. The estuary was modelled using a curvilinear grid, with highest resolution focused on the estuary, its entrance and inflowing rivers. Model forcing included tides, low-frequency sea level fluctuations, wind stress, surface heat and salt fluxes, river flow and oceanic temperature and salinity. The model was run for a 12-month period from April 2011 – March 2012, and calibrated against temperature and salinity time series data collected at five locations in the estuary by the Department of Water for Western Australia.

At the offshore boundaries of the model, low-frequency (non-tidal) fluctuations in sea level, velocitiy, temperature and salinity were taken from the operational model OceanMAPS (operated by the Bureau of Meteorology) output for the Australasian region and combined with a global tide model. Boundary values of temperature and salinity were also taken from the OceanMAPS model. The Leschenault model output exhibited very good agreement between observed and modelled temperature in the estuary over the annual cycle. The comparison between observed and modelled salinity was also good throughout most of the estuary; the weakest agreement occurred in the Collie River, where limited spatial resolution coincides with complex salt wedge dynamics. Nevertheless, the model reproduced the fundamental aspects of salt wedge dynamics in the Collie River.

Currents in the Leschenault Estuary were dominated by tides, particularly in the southern basin around the entrance channel. In the Cut, tidally-driven velocities exceeded 1.5 m s^{-1} at times. Water entering through the Cut during flood tide was largely diverted northward into the central estuary; a secondary current generated an anti-clockwise circulation in the southern basin. During ebb tides, the circulation was reversed, with southward flow in the northern and central basins, and a clockwise flow in the southern basin. Away from the entrance channel, tidal currents quickly became weaker and, around the mouths of the major river channels such as the Preston and Collie Rivers, currents due to the river flow at times overpowered the tidal currents and became uni-directional during periods of high river flow.

The seasonally-averaged circulation fields exhibited a classical estuarine circulation during winter 2011, and an inverse estuarine circulation during summer 2011-12. The winter-mean surface circulation in the estuary was seaward, forced by elevated freshwater inputs into the estuary, with current speeds of the order of 1 cm s^{-1} in the main body of the estuary; in the southern basin, current speeds were stronger, typically 3 – 4 cm s^{-1}, driven by the freshwater discharge from the Collie and Preston Rivers. The bottom layer winter-mean currents in the main estuary were landward and of the same strength as the near-surface velocities. During summer, high evaporation in the shallow northern estuary combined with low river discharge led to an inverse circulation pattern in the central and northern estuary, with landward mean surface currents and

seaward mean currents at depth. Summer-mean current strengths were slightly stronger than the winter-mean values, with values of about 2 cm s^{-1}. In the southern basin, the circulation pattern was less structured, but appeared generally seaward at the surface, driven by the weak river flows and not affected by high evaporation.

A high river flow event occurred during August 2011, and had a major impact on the dynamics of the southern basin of the estuary; the basin was filled with fresh river water, which was gradually ejected from the estuary through the Cut, emerging as a buoyant plume into Geographe Bay with velocities in the central plume exceeding 0.5 m s^{-1}. Impacts of the river flow on the northern and central estuary basins were less, with only a gradual freshening of the northern and central basins.

The conceptual division of the Leschenault Estuary into three distinct basins was emphasized by tracer simulations carried out during the study. A simulation of the dispersion of a seasonally-released tracer throughout the whole basin was performed, as were simulations of continuous releases of tracer at seven point sources in the estuary. Tidal currents in the northern estuary are weak, and the dynamics there are strongly influenced by the freshwater discharge from the Parkfield Drain. Exchange and dispersion of tracer in the region was slow. In the central region, no river discharges are present, and dynamics are controlled by weak tidally-driven mixing with the northern and southern basins. Again, tracer dispersion was slow. The southern basin of the estuary was clearly the most dynamic, with water exchanged with the adjacent ocean through the Cut and the Collie and Preston Rivers discharging into the basin. The flushing of the southern basin was much more rapid than that of the northern or central basins. The flushing time of the whole estuary varied from 9 – 32 days, but most of the tracer lost from the system in these simulations was predominantly from the southern basin.

The dynamics of the Collie River were dominated by the salt wedge in the lower reaches of the river. The model results illustrated some of the variability in the position and strength of the interface between the fresh and salt water. During high flow events, salt water may be purged completely from the river, and the freshwater extend across the surface of the southern Leschenault Estuary into the Cut. At other times, salt water may penetrate far upstream in the bottom layer of the river. Due to resolution issues, the performance of the model was weakest in the Collie River, and a more accurate simulation of the Collie River dynamics may require a much higher resolution model of the river alone.

Some tentative simulations of the potential impacts of projected climate change on the Leschenault Estuary were made. In the warmer drier climate expected for 2050, the Leschenault Estuary was predicted to also be warmer and saltier than at present. The impacts on the dynamics of the estuary were small, but the ecological implications of the higher temperatures and increased salt content may be greater. The strength of the predicted impacts increased with higher emissions scenarios.

1. Background

The Leschenault Estuary (Figure 1.1) lies to the north of Bunbury, in the south-west of Western Australia. The estuary and its source river catchments are subject to increasing pressure from urban and industrial expansion, increasing water demand, and from changing and intensifying land use (DoW, 2007). The Leschenault catchment area is 4840 km^2, of which 2830 km^2 is above Wellington Dam, which was completed in 1960. The major rivers are the Wellesley, Brunswick and Collie, which flow to the estuary's south-east via the lower Collie River, and the Ferguson and Preston which flow into the south of the estuary via the Preston River. The Parkfield Drain, constructed in 1977, flows into the north of the estuary. Land use in the Leschenault catchment is highly diversified (Dow, 2007), incorporating residential, commercial and agricultural activities. Large areas of the catchment are irrigated, used primarily for dairying and horticulture. As a result of the catchment runoff that drains into the estuary, the estuary reflects the state of the catchment environment. Water quality in the estuarine portions of the rivers is poor, with nutrient and chlorophyll concentrations greater than ANZECC (2000) guidelines; and these areas suffer periods of anoxia and hypoxia. At the sites monitored in the main estuary, although nutrient and chlorophyll data generally comply with the ANZECC guidelines, dissolved oxygen concentrations are at times less than desired levels.

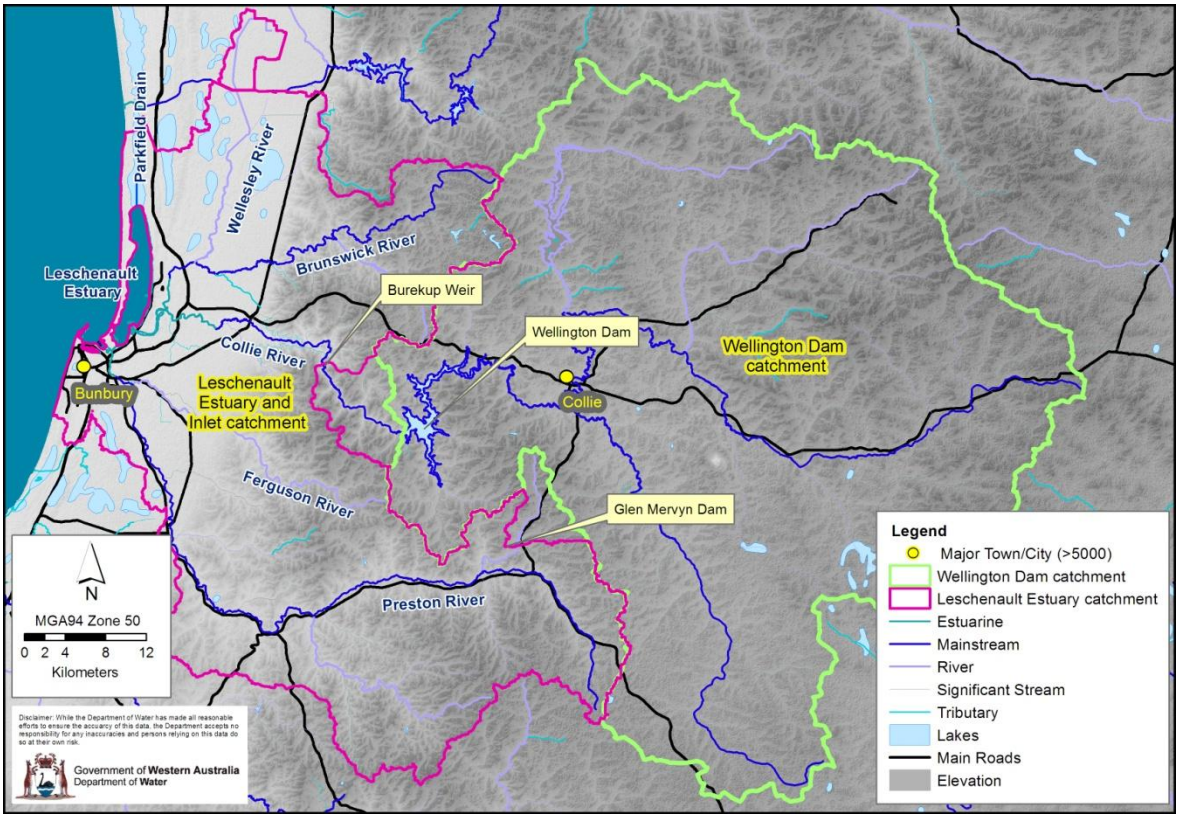

Figure 1.1: Leschenault Estuary and surrounding catchment area. [Figure supplied by Peta Kelsey, Western Australia Department of Water].

The morphology of the Leschenault Estuary has evolved significantly over the past century. Originally known as the Leschenault Inlet, its only connection to the sea lay at the southwestern extreme of the inlet, close to Bunbury. In 1951, in order to avoid excessive accumulation of silt in the Bunbury port area, the original entrance was closed, and a new artificial entrance, known as "The Cut", was excavated through the sand dunes opposite the mouth of the Collie River (Figure 1). The Preston River was subsequently re-routed to its present course in 1968–9, and construction work in the 1970s resulted in the separation of the small Leschenault Inlet at the southern end of the main water body. Exchange between the Leschenault Estuary and the sea now occurs solely through the Cut.

The Leschenault is a shallow micro-tidal estuary, with the barotropic tide having a range up to about 0.6 m. Tides exhibit a neap-spring cycle over a period of approximately 14 days, with ranges at springs of ~0.6 m and as little as 10 cm during neap tides. Low-frequency (sub-tidal) oscillations in coastal sea surface elevation are of a comparable magnitude to the tidal oscillation, and may be expected to drive a discernible circulation in the estuary, as has been recorded in the nearby Swan estuary (O'Callagan et al, 2007). Despite water depths of the order of 2 m throughout the estuary, significant stratification may develop during periods of high river flow. When river flows are low, the estuary is only weakly stratified. Maximum currents during the spring phase may be as large as 1.5 ms^{-1} in the Cut.

As discussed above, water quality in the estuary is below acceptable standards for nutrients, chlorophyll and oxygen. The lower river reaches exhibit poor water quality and act as sinks for riverine sediments and nutrients; fish kills have been known in the lower river reaches of the Collie and Brunswick Rivers (DoW, 2007). Water quality in the estuary reflects increasing pressures on the catchment and changes in climate. This project aims to provide a better understanding of the hydrodynamics of the estuary and to provide a platform for further modelling of the water quality and biogeochemistry of the system.

2. Objectives

This study aims to implement a numerical hydrodynamic model that will provide predictive capacity for currents and mixing within the Leschenault Estuary and its river systems. The model has been calibrated against data collected by moored temperature and conductivity sensors over an annual cycle through 2011–12. Insight into exchange mechanisms of the estuary with the adjacent ocean, flushing times, tracer dispersal distributions and residual flows can be gained from application of the model. The model is designed to ultimately aid management decisions relating to contaminant management, and form the basis for subsequent sediment transport and biogeochemical numerical investigations. The model was forced with river discharge data, wind stress, surface heat and freshwater fluxes, and surface elevation, current velocity, temperature and salinity on the offshore limits of the domain. The hydrodynamic model, its inputs, and model output are discussed in more detail below. Analyses are presented addressing the flushing characteristics of the Leschenault Estuary, passive tracer distributions in response to the circulation, and residual flow dynamics. The limitations of the model, effort required to improve confidence in model solutions and data requirements to facilitate these improvements, are discussed.

3. The Hydrodynamic Model

The hydrodynamic model used to simulate the flow and mixing of the Leschenault Estuary is SHOC (Sparse Hydrodynamic Ocean Code; Herzfeld, 2005). This model has been developed by the Environmental Modelling group at CSIRO (Commonwealth Scientific and Industrial Research Organization) Division of Marine Research over the past fifteen years. SHOC is intended to be a general purpose model applicable to scales ranging from estuaries to regional ocean domains, and has been successfully applied to a variety of applications encompassing these scales to date. SHOC is a three-dimensional finite difference hydrodynamic model based on the primitive equations. Outputs from the model include three-dimensional distributions of velocity, temperature, salinity, density, passive tracers, mixing coefficients and sea level. The equations forming the basis of the model are similar to those described by Blumberg and Herring (1987). SHOC is based on the MECO model (Model for Estuaries and Coastal Oceans; Walker and Waring, 1999) with added functionality to allow distributed processing over multiple computing processors. SHOC also employs a sparse coordinate system internally that allows the representation of unused land in the model to be excluded. Inputs required by the model include forcing due to wind, atmospheric pressure gradients, surface heat and water fluxes and open boundary conditions (e.g. tides). A schematic of the major forcing mechanisms captured by SHOC is included as Figure 3.1. SHOC is based on the three-dimensional equations of momentum, continuity and conservation of heat and salt, employing the hydrostatic and Boussinesq assumptions. The equations of motion are discretized on a finite-difference stencil corresponding to the Arakawa C grid.

The model uses a curvilinear orthogonal grid in the horizontal and a choice of fixed ‘z’ coordinates or terrain following ‘σ’ coordinates in the vertical. The curvilinear horizontal grid was particularly useful in this application since it enabled high resolution to be specified in areas of the study region where small scale motions were present and less resolution where they were not. The ‘z’ vertical system allows for wetting and drying of surface cells, useful for modelling regions such as tidal flats where large areas are periodically dry. SHOC has a free surface and uses mode splitting to separate the two-dimensional (2D) mode from the three-dimensional (3D) mode. This allows fast moving gravity waves to be solved independently from the slower moving internal waves allowing the 2D and 3D modes to operate on different time-steps, resulting in a considerable improvement in computational efficiency. The model uses explicit time-stepping throughout except for the vertical diffusion scheme which is implicit. The implicit scheme guarantees unconditional stability in regions of high vertical resolution. A laplacian diffusion scheme is employed in the horizontal on geopotential surfaces. Smagorinsky mixing coefficients may be utilized in the horizontal.

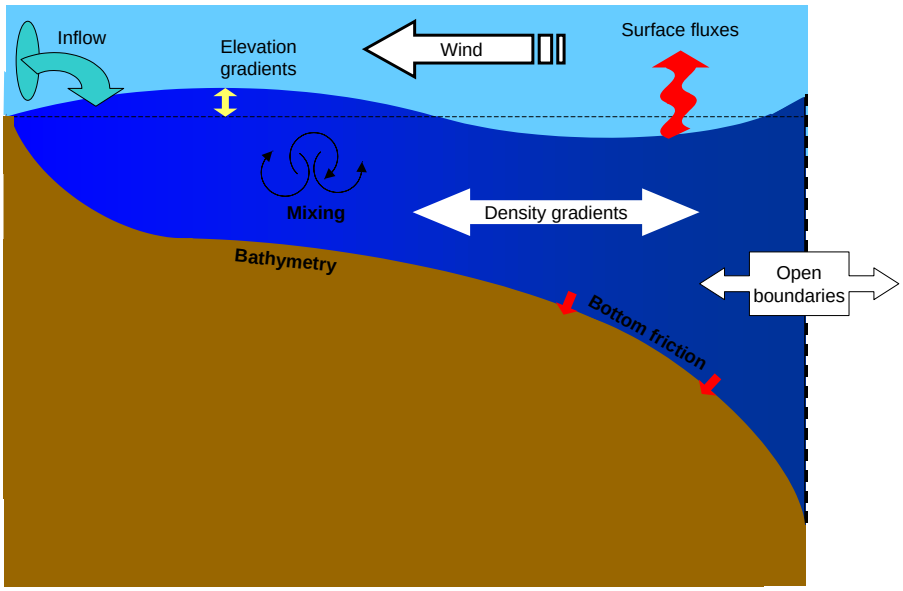

Figure 3.1 : Schematic of forcing mechanisms in SHOC

SHOC can invoke several turbulence closure schemes, including k-ε, k-ω, Mellor-Yamada 2.0 and 2.5, and Csanady-type parameterisations. A variety of advection schemes may be used on tracers and 1st or 2nd order can be used for momentum. This study used the Van Leer advection scheme (Van Leer, 1979). SHOC also contains a suite of radiation, extrapolation, sponge and direct data forcing open boundary conditions. Input and output is handled through netCDF data formatted files, with the option of submitting ASCII text files for simple time-series forcing. The netCDF format allows input of spatially and temporally varying forcing and initialization data in a grid and time-step independent manner. SHOC is capable of performing particle tracking and may be directly coupled to ecological and sediment transport models.

4. Model Domain

To model the Leschenault Estuary, a curvilinear numerical grid was constructed (Figure 4.1). Curvilinear grids allow, within reasonable limits, for spatial resolution to be focused on the particular area of interest, with lower resolution elsewhere in the domain, improving model efficiency. For the Leschenault grid, spatial resolution was highest in the Cut and the central and upper reaches of the Collie River, with grid spacing of about 20 – 30 m. In the main body of the estuary, the grid spacing was of the order of 100 m (Figure 4.2), and outside the estuary it increased gradually with distance from the Cut, reaching about 2500 m along the outer periphery of the model domain (Figure 4.1).

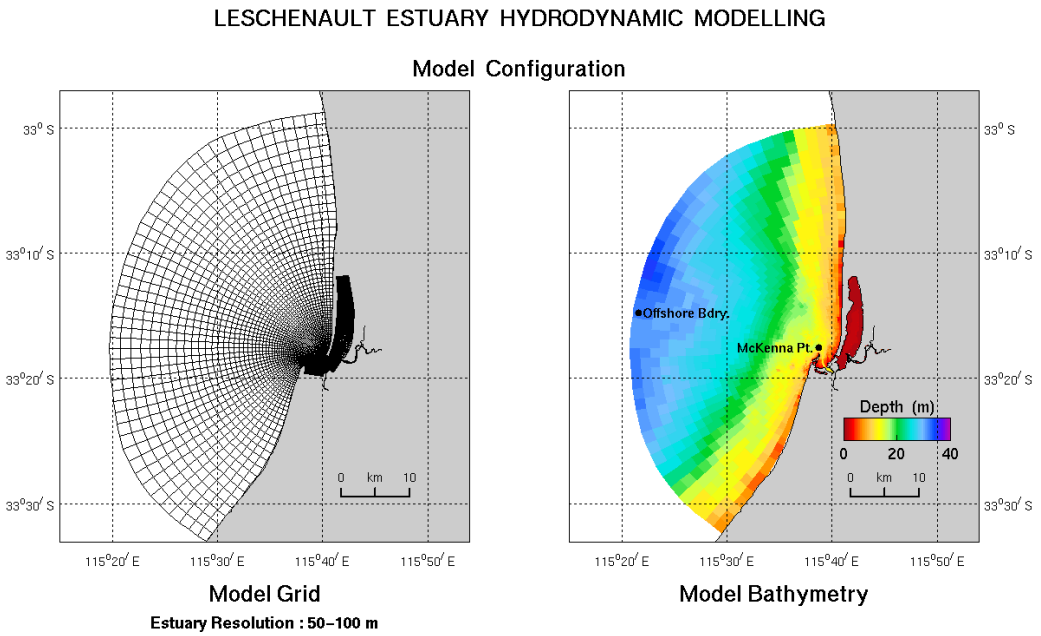

Figure 4.1 : Leschenault Estuary model domain bathymetry and grid. The grid resolution (left) increases from the outer boundary into the estuary.

The Collie River estuary was resolved in three dimensions as far as the junction with the Brunswick River (Figure 4.3). Upstream of the junction, both the Collie and Brunswick Rivers were resolved in two dimensions (laterally-averaged, Figure 4.4). This was necessary so that very fine cross-river resolution did not adversely compromise the time step used, hence delivering unacceptable run time ratios. The grid spacing was ~20m cross-river in the lower estuary, while the along-river resolution tended to be slightly greater (Figure 4.4). There were 18 layers in the vertical, with 0.5m resolution at the surface increasing to 5m resolution near the maximum depth of 40m. This domain consisted of mostly land cells, with 9% of the surface layer comprising wet cells and 3% of the 3D domain being wet.

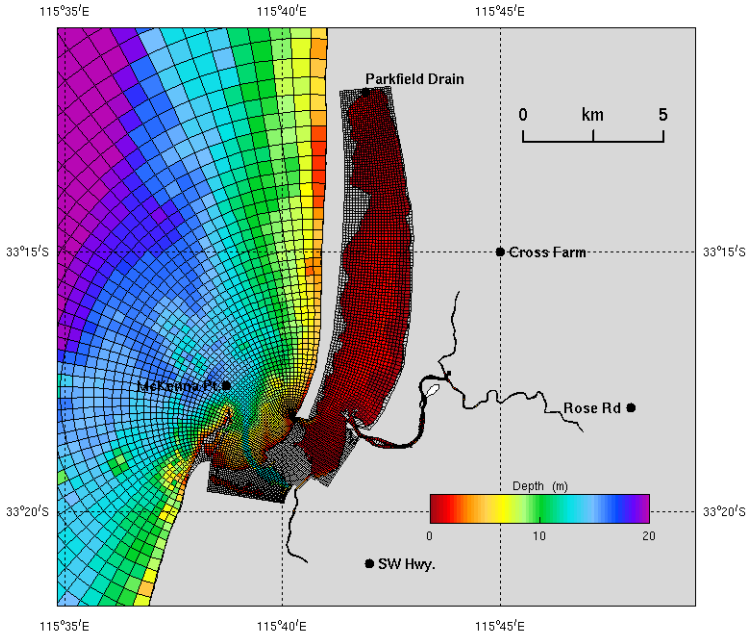

Figure 4.2 : Model bathymetry and grid in the Leschenault Estuary vicinity. The locations on land indicate the gauging stations used for river flow inputs.

The run-time ratio of the model was approximately 60:1 (i.e. the model simulates 60 days of results in 1 day of real time). This was determined by the stability constraints on the model, which limited the maximum time-step allowed for 2D and 3D modes. These constraints are in turn dependent on the grid resolution, the water depth, stratification and the size of the grid. Considerable effort was invested into optimizing these time-steps so as to achieve the largest run-time ratio possible. The model speed is moderate, allowing a year-long simulation to be completed in around one week real time.

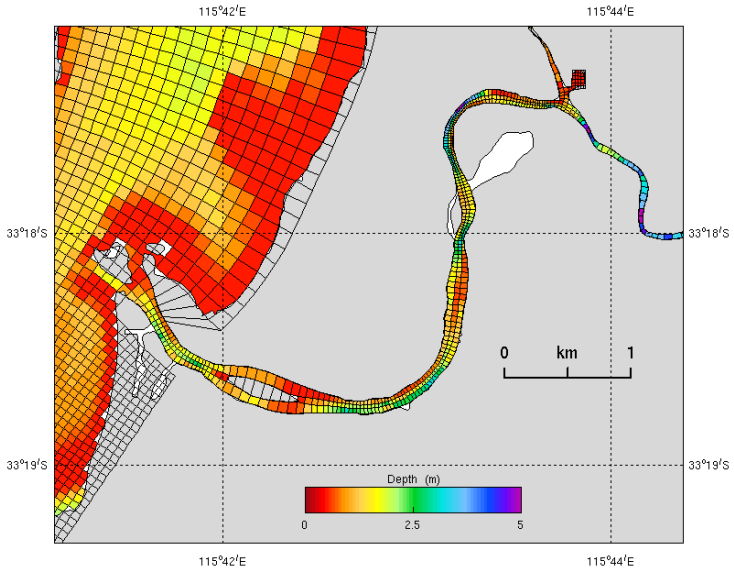

Figure 4.3 : Model bathymetry and grid for the lower Collie River.

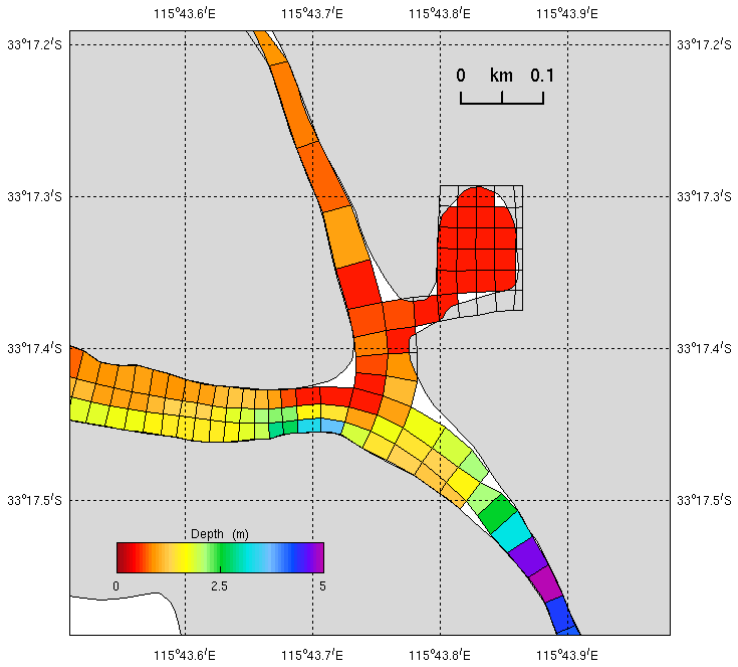

Figure 4.4 : Model bathymetry and grid for the junction between the Collie and Brunswick Rivers.

5. Input Data

The model was forced with wind stress, flows from four rivers, surface heat and freshwater (i.e. the difference between precipitation and evaporation) fluxes, and elevation, current velocity, temperature and salinity on the oceanic open boundary. The simulations described in this report extended from 01 April 2011 to 31 March 2012, coincident with the data collection programme. The model was spun-up from rest over a two-week period (from 17 March – 01 April 2011) in order to provide initial conditions on 01 April 2011. Initial conditions of temperature and salinity on 17 March were taken from modelled ocean conditions (see §5.3 below). The sources of the forcing data are detailed below.

5.1 Atmospheric Forcing

Meteorological data are available from the Bureau of Meteorology (BoM) weather station at Bunbury. However, in order to force the model with spatially varying meteorological parameters, the model was forced using the BoM atmospheric model ACCESS (http://www.bom.gov.au/weather-services/about/service-changes/modelchangeover.shtml), which provides predicted hourly air temperature, atmospheric pressure, wind speed and direction, dew point temperature and cloud cover at 10 km resolution. Using ACCESS products to force the hydrodynamic model also enables a forecast capability, since the BoM routinely provides forecasts of several days. The ACCESS model output compares well with observed wind speed and direction at Bunbury (Figure 5.1), providing confidence in the accuracy of the model forcing.

5.2 Ocean Boundary: Surface Elevation and Velocity

Along the open boundary of the model domain, time series of surface elevation, current velocity, temperature and salinity are supplied from a 10 km resolution Australasian ocean model, OFAM, which underpins the Bluelink operational forecasting system (Oke et al., 2008). OFAM is run operationally at the BoM, and provides daily predictions of ocean temperature, salinity and non-tidal current velocity in the Australasian region (in a product called OceanMaps, http://www.bom.gov.au/bluelink/products/prod_oceanmaps.html). Velocities at the location of the Leschenault model domain boundary were extracted from OceanMaps for the simulation period, and supplemented by tidal current velocities using the global tide model of Cartwright and Ray (1990). The resulting velocity time series were used to force the Leschenault model. Forcing the local area model by velocity fields from a larger scale model provides a stable and accurate open boundary condition (Herzfeld, 2009; Herzfeld and Andrewartha, 2012). The open boundary condition is combined with a local flux adjustment scheme, using time series of surface elevation

(also taken from OceanMaps and supplemented by tidal elevations), to ensure that tides and sea level are accurately predicted by the model.

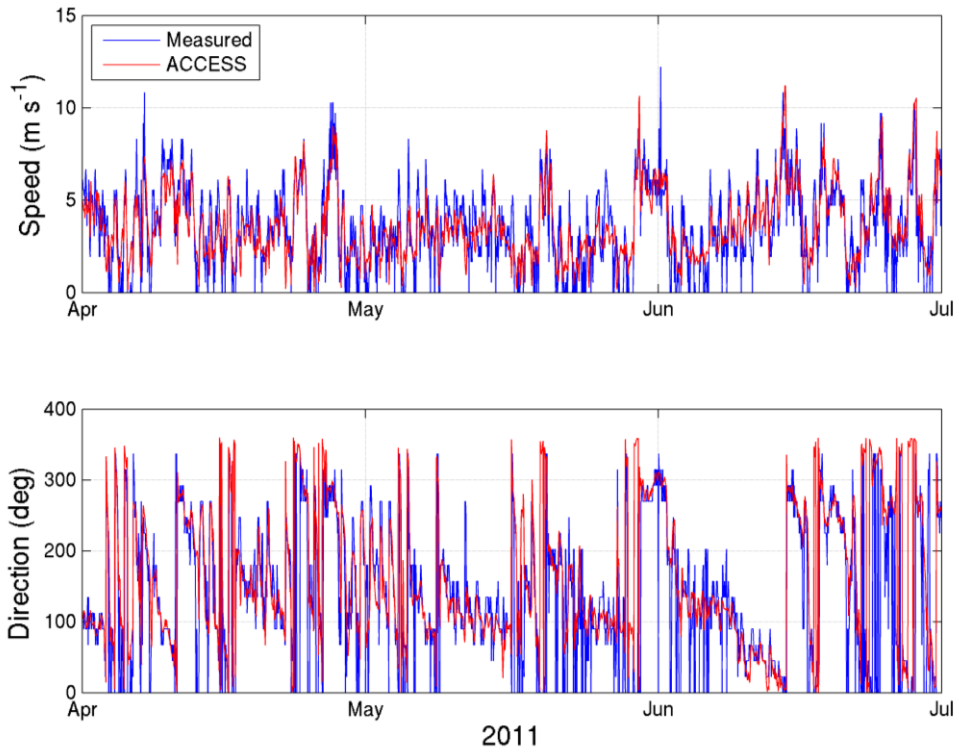

Figure 5.1 : Hourly wind speed (m s^{-1}) and direction (°N) at Bunbury from the ACCESS product for April – June 2011, compared against observations at Bunbury.

Sea level data were obtained at hourly intervals for Bunbury. The time series for April 2011 – March 2012 is presented in Figure 5.2.1. These data were used to calibrate the model. It is notable that the low-frequency variability in the sea level record, due to coastal trapped waves, storm surges etc) is of the same order of magnitude as the tidal fluctuations. Similar low-frequency surface oscillations were found to play a significant role in the dynamics and hydrography of the nearby Swan estuary (O'Callaghan et al, 2007).

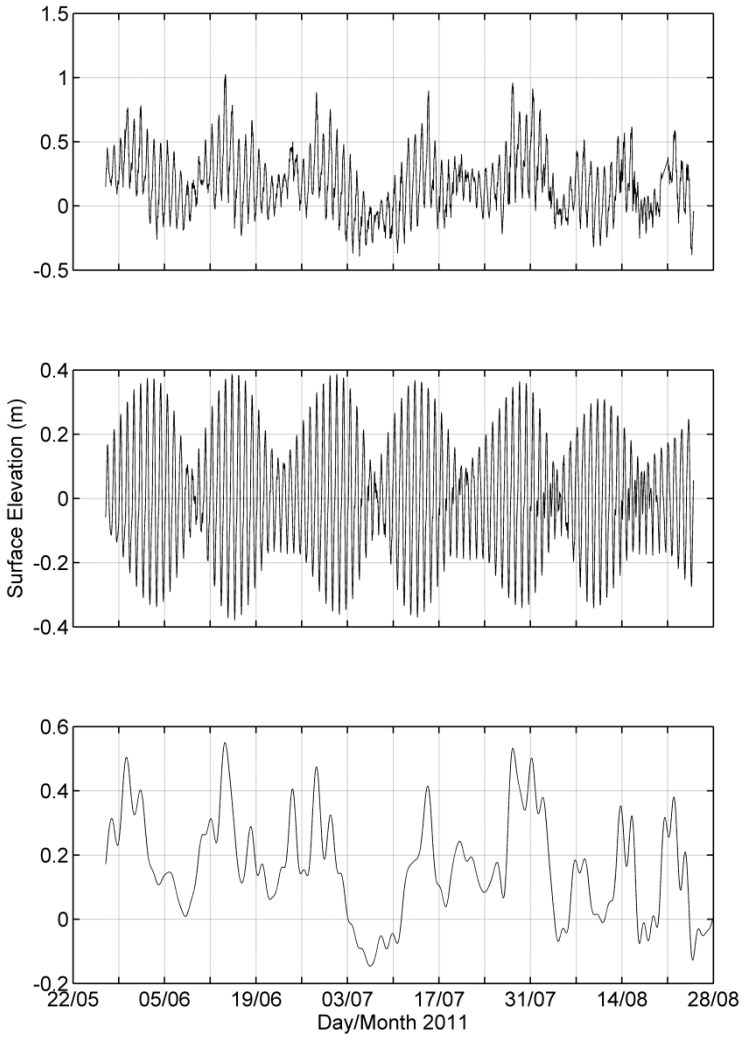

Figure 5.2.1 : Observed sea level at Bunbury for May – August 2011: observed sea level (top); tidal component (middle); sub-tidal component (bottom).

The major tidal constituents (see e.g. Pugh, 1987) and their amplitudes derived from the observed Bunbury sea level time series are presented in Table 5.2.1. It is evident from Table 5.2.1 that the dominant constituents in the region are those due to K_1 and O_1, hence the tide possesses a largely diurnal character. The largest semi-diurnal constituent, M_2, is one-third of the amplitude of K_1. The significant contribution of low-frequency constituents (Mf, MSm, MSf, Mm) to the total sea level is also evident.

Using just the OFAM sea level coupled with the global tide model to force the open boundaries of the Leschenault model did not result in optimal model performance in the vicinity of the estuary. This was due to differences in the low-frequency sea level fluctuations predicted by OFAM from those observed. The boundary condition was improved by relaxing the tidal signal at the boundary toward the observed values observed at Bunbury, with an appropriate time lag. This approach led to an improved boundary condition.

Tidal Constituent Name	Frequency (cycles/day)	Amplitude (m)	Phase (deg)
K_1	1.0027	0.168	298
O_1	0.9295	0.120	283
M_2	1.9323	0.054	292
P_1	0.9973	0.051	290
S_2	2.0000	0.048	293
Mf	0.0732	0.033	73
MSm	0.0314	0.033	34
Q_1	0.8932	0.032	269
MSf	0.0677	0.028	321
N_2	1.8960	0.018	337
Mm	0.0363	0.017	200
K_2	2.0055	0.016	288
MU_2	1.8645	0.008	301
J_1	1.0390	0.008	333

Table 5.2.1 : Tidal Harmonics for Bunbury sea level.

5.3 Temperature and Salinity

The temperature and salinity (T/S) distributions used as initial conditions in the Leschenault model were initialized on 17 March 2011 to 23^{o}C and 36 psu respectively, approximated from the large scale ocean model (OceanMaps, Figure 5.3.1). The temperature solution in the local model was found to be dominated by local atmospheric exchanges (Section 6.3), and attained equilibrium with the atmospheric fluxes relatively quickly (within the two-week spin-up period), hence the choice of initial condition was not critical. Similarly, the open boundary conditions used proved relatively non-critical due to the atmospheric dominance. The salinity solution was similarly quite insensitive to the initial condition, also having a rapid spin up time. The exception was for the northern part of the estuary, where evaporation during the previous summer had raised the salinity. No data were available for the initialization period, but observations from mooring location ‘Estuary 3’, beginning in May 2011, indicated salinities of about 40 psu.

The modelled salinity in the Leschenault Estuary was not particularly sensitive to the open boundary salinity, since the fluctuations in the open ocean were small relative to the fluctuations in the estuary salt content. Time series of the surface temperature and salinity at a location on the open boundary of the model to the west of the Leschenault Estuary (33° 15’ S 115° 20’ E) are shown in Figure 5.3.2. The temperature record displayed the annual cycle of heating and cooling, peaking in late January / early February, and reaching its minimum in August. Salinity at the open

boundary varied over a range of about 35.75 ± 0.75 psu, with highest values occurring in the summer and lowest in late winter and early spring.

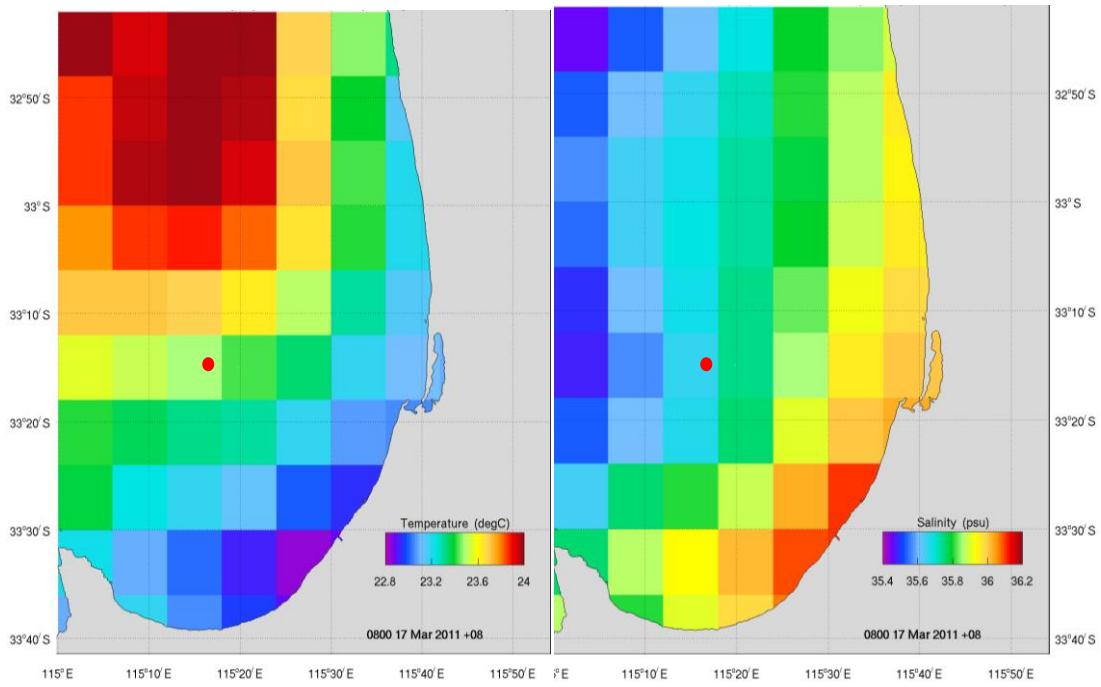

Figure 5.3.1: Sea surface temperature (left) and salinity (right) from OceanMaps (courtesy: Bureau of Meteorology) on 17th March 2011. The red dot marks the location on the open boundary of the Leschenault Estuary model from where the time series in Figure 5.3.1 are taken.

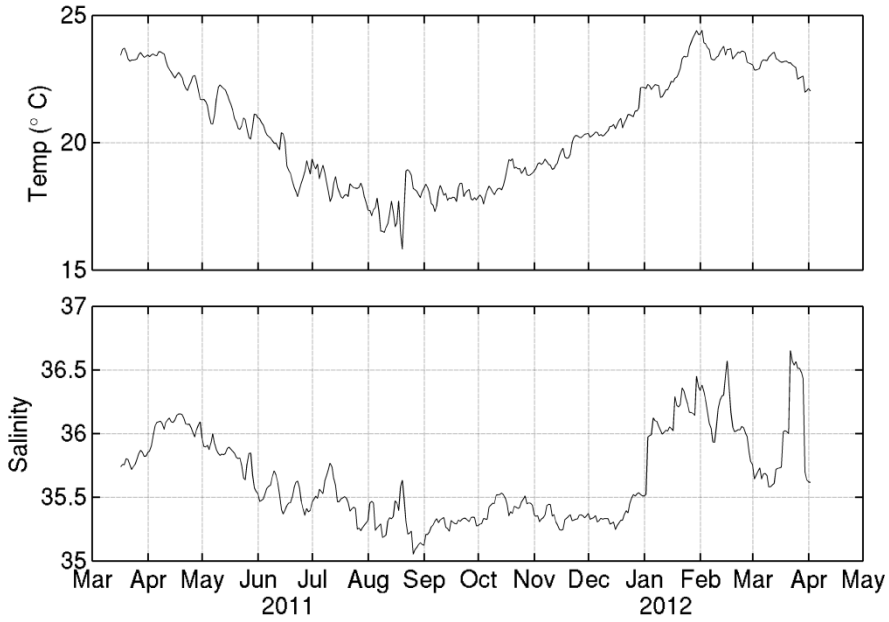

Figure 5.3.2 OceanMaps surface temperature and salinity at the open boundary of the Leschenault model domain (33° 15' S 115° 20' E).

5.4 River Flow

River flow records were provided by DoW for the Collie River at Rose Road, the Brunswick River at Cross Farm, and for the Preston River by combining flows at SW Highway with Ferguson river flows at Boyanup. Flows in the Parkfield Drain were also estimated using the Brunswick River flows appropriately weighted by relative catchment size. The freshwater input from the Parkfield Drain appears to be an important factor in the flushing of the northern part of the estuary. Daily flows are displayed for the simulation period in Figure 5.4.1.

The temperature and salinity of the Collie and Ferguson Rivers were measured throughout the year and these values were applied also to the Brunswick and Preston Rivers respectively. The river temperature time series are shown in Figure 5.4.2. Salinity values were essentially zero, and are not shown.

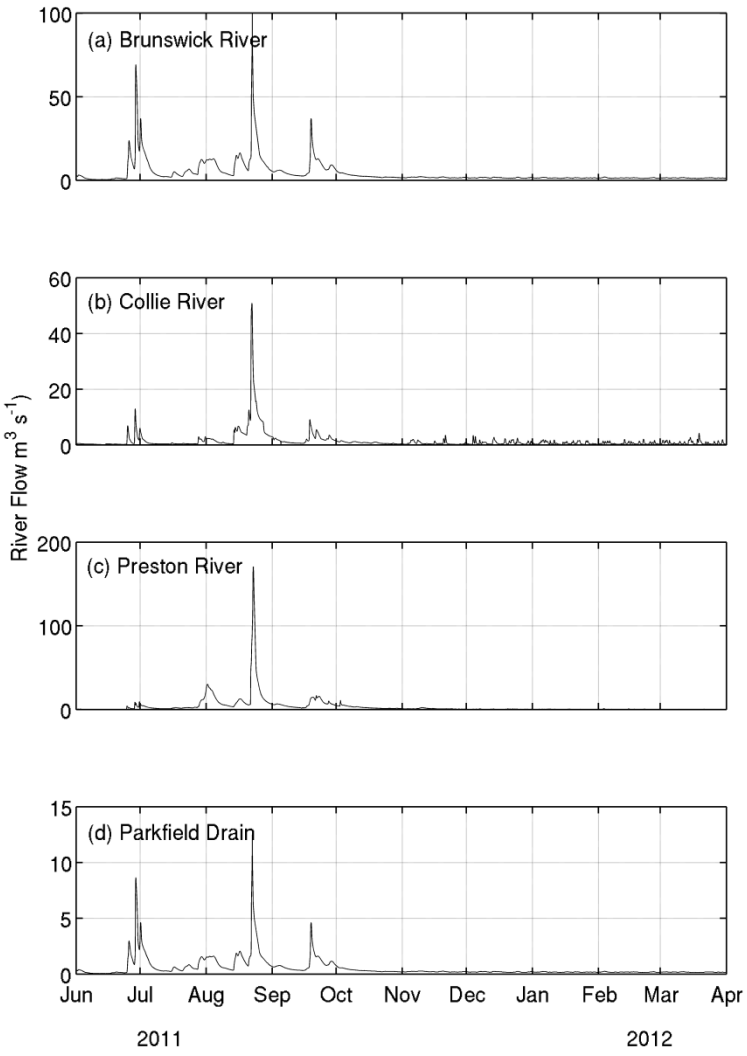

Figure 5.4.1: Measured(Collie, Preston, Brunswick) and modelled (Parkfield) flows in the rivers entering the Leschenault Estuary during 2011 – 12.

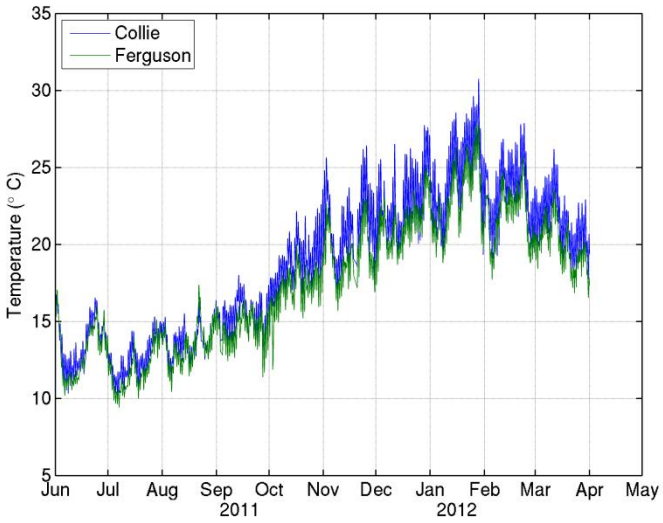

Figure 5.4.2: Measured temperature in the Collie and Ferguson rivers during 2011-12.

5.5 Heat and Salt Fluxes

Heat fluxes were computed from meteorological parameters provided by the ACCESS model by the methods outlined in Herzfeld (2005, Chapter 9). Short wave radiation was estimated from the sun's hour angle at the latitude corresponding to the Leschenault Estuary, and corrected for cloud cover. Long wave radiation was calculated using the model sea surface temperature and ACCESS air temperature, also correcting for cloud cover. Sensible and latent heat fluxes were calculated using the bulk method (Kondo, 1975), requiring wet and dry bulb air temperature, pressure and wind-speed measurements as input. The heat flux components and net heat flux for the simulation period are illustrated in Figure 5.5.1. Heat fluxes are further discussed in §7.2.

The salt (or freshwater) flux is defined as the difference between evaporation minus precipitation. Evaporation over water is difficult to measure, and this quantity was obtained from the latent heat flux computed by the bulk method divided by the latent heat of evaporation. The precipitation used was from the ACCESS (Figure 5.5.2).

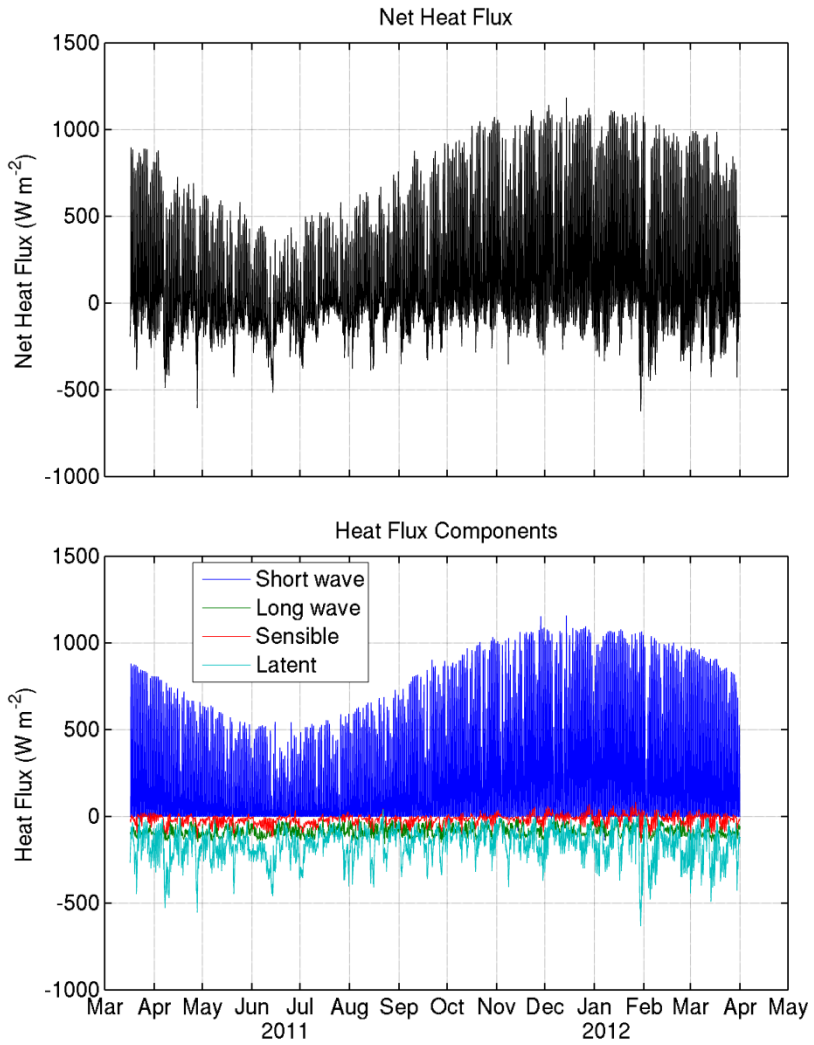

Figure 5.5.1 : Heat fluxes for 2011 – 12.

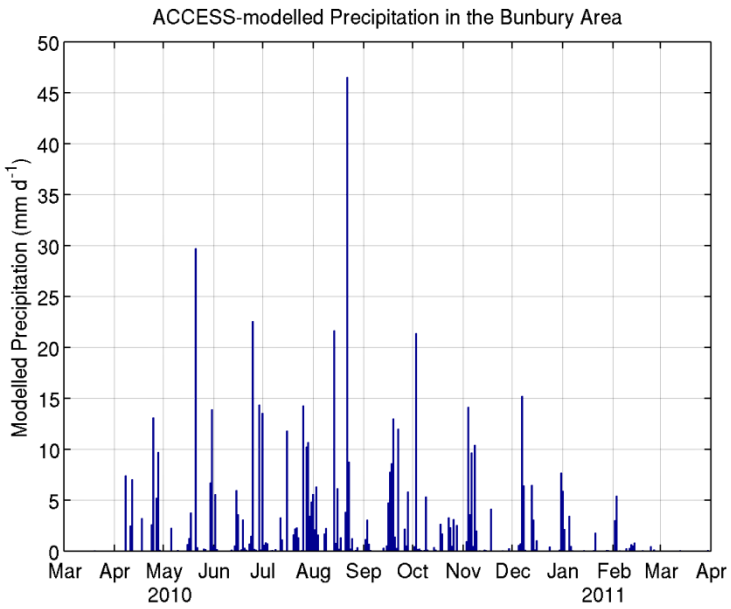

Figure 5.5.2 : Modelled daily precipitation at Bunbury (mm) from ACCESS.

6. Field Data

A data collection programme was maintained by Western Australia Department of Water throughout the first half of the study period, from May – December 2011. YSI temperature and conductivity loggers were deployed on moorings at five sites in the estuary (Figure 6.1).

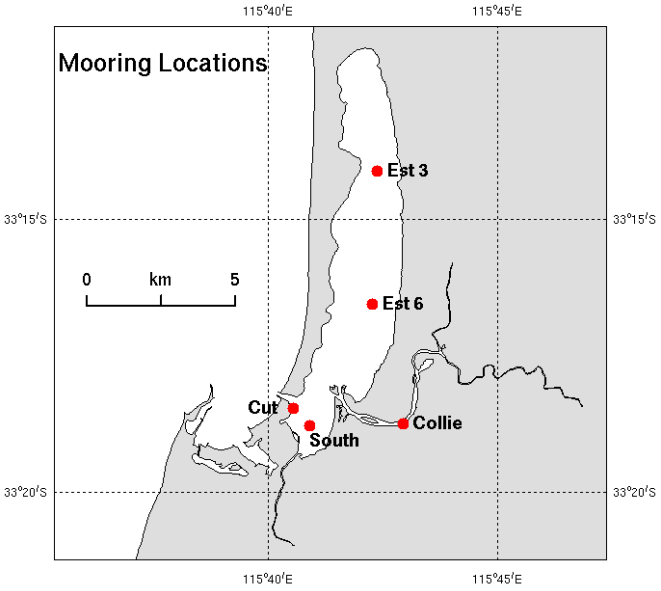

Figure 6.1. Locations of the moorings deployed in the Leschenault Estuary by DoW during 2011 – 12.

The mooring deployments provided hourly data on temperature and salinity conditions in the estuary. At the Cut and Collie locations, two loggers were deployed, providing near-surface and near-bottom data. At Est 3, Est 6 and South locations, a single logger was deployed. Locations and depths of the instruments are presented in Table 6.1.

Name	Latitude (°S)	Longitude (°E)	Water depth (m)	Sensor depth(-)/height(+) (m)
Collie Surface	33.3124	115.7157	2	-0.5
Collie Bottom	33.3124	115.7157	2	+0.4
Cut Surface	33.3078	115.6757	3	-0.4
Cut Bottom	33.3078	115.6757	3	+0.4
Est 3	33.2352	115.7064	1.2	-0.6
Est 6	33.2759	115.7047	1	-0.4
South	33.3130	115.6818	1	-0.25

Table 6.1. Location and depth of the moored temperature and conductivity loggers deployed in the Leschenault Estuary by DoW during 2011 – 12. Sensor depths below the water surface are given as negative values, sensor heights above the seabed are positive.

Sea level data from Bunbury, obtained from the Department of Planning and Infrastructure, were also used to calibration the model, particularly in terms of fine-tuning the open boundary condition.

7. Model Output

7.1 Background

The Leschenault Estuary is classified as a micro-tidal estuary. The climate for the region involves a cool wet winter and a dry hot summer. During the winter, flows in Collie and Brunswick increase from background levels of about 1 $m^3 s^{-1}$ to values exceeding 100 $m^3 s^{-1}$ during flood events. On shorter timescales, a small predominantly diurnal tide undergoes a neap-spring oscillation on a fortnightly time scale, with maximum ranges of ~0.7 m during the spring phase and less than 0.1 m during the neap. During spring tides, large currents are generated in the Cut, but currents are weaker in the estuary interior. Much of the estuary stratifies during periods of high river flow, despite its shallow nature. In the Collie River, a salt wedge intrudes as far as the Australind Bypass Bridge during dry periods, but when river flow is high, the saltwater may be pushed out of the lower Collie reaches into the estuary. When the flood abates, the salt wedge intrudes back into the Collie River. In the lower reach of the river, the salt wedge appears to return quite rapidly following cessation of the flood event.

7.2 Model Calibration

The model was primarily calibrated against sea level, temperature and salinity. Calibration against surface elevation provides confidence that modelled tidal flows, which dominate the circulation in the region, are broadly accurate. Calibration of temperature and salinity was performed using data from the moored instrumentation (Figure 6.1). The first stage of the calibration process was to fine-tune the application of the open boundary conditions, by combining tidal characteristics, OceanMaps sea level and velocity, and observed sea level, to produce the best fit against the observed sea level data at Bunbury. The second stage involved selecting advection schemes, mixing schemes and surface flux parameter settings to provide the best fit against the measured temperature and salinity time series. This second calibration stage was performed using data from September and October 2011, when surface heating was producing strong warming of the estuary water. Once the best simulation for September and October was achieved, the model was run for the whole year, and some final fine-tuning of parameter values undertaken e.g. horizontal viscosity and diffusion coefficients and background vertical diffusion coefficients.

The ability of the model to reproduce the observations was tested quantitatively, using methods described by *Willmott et al.* (1985). We calculated the root-mean-square (rms) error between the model predictions and the data, given by:

$$rms = \left[\frac{1}{N} \left(\sum_{j=1}^{N} (p_j - o_j)^2 \right) \right]^{1/2}$$

where p_j and o_j are predicted and observed values respectively and N is the number of data points in the calculation. The model skill, d_2, was estimated by:

$$d_2 = 1 - \left[\sum_{j=1}^{N} (p_j - o_j)^2 \right] \Big/ \left[\sum_{j=1}^{N} (| p_j - \bar{o} | + | o_j - \bar{o} |)^2 \right]$$

where ō is the arithmetic mean of the observed data. A perfect agreement between model and data would give $d_2 = 1$, with decreasing values indicating declining performance down to zero skill ($d_2 = 0$).

The modelled and measured sea level at Bunbury for the whole simulation is shown in Figure 7.2.1. The model performs well in terms of sea level, capturing the diurnal tidal character, the spring-neap cycles, and the low-frequency fluctuations. The root-mean-square (RMS) error for the entire simulation is 0.05 m. A more detailed comparison between modelled and observed sea level, for July – August 2011, is shown in Figure 7.2.2. The figure shows clearly how well the model reproduces the observed tidal sea level at Bunbury.

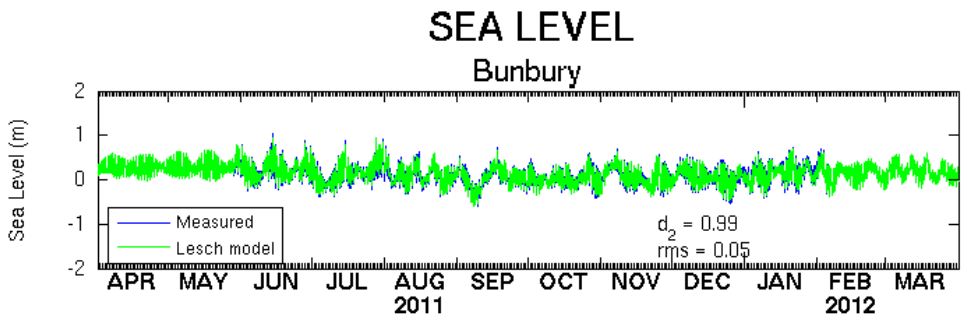

Figure 7.2.1 : Modelled and measured sea level at Bunbury (observation = blue, model = green)

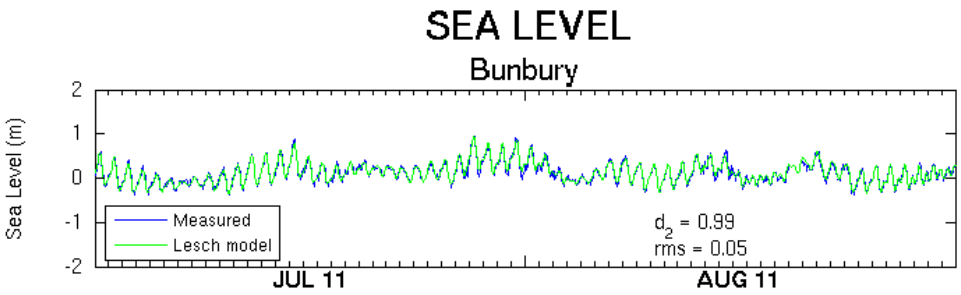

Figure 7.2.2 : Modelled and measured sea level at Bunbury for July – August 2011 (observation = blue, model = green)

The boundary forcing of the model was tuned to provide the best fit to the data at Bunbury, so the good agreement between the model and data is not unexpected. Nevertheless, the good agreement provides confidence in the accuracy of the model forcing at the entrance to the estuary.

Temperature and salinity data from the moored sensors were inevitably patchy. Of the sensors listed in Table 6.1, useful datasets were acquired from all sensors except for the surface record at the Cut; we used data from the other sensors to calibrate the model.

The comparison between modelled and observed temperature for the full annual simulation is shown in Figure 7.2.3. The annual cycle of heating and cooling is evident and the observed and modelled time series are closely matched. The model also reproduced fluctuations with time scales of a few days, likely due to either fluctuations in the next heat flux or advection within the estuary. The skill indices for each location typically have values greater than 0.9, and RMS errors are of the order of 1°C, less than 10% of the data range. These results clearly show that the model successfully captured the evolution and variability of temperature in the estuary over a seasonal cycle.

The temperature comparison for winter (July – August 2011) is shown in greater detail in Figure 7.2.4. The model captured much of the tidal variability in temperature during this period, but some discrepancies are evident. Nevertheless, the level of agreement between model and data overall is good. It is interesting to note that a clear tidal signal is evident in the surface sensor location in the Collie River, but is almost entirely absent from the lower sensor at the same location. The model successfully reproduced this effect.

During summer, limited observations were available for comparison. The few data available, for example at Estuary 3 and Collie Bottom, indicate that the model was accurately tracking rising temperatures in the estuary (Figure 7.2.5). Over summer, water temperatures exceeded 28 C in the main body of the estuary and in the Collie River. Daily variability in water temperature was successfully captured in the model.

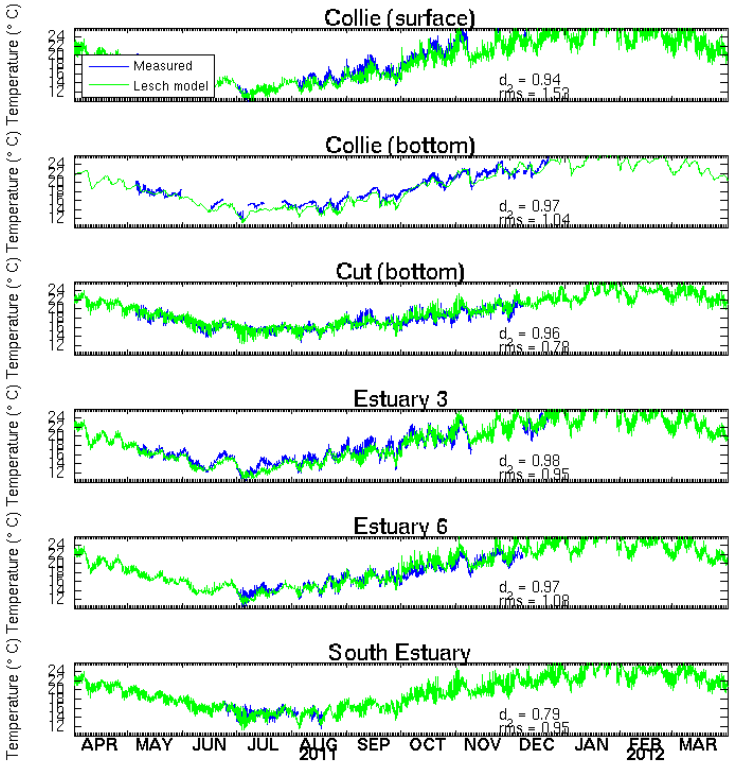

Figure 7.2.3. Observed and modelled temperature for 2011 – 12 at six sensor locations. Measured data are in blue, model predictions in green. Skill indices and RMS errors for each location are noted.

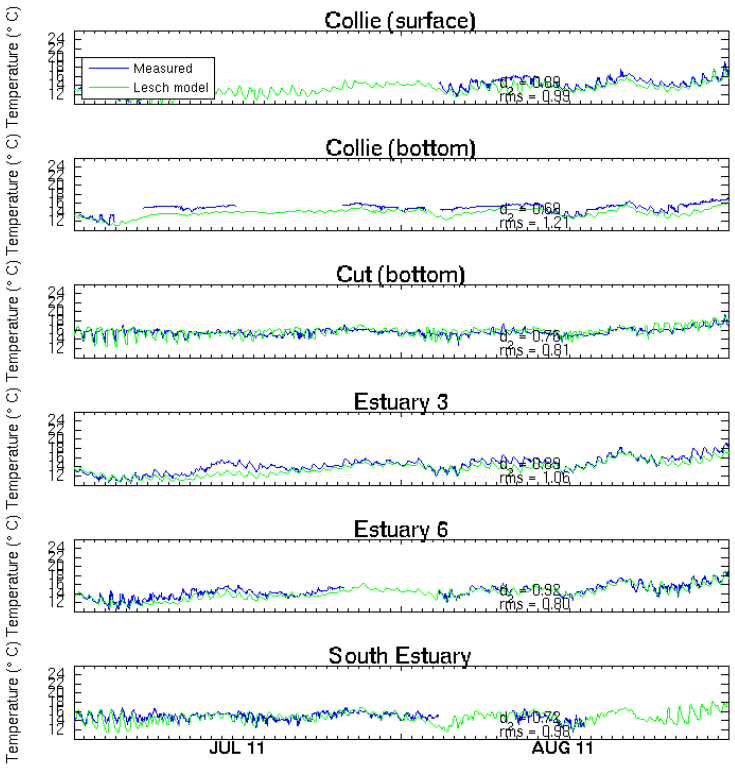

Figure 7.2.4. Observed and modelled temperature for July – August 2011 at six sensor locations. Measured data are in blue, model predictions in green. Skill indices and RMS errors for each location are noted.

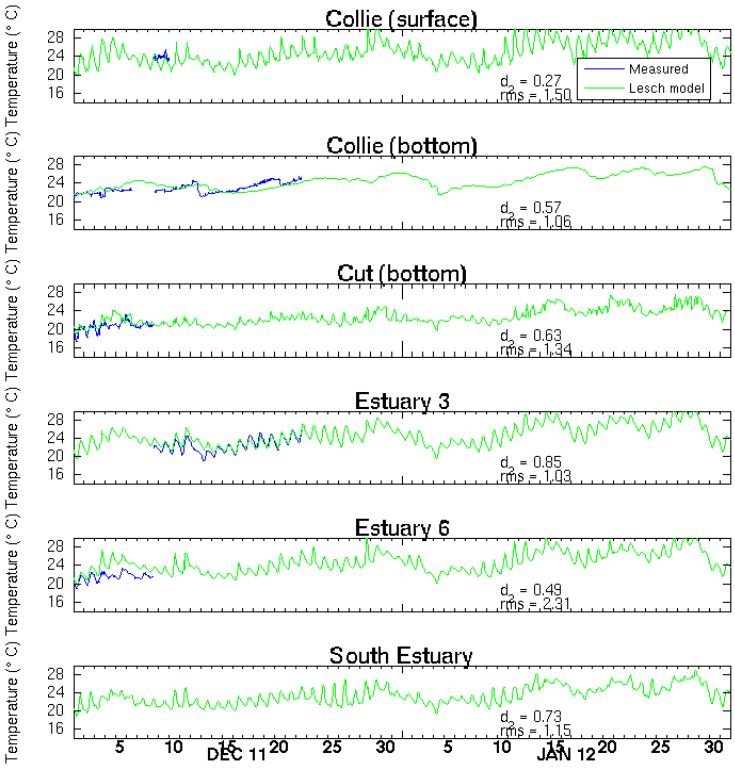

Figure 7.2.5. Observed and modelled temperature for December 2011 – January 2012 at six sensor locations. Measured data are in blue, model predictions in green. Skill indices and RMS errors for each location are noted.

Modelled and observed salinity at the sensor locations during 2011 – 12 is shown in Figure 7.2.6. The model generally reproduced the seasonal variability and the shorter-term fluctuations in salinity, but there were discrepancies between the model and the observations. In the main body of the Leschenault, as evidenced by data from the Cut, Estuary 3, Estuary 6 and South Estuary sensors, the model captured the majority of the salinity variability. The model tended to underestimate the salinity at Estuary 3, which is probably caused by over-estimated flows in the Parkfield Drain. In early simulations, when freshwater input from the Parkfield Drain was not included in the model, the modelled salinity at Estuary 3 was significantly higher than the observations and did not capture the observed variability. The freshwater input from this source is clearly essential to accurately model the northern part of the estuary, and improving the knowledge of flows in the Parkfield Drain could improve the simulations here.

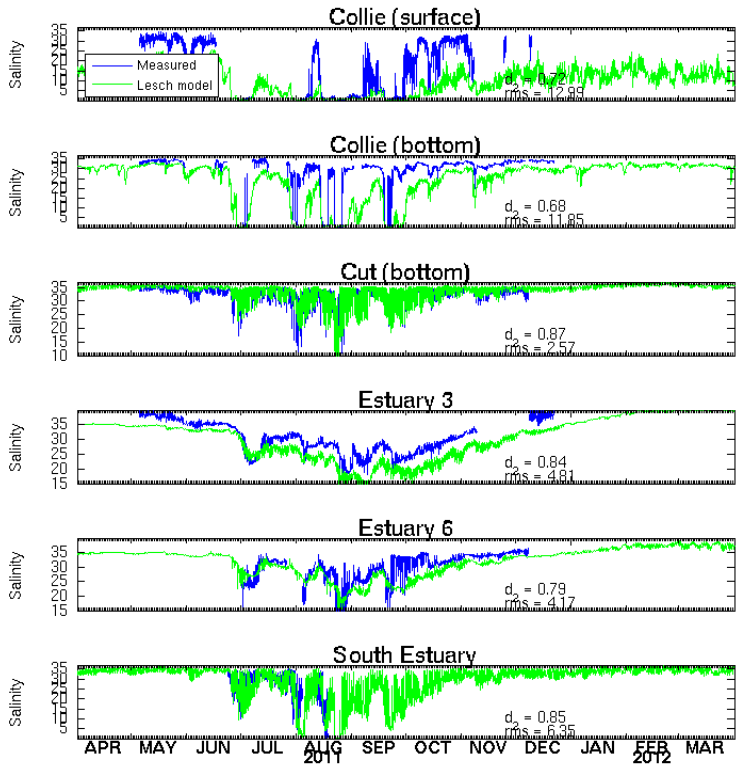

Figure 7.2.6. Observed and modelled salinity for 2011 – 12 at six sensor locations. Measured data are in blue, model predictions in green. Skill indices and RMS errors for each location are noted.

At Estuary 6 and South Estuary locations, the model captured the broad variability observed in the available salinity data. During the summer, salinities in the main estuary body approached 40 psu, due to strong evaporation, evident at Estuary 3 (Figure 7.2.6). The model successfully reproduced these elevated values, by using the latent heat flux formulation built into the model. Model skill scores in the main estuary were typically greater than 0.8, with RMS errors of 2 – 6 psu (10 – 25% of the range of values). In the Collie River, the model skill was slightly less, at about 0.7 and larger RMS errors.

The biggest discrepancy between the predicted and observed salinity time series occurred in the Collie River. The observations indicate the up- and down-estuary movement of a salt wedge. During periods of high river flow in the Brunswick and Collie Rivers, salt water is driven out of the lower Collie; when the flow reduces, the salt wedge appears to rapidly return up the estuary, within a time frame of the order of a day (Figure 7.2.6, Collie (bottom)). Although the model generally reproduced this pattern of events, the salt wedge intrusion following a high flow event occurred more slowly, taking the order of a week. Quite often, the modelled salinity did not return to full estuary values before the next flow event. It should be noted here that the lower Collie River is a region of very strong salinity gradients, particularly vertically, and that any discrepancy between the location at which model output is extracted and the actual observation location could lead to significant differences between modelled and observed time series. The model reproduces the fundamental dynamics of salt wedge intrusion along the Collie River, with a very sharp pycnocline

(discussed further in §8.7). Given the limits to spatial resolution that is possible for this part of the domain, whilst allowing practical run times for the domain as a whole, we believe the model is performing satisfactorily in the Collie.

Winter salinities at the mooring locations are shown in Figure 7.2.7. The model largely captured the tidal variability in the observations: large tides at the Cut and the South mooring were reproduced, as were the weaker tides at Estuary 3 and Estuary 6. The limitations of the model in the Collie River are evident. The RMS errors are quite large, due to the strength of the salinity gradients spatially and over time, but the skill indices for the main body of the estuary are satisfactory.

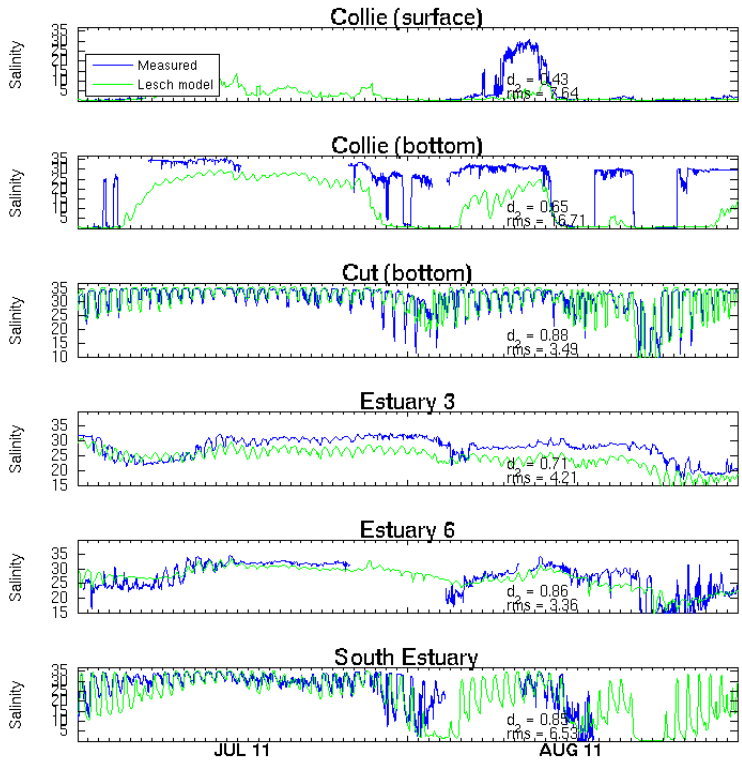

Figure 7.2.7. Observed and modelled salinity for July – August 2011 at six sensor locations. Measured data are in blue, model predictions in green. Skill indices and RMS errors for each location are noted.

During summer, the limited data available prevent proper calibration. Those data indicate that the model slightly underestimated salinity in the northern estuary (Figure 7.2.8, Estuary 3); as noted previously, this is probably due to the relatively poor specification of flows in the Parkfield Drain. The discrepancy between modelled and observed salinities at Estuary 3 originates in late September (Figure 7.2.6), following a small flood event, and appears to persist thereafter. In the central estuary, (at Estuary 6 and the Cut), the model appeared to be tracking the observed data well.

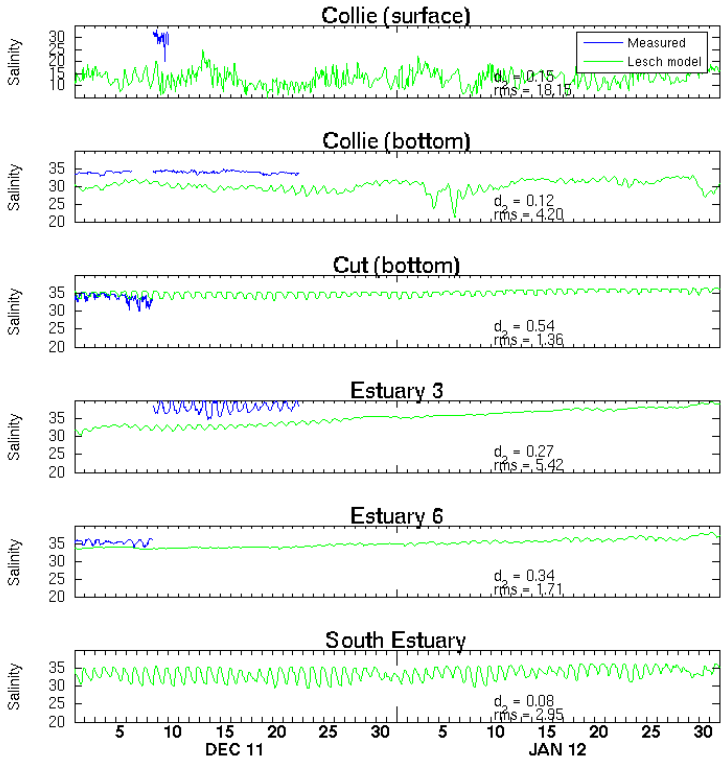

Figure 7.2.8. Observed and modelled salinity for December 2011 – January 2012 at six sensor locations. Measured data are in blue, model predictions in green. Skill indices and RMS errors for each location are noted.

7.3 Sensitivity

During the calibration procedure an assessment of the sensitivity of model parameters and processes was made. This provides insight into the parameters and processes which may critically affect the model solutions. The calibration presented in Section 7.2 is the end result of the sensitivity analysis; the key parameters of the calibration procedure and model process requirements are detailed below.

The bathymetry used in the model proved critical in reproducing the salt wedge dynamics in the Collie River. The vertical spatial resolution in the river was 0.5 m; to increase this resolution (i.e. increase the number of layers in the vertical) throughout the model domain leads to impractical run times. Yet water depths in the Collie River are only of the order of 1 m in many places, allowing only two grid cells in the vertical. This leads to difficulty in simulating salt wedge dynamics, when water in the surface model cell mixes directly with water in the bottom cell. The Collie River contains numerous deeper pools, typically 3 – 4 m deep, connected by shallower reaches (Figure 7.3.1).

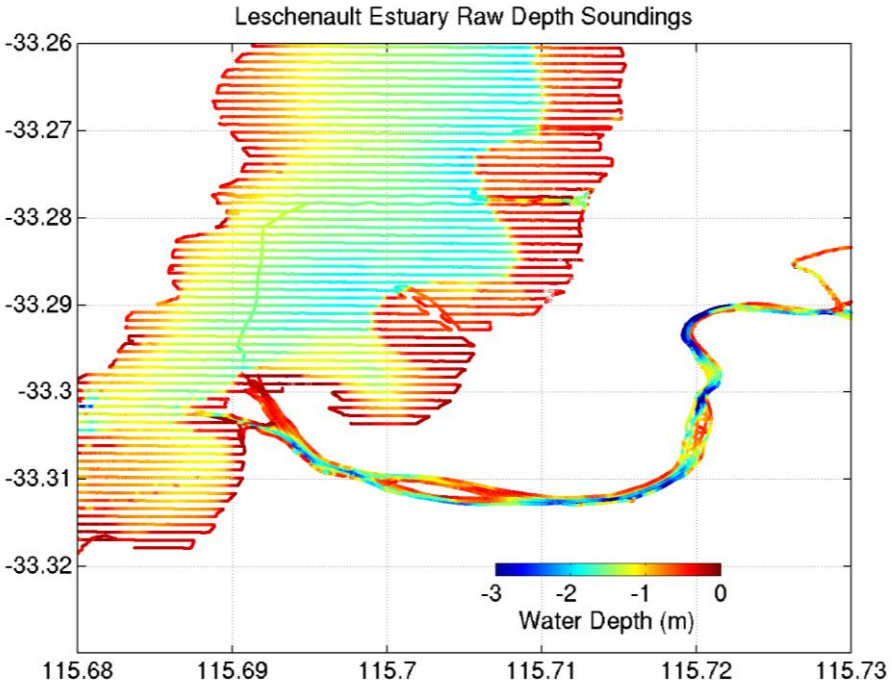

Figure 7.3.1 : Raw bathymetry data in the Collie River.

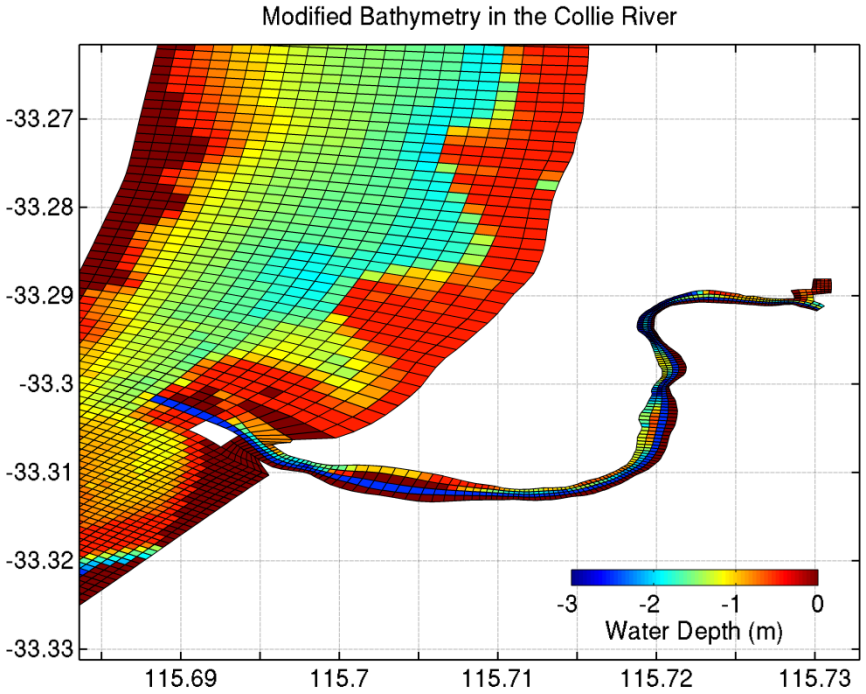

Figure 7.3.2 : Modified bathymetry in the Collie River, with a 2.5 m deep channel introduced up to the Collie-Brunswick junction.

In order to enable the model to reproduce the salt wedge dynamics, the bathymetry was modified by connecting these deeper pools by a channel of constant depth. In effect, an artificial channel, 2.5 m deep, was created from the mouth of the Collie River as far as the junction with the

Brunswick River (Figure 7.3.2). This channel allowed salt water to penetrate from the Leschenault Estuary up the Collie River to the Collie/Brunswick junction and beyond. As was noted earlier, the response of the salt wedge to reduced flow was still, even with the introduction of the artificial channel, slower than observed. All model runs described in this report use the model bathymetry with the artificial channel. The cause of the problem is thought to be the spatial resolution, both horizontally and vertically, which is insufficient to resolve the key dynamics of salt wedge propagation; however, as remarked above, the spatial resolution cannot be increased without rendering the model run times impractical.

The first critical process addressed in the model was the parameterization of atmospheric heat and freshwater fluxes across the ocean surface. In the model, the surface heat and freshwater fluxes are computed from standard meteorological measurements (Herzfeld, 2005, Chapter 9). Incoming short-wave (solar) radiation and outgoing long-wave radiation values were calculated from the formulae of Zillman (1972), corrected for modelled cloud cover as provided by the ACCESS model output. Sensible heat (the transfer of heat by convection and conduction) and latent heat (the transfer of heat during evaporation) fluxes were calculated using bulk formulae from standard meteorological variables, and introduce the most uncertainty into the heat flux calculations (see below). The freshwater (or salt) flux arises from the difference between evaporation and precipitation, which leads to a net change in freshwater content (and therefore salinity) of the estuary.

In shallow areas (i.e. much) of the Leschenault Estuary, localized observed temperature increases are due to the effects of surface heating and cooling on water of varying depth. Salinity was also observed to increase in the central estuary during summer due to evaporation. The choice of bulk scheme used to derive the sensible and latent heat fluxes across the sea surface can therefore be an important factor in the accuracy of simulated temperatures. There are numerous bulk schemes in existence; Blanc (1985) reviewed ten schemes and concludes that each scheme provided different results when applied to the same data, highlighting the inherent uncertainty in the bulk method. During the present study, two schemes were tested by simulating the spring heating period (September – October 2011); the bulk scheme of Kondo (1975) provided better agreement between measured and model results than the algorithm of Large and Pond (1981) and was then used throughout the study.

The short wave radiation component incident on the sea surface may be partitioned so that a fraction is input as the surface boundary condition (in addition to the sensible, latent and long wave components) and the remaining fraction is allowed to penetrate the water column to a depth determined by an attenuation coefficient. This partitioning represents the preferential absorption of longer wavelengths of short wave radiation within the first few meters (Simpson and Dickey, 1981). It was determined that the best temperature calibration occurred when 20% of the shortwave radiation was allowed to penetrate the water column with an attenuation coefficient of 0.1 m^{-1}; the

remaining 80% of incident radiation was absorbed into the surface layer. During the calibration process, many simulations were performed with different combinations of the transmission and attenuation coefficients. Attenuation was varied from 0.1 to 0.5 m^{-1}, with transmission varied from zero to 100%. Some of the radiation that is transmitted through the water column reaches the seabed, and the impact of that radiation is controlled by a third parameter, the bottom absorption parameter. The bottom absorption parameter specifies the fraction of the radiation incident on the seabed that is absorbed into the seabed, thereby having no effect on the water column; the remainder is assumed to heat the bottom layer of the water column (p. 64, Herzfeld & Waring, 2012). For the calibration process, the bottom absorption parameter was varied over the range 0.1 – 0.9. The ensemble of temperature time series resulting from all these simulations is shown in Figure 7.3.3, together with the observed temperature. The ensemble envelope indicates the sensitivity of the model to these parameters. The parameter values of the ensemble member having the best overall agreement with the data were chosen for subsequent model runs. Attenuation coefficients are likely to be spatially variable, responding to different loads of suspended sediment in the water column, and the use of a constant extinction in the model may account for some of the minor discrepancies between modelled and measured temperature in the Leschenault Estuary. (Figure 7.2.3).

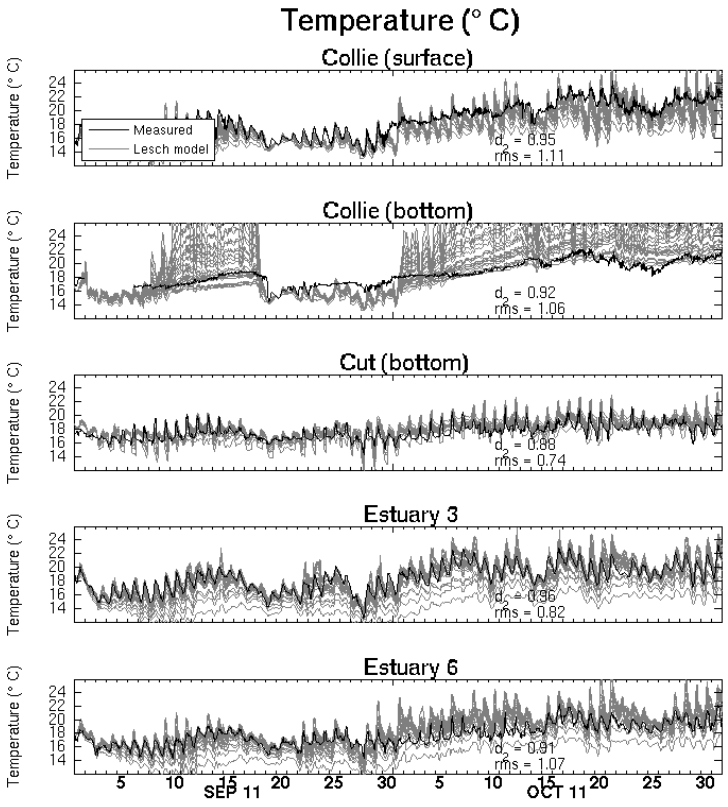

Figure 7.3.3: Time series of temperature from the ensemble of model runs to choose the heat flux parameters. Each ensemble shown in light gray. The temperature data are overlain in black.

Horizontal viscosities and diffusivities were set to constant values of 20 $m^2 s^{-1}$ and 10 $m^2 s^{-1}$. A time- and space-varying horizontal diffusivity scheme (Smagorinsky, 1963) was also tested, but the constant values were found to provide a more stable and accurate solution.

For vertical viscosity and diffusion, the k-ω scheme of Umlauf et al. (2003) was found to provide the best results and to produce the most stable model. The background vertical diffusion coefficients were set to $1x10^{-7}$ $m^2 s^{-1}$; this value used is lower than typical values used in coastal ocean models (e.g. Warner et al., 2005), but increasing the background values affected the model solution in the Collie River. In particular, the vertical salinity gradient across the salt wedge interface was weakened as the background mixing levels were increased. Decreasing the background mixing by an order of magnitude had minimal effect on the solution, presumably because the numerical mixing inherent in the implicit mixing scheme introduced vertical diffusion of this order of magnitude.

No manipulation of the open boundary was attempted during the project. The boundary is sufficiently far removed from the estuary, and fluctuations of temperature and salinity along the boundary are sufficiently small compared to the variability in the estuary, for the boundary to be considered a minor influence on estuary conditions. Salinity along the open boundary of the model typically varied in the range 35 – 37 psu. Uncertainty in the boundary salinity is very small compared to the variability in the Leschenault Estuary, and considered very unlikely to have a significant impact on the estuary predictions. Likewise, the uncertainty in the model boundary temperature is unlikely to significantly influence predictions of estuary temperature.

8. Solutions

8.1 Tides

The circulation in the Leschenault Estuary at any instant in time is dominated by the tide, moderated by the magnitude of freshwater flow into the estuary. Surface flood and ebb currents are opposed and enhanced respectively by the estuarine circulation. During winter, therefore, surface ebb currents were stronger than surface flood currents on both spring (Figure 8.1.1) and neap (Figure 8.1.2) tides. These snapshots were taken at the state of the tide indicated in Figure 8.1.3. Currents were significantly weaker during the neap tide in comparison to the spring tide, where maximum current speeds approached 2 m s^{-1} through the Cut. The sea surface height within the Leschenault Estuary lags behind the external sea level, as exchange is constricted through the narrow entrance channel. The phase of the tide can be traced along the main estuary and up the Collie River by comparing the times of high and low water at the monitoring locations (Figure 8.1.3). During the period illustrated in Figure 8.1.3, high water inside the estuary occurred about two hours after high water at Bunbury, and the lag for low water was about six hours. The tidal choking through the Cut also reduces the tidal range inside the estuary relative to that outside. Observations of surface elevation in the northern estuary and the Collie River would be useful to verify the tidal progression up the estuary.

During flood tide, there is considerable variability in the strength and direction of the currents at any particular location in the estuary. The flood jet entering the Leschenault basin through the Cut is steered northwards along the western shore of the estuary, with weak currents on the east shore to the north of the Collie River. The flood tide jet is gradually steered into the centre of the estuary, and becomes progressively weaker as the head of the estuary is approached. In the southern basin, where the Preston River discharges, the flood tide sets up an anti-clockwise circulation pattern. Note that the plot for neap currents (Figure 8.1.2) shows that the currents outside the estuary offshore from Bunbury have already reversed and are southward along the WA coast, whereas for springs the external current direction is northward.

During ebb tide, the circulation is generally reversed, with southward flow in the central main estuary and a clockwise circulation in the southern basin. Again, variations exist in the strength and direction of the flow at any particular location. At the time of the spring ebb shown, the tide outside the estuary has begun to rise, and coastal currents are northward. Hence the ebb jet emerging from the Cut is turned northwards. During the neap tide ebb shown, the emerging jet is directed westwards across the Koombana Bay before joining the northward flow along the WA coast.

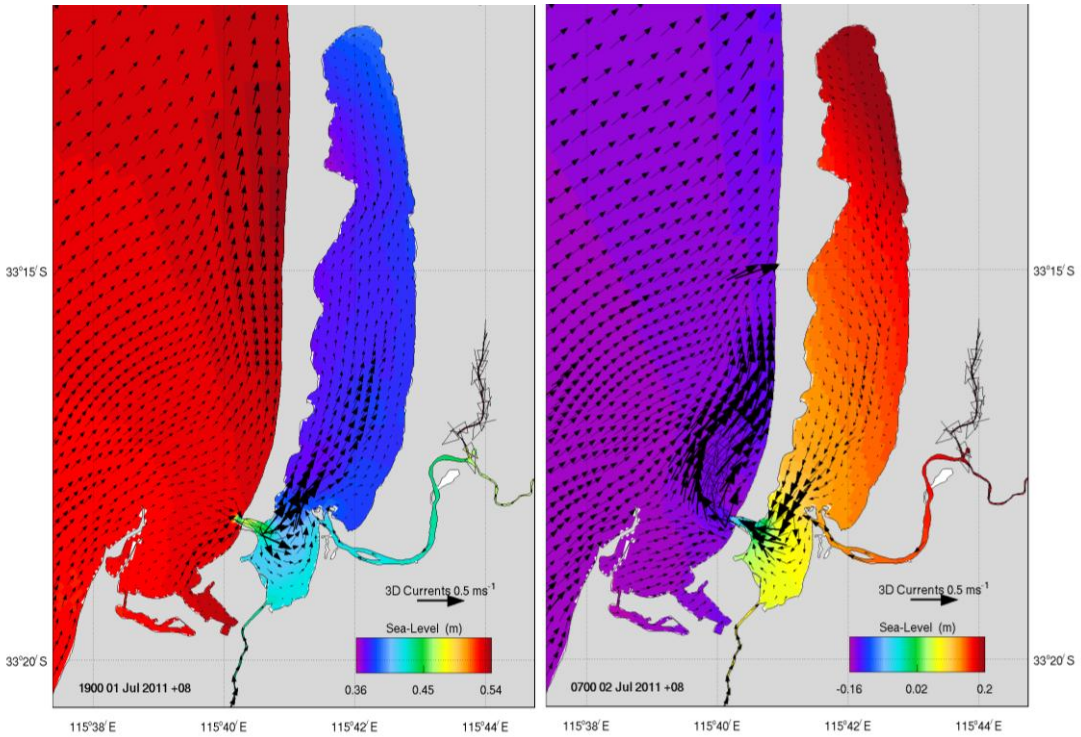

Figure 8.1.1 : Surface flood (left) and ebb (right) currents (ms^{-1}) during spring tides. The coloured shading represents values of sea surface height (eta).

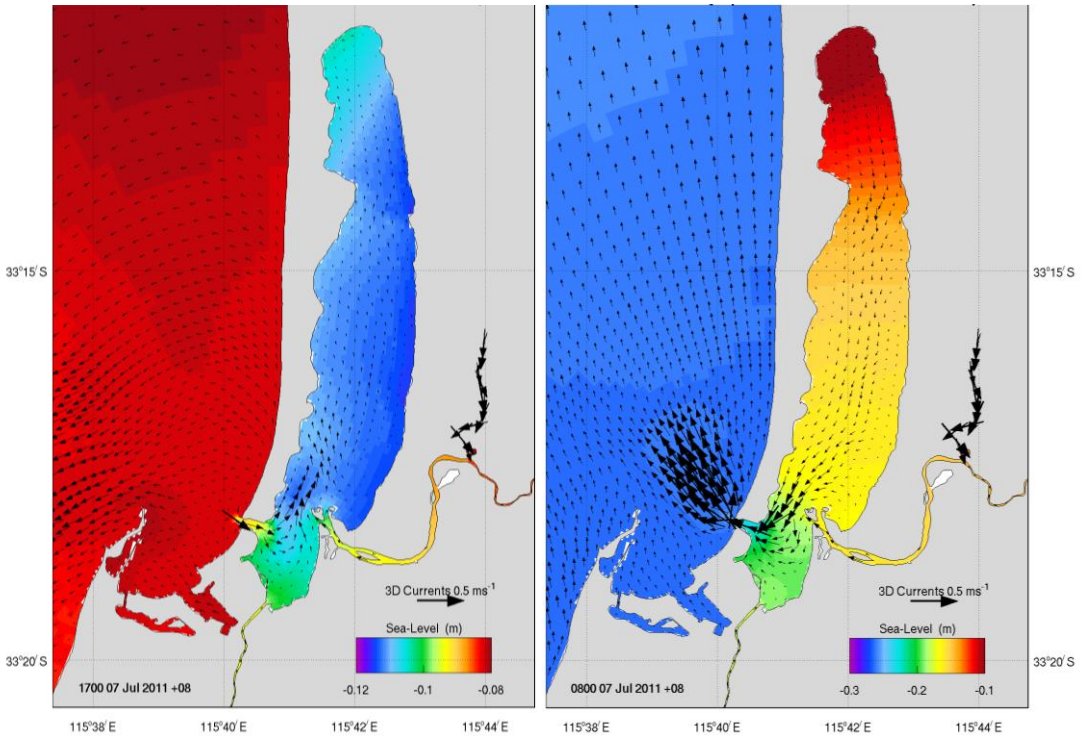

Figure 8.1.2 : Surface flood (left) and ebb (right) currents (ms^{-1}) during neap tides. The coloured shading represents values of sea surface height (eta).

There is little depth dependency on the tidal currents in the main Leschenault Estuary (this is not true of the lower Collie River). Maps of the near-bed currents (at 1.3 m depth) and the depth-averaged currents show very similar features to the surface currents. Typical current speeds in the main estuary during spring flood are typically 1.5 m s^{-1} though the Cut, 0.5 m s^{-1} in the flood jet adjacent to the mouth of the Collie River, about 0.10 m s^{-1} at Est 3 and Est 6, decreasing to 0.05 m s^{-1} in the northern part of the main estuary (Figure 8.1.4). Note that the velocity time series from the Cut shown in Figure 8.1.4 are taken from a location just inside the Cut channel (Figure 6.1); at this particular location, flood currents are southeastward into the southern basin, and ebb currents towards the northwest.

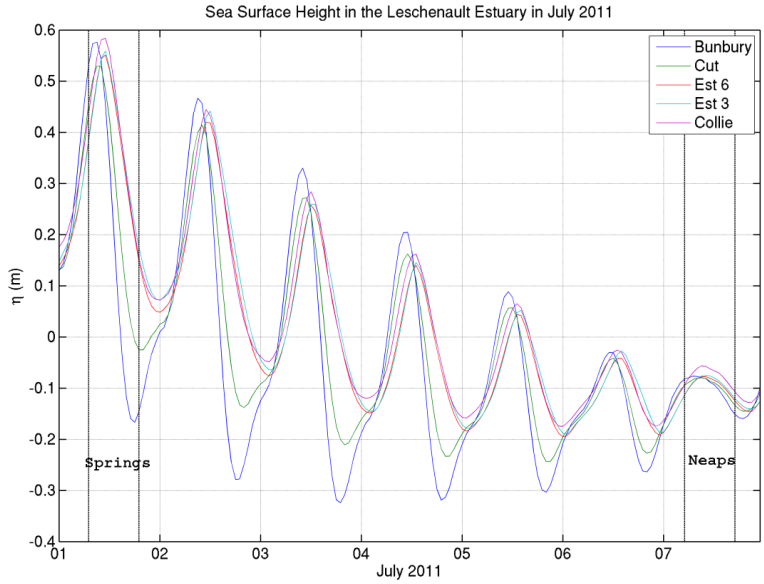

Figure 8.1.3. Sea surface height during the first week of July 2011 at five locations in the Leschenault Estuary. The four vertical dashed lines indicate the times when the surface current snapshots in Figures 8.1.1 and 8.1.2 were taken at springs and neaps.

In the Collie River, stratification is stronger, and there was a more marked difference between near-surface and near-bottom currents (Figure 8.1.5). Downstream (south-westward) flows were stronger in the surface layer, with a greater tendency to upstream (north-eastward) flow near the seabed. This is consistent with a strong density-driven estuarine circulation in the lower reaches of the river. Nevertheless, the circulation is strongly modulated by tidal currents, and both surface and bottom currents are similarly influenced by major flood events, for example the flood of late August.

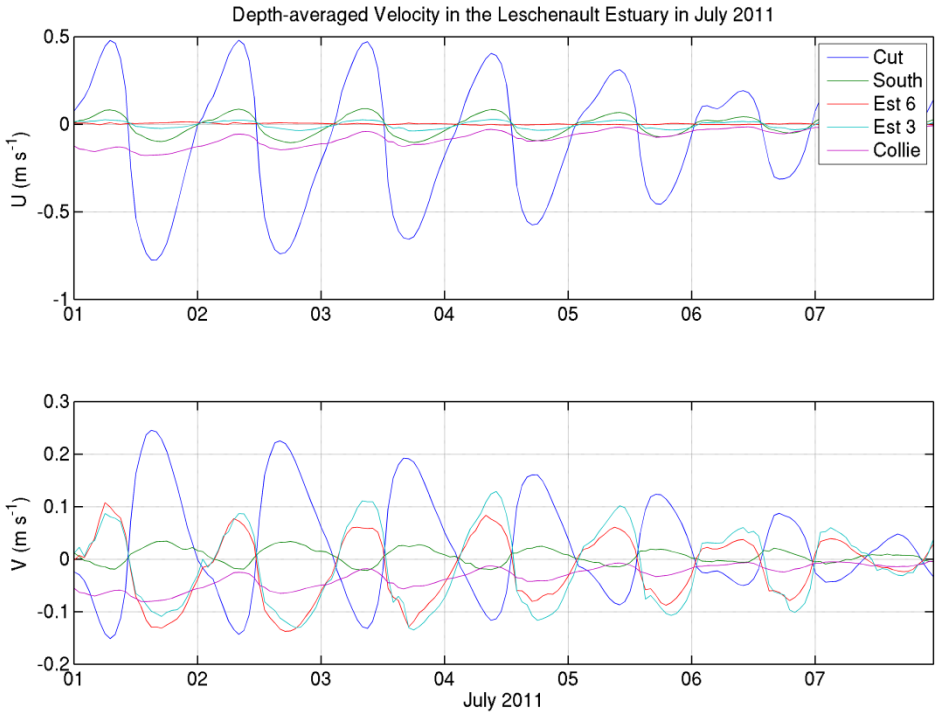

Figure 8.1.4. Depth-averaged velocity components during the first week of July 2011 at five locations in the Leschenault Estuary. U and V refer to east and north components respectively.

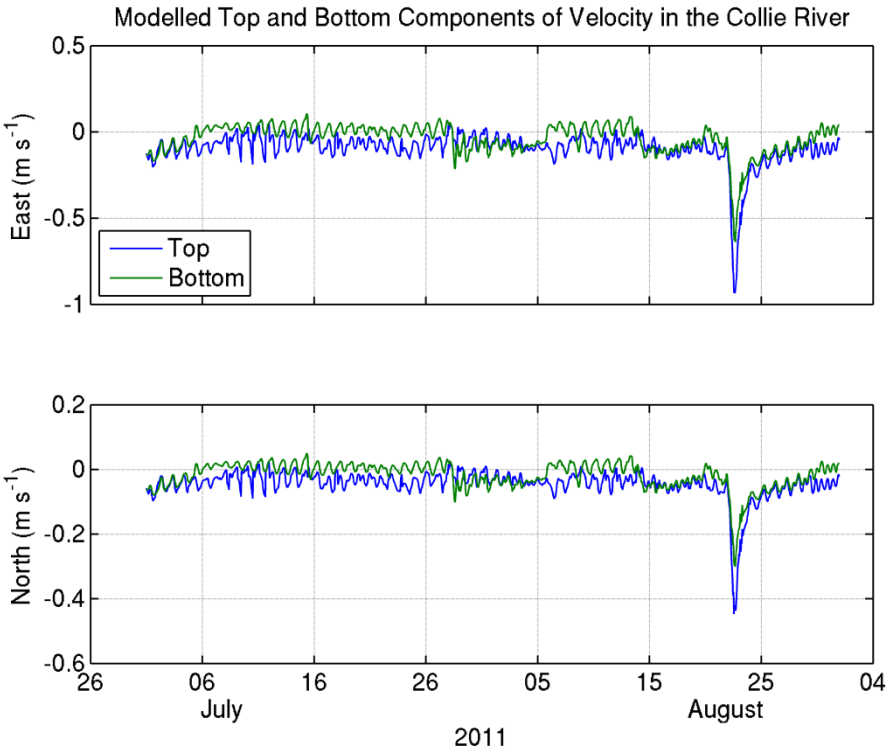

Figure 8.1.5. East and north components of velocity in the Collie River at the near-surface and near-bottom locations of the moored sensors. Positive values are eastward and northward respectively.

8.2 Temperature and Salinity

Each flood tide brings relatively salty coastal water into the estuary. The flood jet entrains ambient estuary water, and the mixture then retreats on the subsequent ebb tide. Similarly, heat is also exchanged between the Leschenault Estuary and the adjacent coastal waters. In Figure 8.2.1, the surface temperature field is shown at different stages of the tide during summer 2012. Two key processes are illustrated: the exchange of water between the estuary and coastal zone via advection through the Cut, and temperature variability of the surface water from atmospheric heating and cooling. At 0900 on 4 January 2012, modelled temperatures in the estuary are typically 20 – 21 °C, about 2 °C cooler than the coastal water due to overnight cooling. By late afternoon, temperatures in the estuary had warmed by about 2 – 2.5 °C to 22 – 23.5 °C, slightly warmer than the coastal temperatures. Daily fluctuations of temperature in the estuary of 2 – 2.5 °C are evident in the temperature data (Figure 7.2.5), so these modelled values are entirely reasonable. The cooler coastal water intrudes into the estuary on the flood tide, spreading north and south, and evident as a patch of cooler water in the estuary. The maximum extent of the patch was reached at high water at 2100 on 4 January. On the subsequent ebb tide, the rapidly cooling estuary water is ejected into the coastal zone, forming a plume of cooler water advected (in this instance) southwards.

The flood/ebb cycle is repeated throughout the year on a daily basis. The contrast between estuary and coastal temperatures is, of course, dependent on season and on the phasing of the tide with daylight hours. Thus in winter, when surface heating may be minimal, the flood tide may inject warmer coastal water into the estuary, and the ebb tide extract cooler estuary water. But the limited extent of the exchange between coast and estuary on each tide is evident from the footprint of cooler water shown in Figure 8.2.1.

Similar maps of surface salinity over a tidal cycle are shown in Figure 8.2.2. Here, the influence of river discharge is illustrated during the dry summer. An example of the effect of high discharge on salinity is shown later. During January 2012, the estuary was largely filled with saltwater. Riverine influences were confined to the northern and southern margins. Strong evaporation during summer increased the salinity in the central estuary to almost 40 psu (Figure 7.2.8, “Estuary 3”). Limited exchange with the coastal ocean, as evidenced in Figure 8.2.1, permitted estuary salinities to become elevated above typical coastal values.

During winter, the influence of fresh river discharge is greater. Figure 8.2.3 illustrates the modelled surface salinity and flows in the southern part of the estuary during July 2011. The intruding saltwater during flood tide has pushed the low-salinity water back toward the river mouths. On the following ebb tide, low-salinity surface water spread throughout the southern basin, almost completely filling it by low water. On the following flood, the low salinity water was again pushed back, and outflow from the Collie River swept northwards into the central estuary.

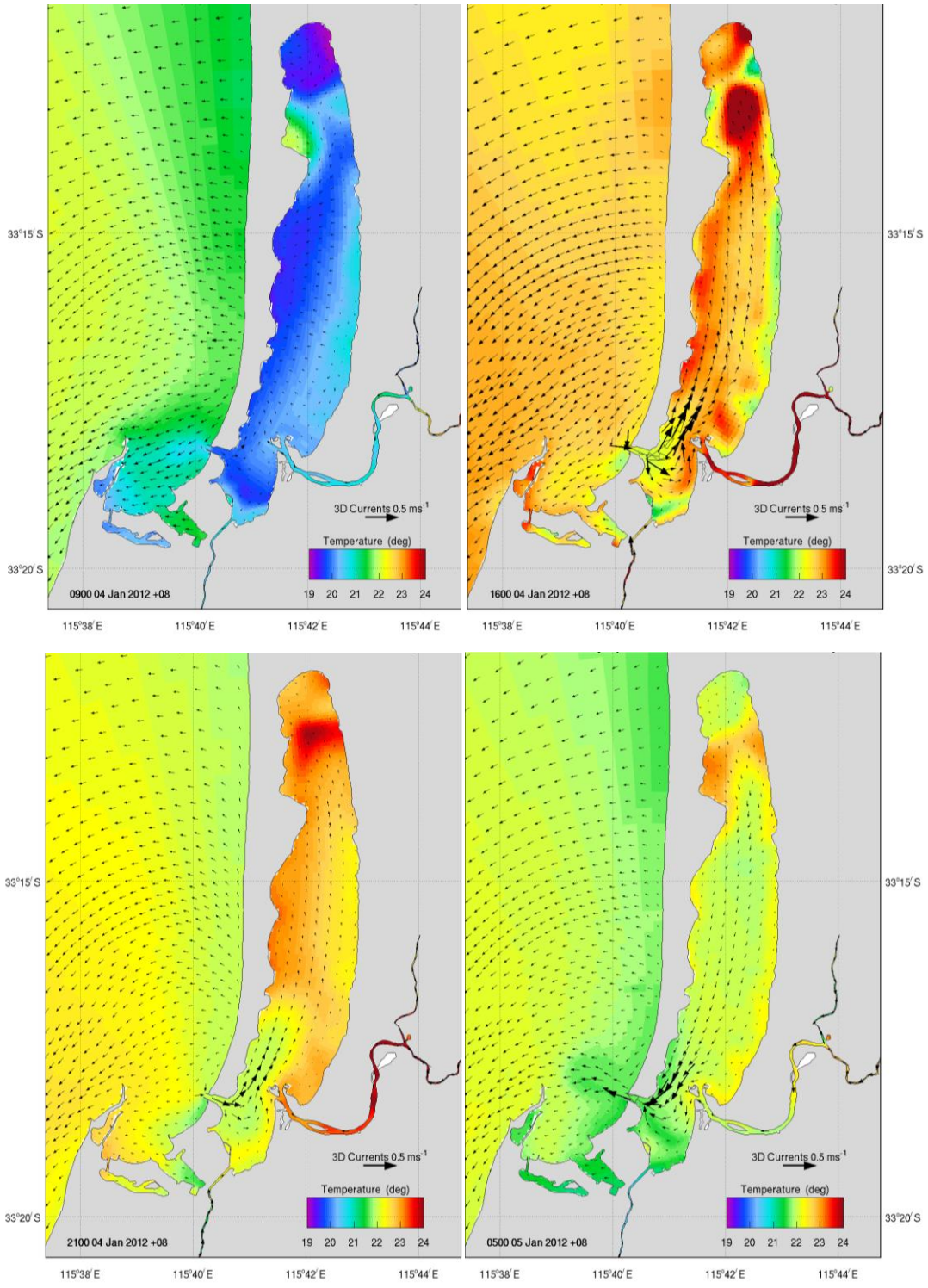

Figure 8.2.1. Fluctuations in the surface temperature field over a tidal cycle during January 2012. The plots show surface temperature and velocity vectors at low water (top left), mid-flood (top right), high water (bottom left) and mid-ebb (bottom right).

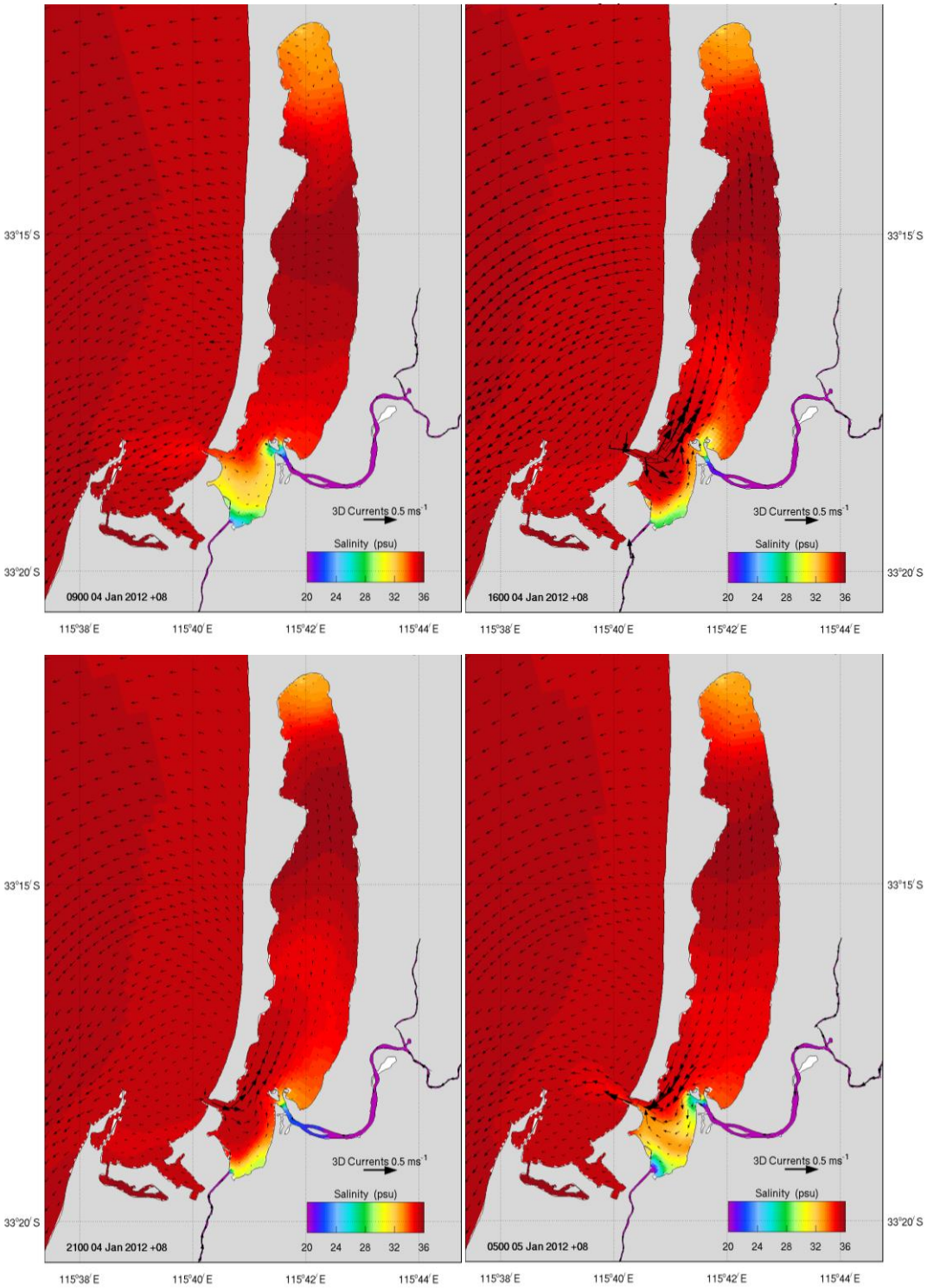

Figure 8.2.2. Fluctuations in the surface salinity field over a tidal cycle during January 2012. The plots show surface salinity and velocity vectors at low water (top left), mid-flood (top right), high water (bottom left) and mid-ebb (bottom right).

The patterns of salinity and temperature fluctuate quite predictably in response to tidal forcing, which has a direct impact on only a small area of the Leschenault Estuary, increased somewhat by horizontal mixing and entrainment of the ambient estuary water. Tidally-induced fluctuations in salinity and temperature distributions are moderated by local heating/cooling and the prevalent river flows. The latter may dominate the water properties in the estuary at times of extreme events, as will be described later.

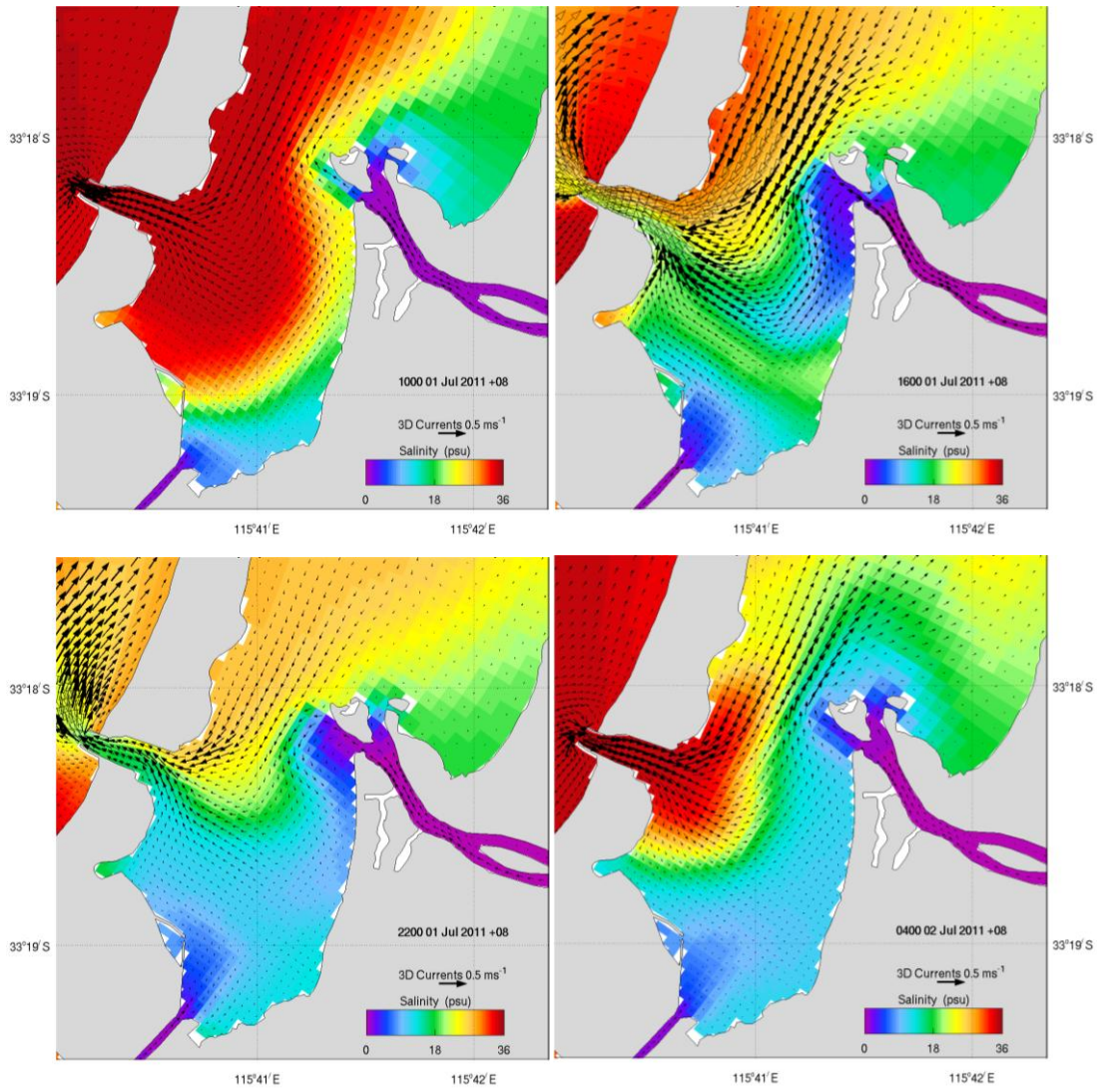

Figure 8.2.3. Fluctuations in the surface salinity field in the southern estuary over a tidal cycle during July 2011. The plots show surface salinity and velocity vectors at high water (top left), mid-ebb (top right), low water(bottom left) and mid-flood (bottom right).

8.3 Seasonal Mean Circulation and Hydrodgraphy

The seasonal-mean circulation in the model domain was determined from the simulations. By averaging the current velocities over long periods, e.g. three months, the tidal circulation is removed and the net residual (non-tidal) circulation revealed. The residual flow fields provide information on the long-term exchange and flushing rates of the estuary. Here, we present the mean summer (01 December 2011 – 29 February 2012) and winter (01 June – 31 August 2011) water properties and circulation fields.

During winter, high river flows and cooler atmospheric conditions led to a typical estuarine circulation (Figure 8.3.1). Surface currents in the estuary were seaward i.e. towards the Cut, with magnitudes in the range 0.5 – 5 cm s^{-1}. The strongest currents occurred around the mouths of the rivers, in particular between the mouth of the Collie River and the Cut. Strong mean currents from the mouth of the Preston River merged with the Collie River plume, enhancing the flow through the Cut. In the northern part of the estuary, a significant mean circulation was driven by the Parkfield Drain discharge; as will be noted later, this discharge plays an important role in flushing the northern part of the estuary. Near the seabed, mean currents throughout most of the estuary were northward during winter, (Figure 8.3.1), typical of partially stratified estuaries, with current speeds of about 1 cm s^{-1}. The exception occurred in the shallow southern portion of the estuary, south of the Collie River mouth, where the mean flow at all depths was seaward. The high river discharge from the Collie and Preston Rivers during winter evidently drove a strong seaward barotropic flow in the southern estuary. Mean sea level in the Leschenault Estuary was a few centimeters higher than the external sea level, particularly off the mouth of the Preston River, which is typical of estuaries with significant freshwater input and restricted exchange with the open sea. Mean currents in the southern basin were about 1 cm s^{-1}.

Mean winter surface temperatures in the estuary ranged from 13.6 °C in the northern estuary to about 16 °C in the Cut (Figure 8.3.2). Outside the estuary, mean coastal water temperatures were about 17 °C. The lowered temperatures in the estuary reflect the input of colder fresh water, and enhanced cooling due to the shallow water depths in the estuary. The limited extent of coastal water influence in the estuary is clearly distinguished by the warmer mean temperatures in the southern estuary around the Cut; the majority of the estuary to the north experiences only weak exchange with the ocean. Likewise, the regions of freshwater influence in the estuary are clearly identified in the map of mean surface salinity (Figure 8.3.2). Mean salinities of about 30 psu in the Cut were slightly diluted to about 29 psu in the central estuary. Towards the mouths of the rivers and drainage channels, mean salinities decreased sharply; thus the entrance and central estuary are dominated by the coastal influence, whereas the northern estuary is controlled by riverine effects. The southern basin is influenced by both.

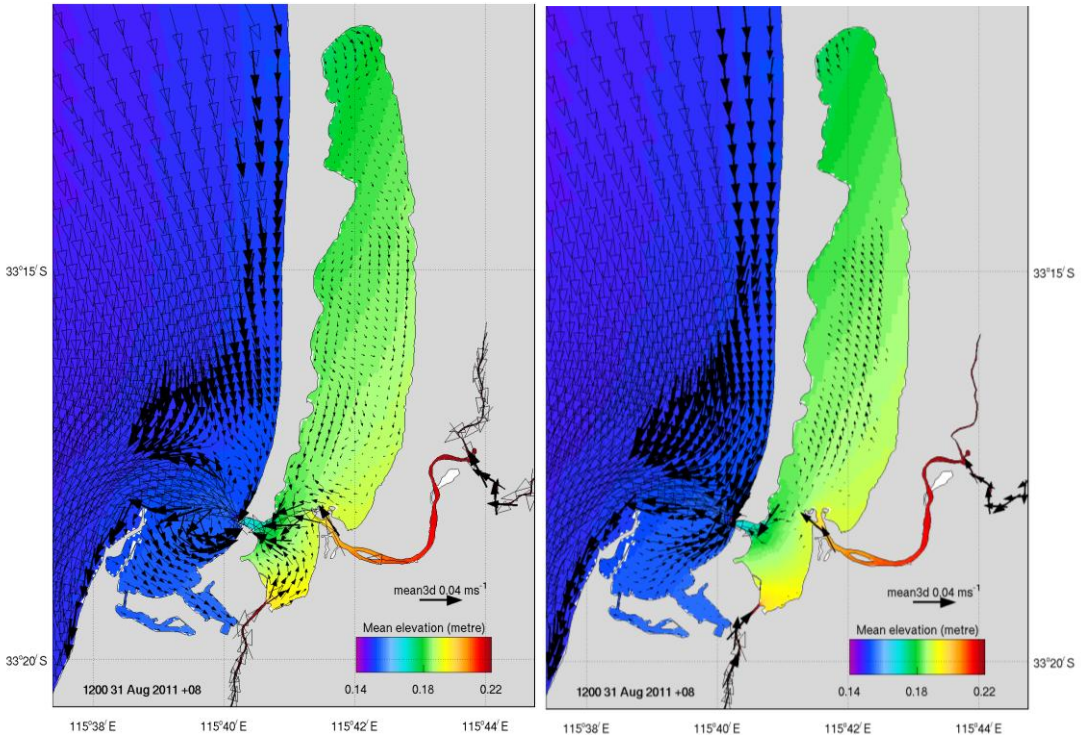

Figure 8.3.1.Seasonal-mean circulation for winter: mean near-surface (left) and near-bed (right) currents averaged over June – August 2011. The near-bed currents are at 1.3 m depth below mean sea level. Open (unfilled) vectors indicate currents greater than 0.04 m s^{-1}. Colouring indicates mean sea surface height (m).

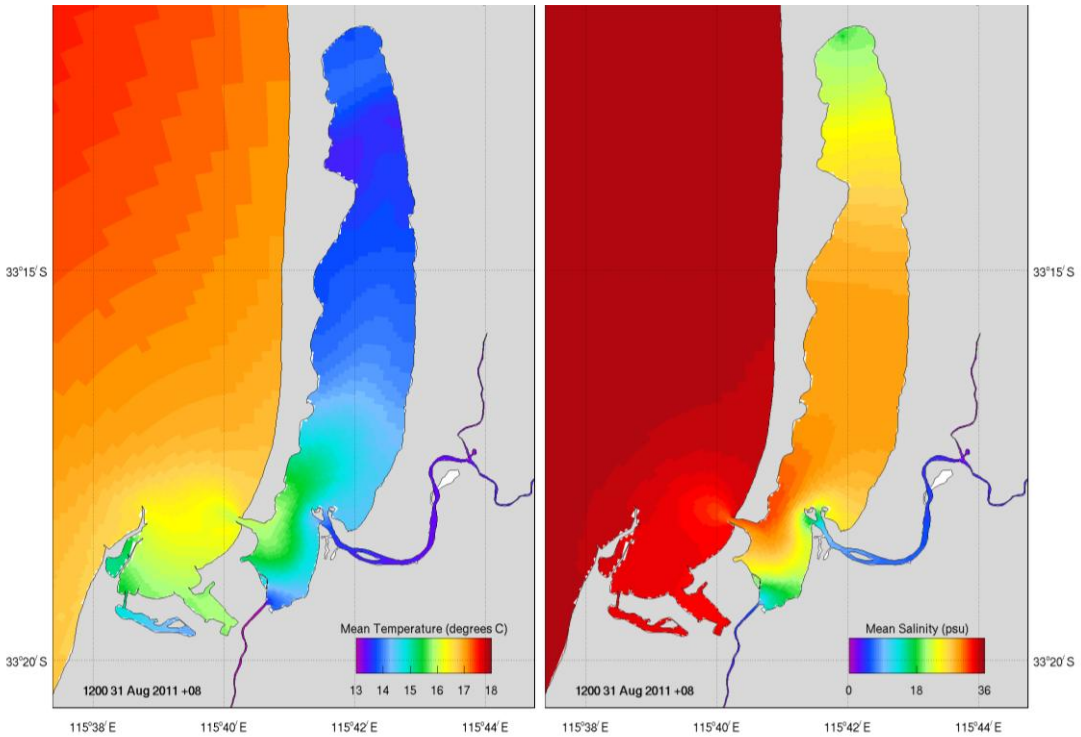

Figure 8.3.2.Seasonal-mean surface temperature (left) and salinity (right) for winter 2011. The model results are averaged from 01 June – 31 August 2011.

In summer, the mean circulation was reversed, with inflowing surface currents and a deeper outflowing layer (Figure 8.3.3), typical of “inverse” estuaries. High evaporation during summer led to high surface salinities in the northern part of the estuary (Figure 8.3.4), which drive the inverse circulation. Mean salinities reached almost 37 psu in the central estuary. Surface gradients towards the river mouths were still apparent, but weaker than in winter, as river flows were reduced. Mean summer surface temperatures reached 24.5 °C in the central estuary, over 1 °C warmer than the adjacent coastal waters, which had surface temperatures of 23 °C. Mean river water temperatures were slightly less than those in the central estuary, leading to cooler waters in the northern and southern regions. Mean sea level remained a few centimeters higher than external mean sea level, even with the low summer river flows, indicative of hydraulic control exerted by the entrance channel.

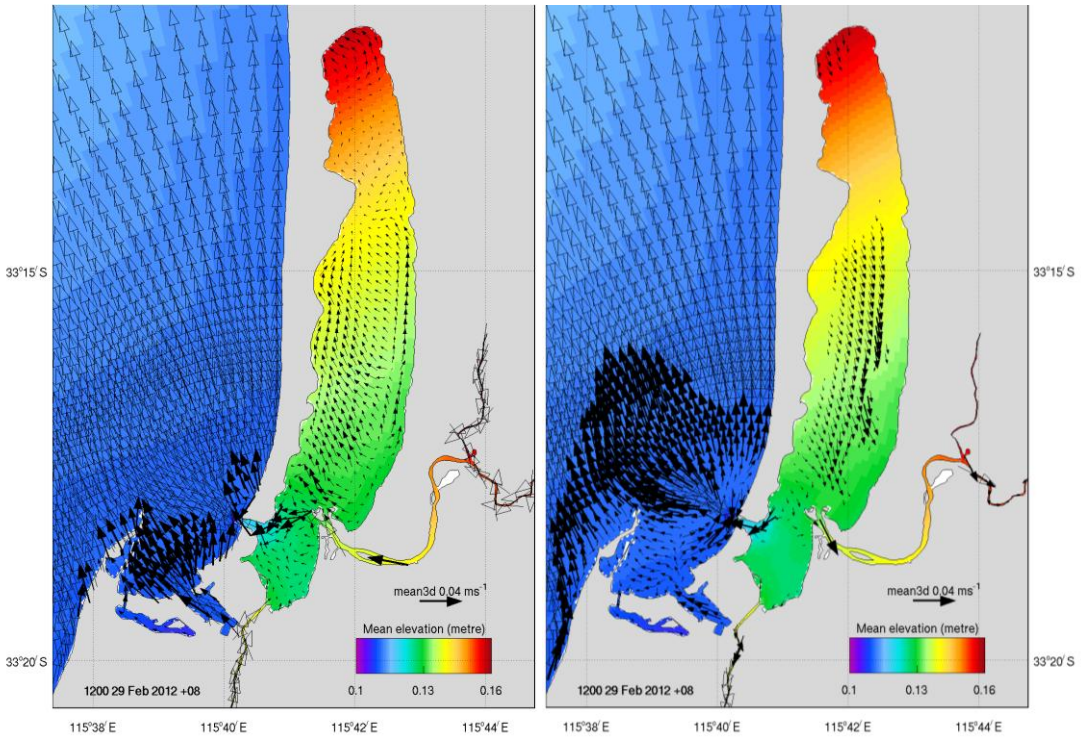

Figure 8.3.3.Seasonal-mean circulation for summer: mean near-surface (left) and near-bed (right) currents averaged over December 2011 – February 2012. The near-bed currents are at 1.3 m depth below mean sea level. Open (unfilled) vectors indicate currents greater than 0.04 m s^{-1}. Colouring indicates mean sea surface height (m).

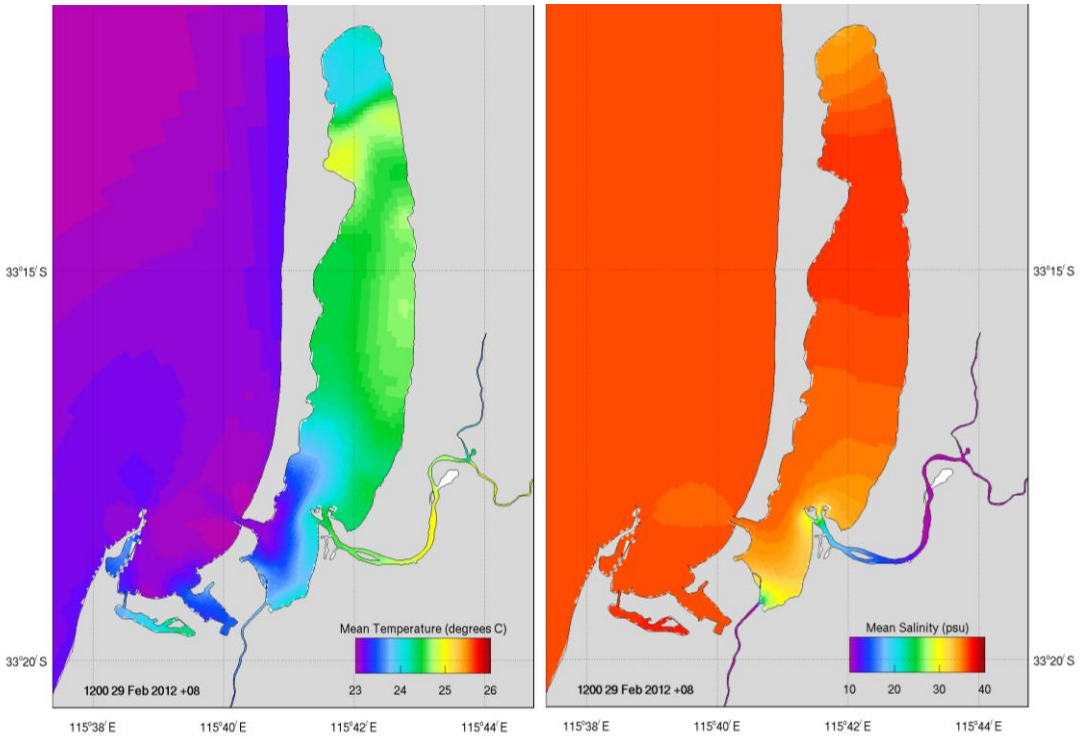

Figure 8.3.4.Seasonal-mean surface temperature (left) and salinity (right) for summer 2011 – 12. The model results are averaged from 01 December 2011 – 29 February 2012.

8.4 High River Flow Events

A feature of the environmental conditions affecting the Leschenault Estuary hydrography and hydrodynamics, particularly during winter, is the incidence of abrupt high flow events in the inflowing rivers in response to heavy rainfall. During the 2011 – 12 study period, a particularly notable event occurred on 22 – 25 August. Daily precipitation peaked at almost 50 mm on 22 August 2011 (Figure 5.5.2), leading to elevated river flows on the following two days (Figure 5.4.1). A sequence of images of model output during this flood event is presented in Figure 8.4.1. Images at 4-hour intervals are shown, beginning at 04:00 22 August and finishing at 08:00 27 August. Each snapshot shows surface salinity overlain by instantaneous velocity vectors. The sequence begins (at 04:00 22 August) near the end of an ebb tide. Twelve hours later (16:00 22 August), at the start of the next ebb tide, the southern estuary began to fill with freshwater as the river discharge rose rapidly. By the end of the ebb tide (04:00 23 August), the southern basin was almost completely filled with freshwater. The plume of water exiting from the Cut was turned northward along the coast by the prevailing tidal flow. Surface currents in the centre of the plume exceeded 0.5 m s^{-1}, and salinities dropped to 10 – 12 psu. At low tide (04:00 23 August), the surface elevation in the estuary was 30 cm higher than the external elevation due to the freshwater input. During the following flood tide, the freshwater plume exiting through the Cut overpowered the flood tide currents, and currents remained seaward through the Cut throughout the flood tide period. The rising tide did cause some blocking of the flow through the Cut, and brackish water from the

southern estuary was diverted northward into the central estuary (12:00 – 16:00 23 August). Meanwhile, the now predominantly southward tidal currents outside the estuary re-directed the brackish plume to the south of Bunbury, and filled Koombana Bay with low-salinity water (20:00 23 August). The buoyant plume along the coast again featured current speeds in excess of 0.5 m s^{-1}, and the southern Leschenault Estuary remained full of fresh water.

Over the following four days, this sequence repeated itself, with buoyant plumes emerging from the estuary and being swept northward and southward by the prevailing tidal currents outside the estuary. As the river flow decreased, flood tide currents slowly resumed through the Cut on the rising tide. The loss of freshwater on each ebb tide, and mixing with the incoming salt water, gradually eroded the pool of freshwater in the southern estuary. Nevertheless, the southern estuary remained brackish at the end of the sequence shown. During the period shown, the northern estuary was flushed by discharge from the Parkfield Drain, while the salinity in the central estuary was gradually lowered through mixing with the northern and southern regions.

The sequence shown here illustrates how high river flows influence circulation and water properties in the estuary and the adjacent coastal zone. The southern basin of the estuary was rapidly and completely flushed by the high river flows, whereas the central and northern estuaries were more moderately affected.

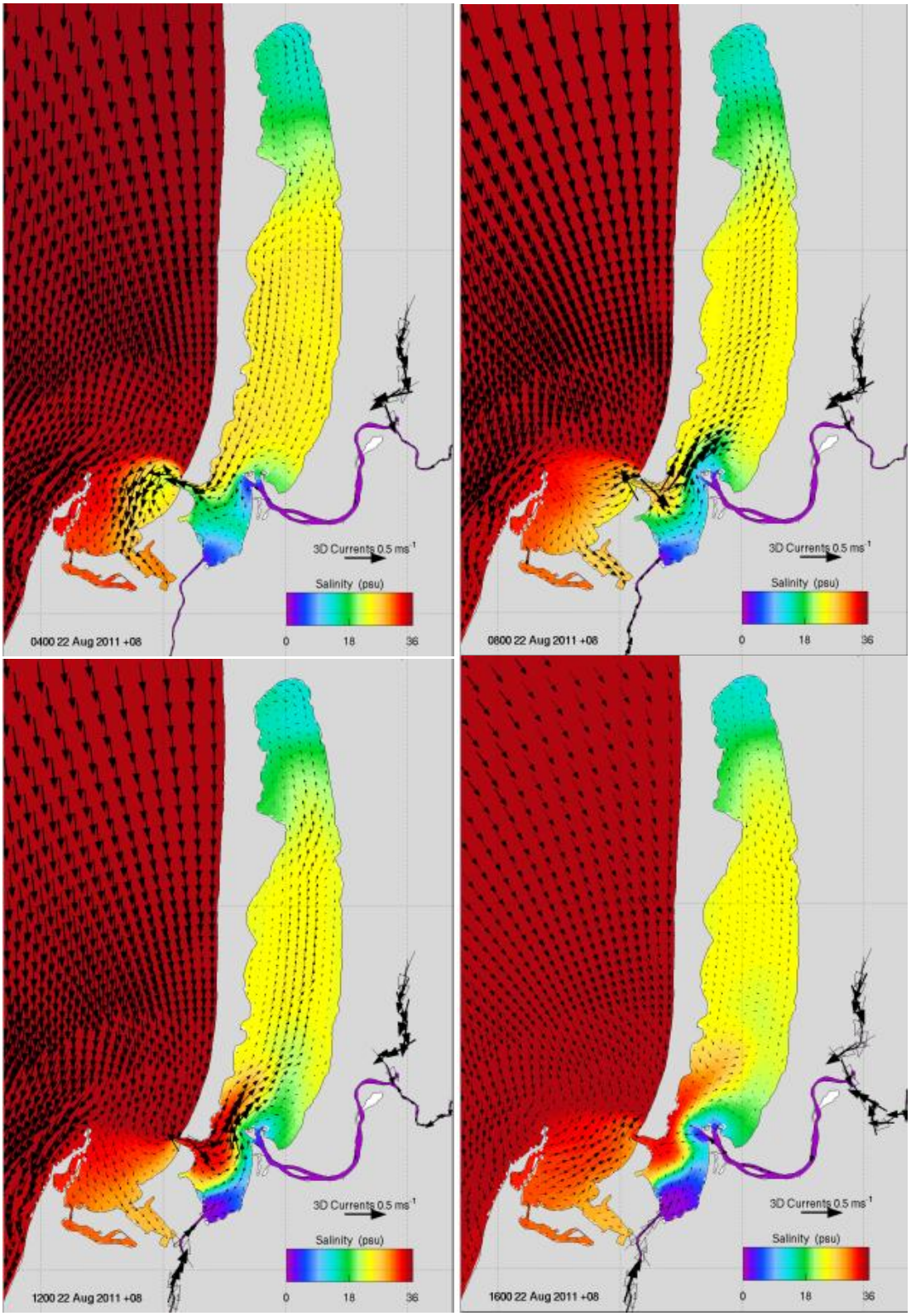

Figure 8.4.1. Near-surface salinity and velocity vectors during the flood event of August 2011. The images are snapshots every 4 hours, starting (top left) at 04:00 22 August 2011, finishing (bottom right) at 16:00 22 August 2011. Open vectors indicate current speed greater than 0.5 m s^{-1}. The salinity scale is from 0 (purple) to 36 (red).

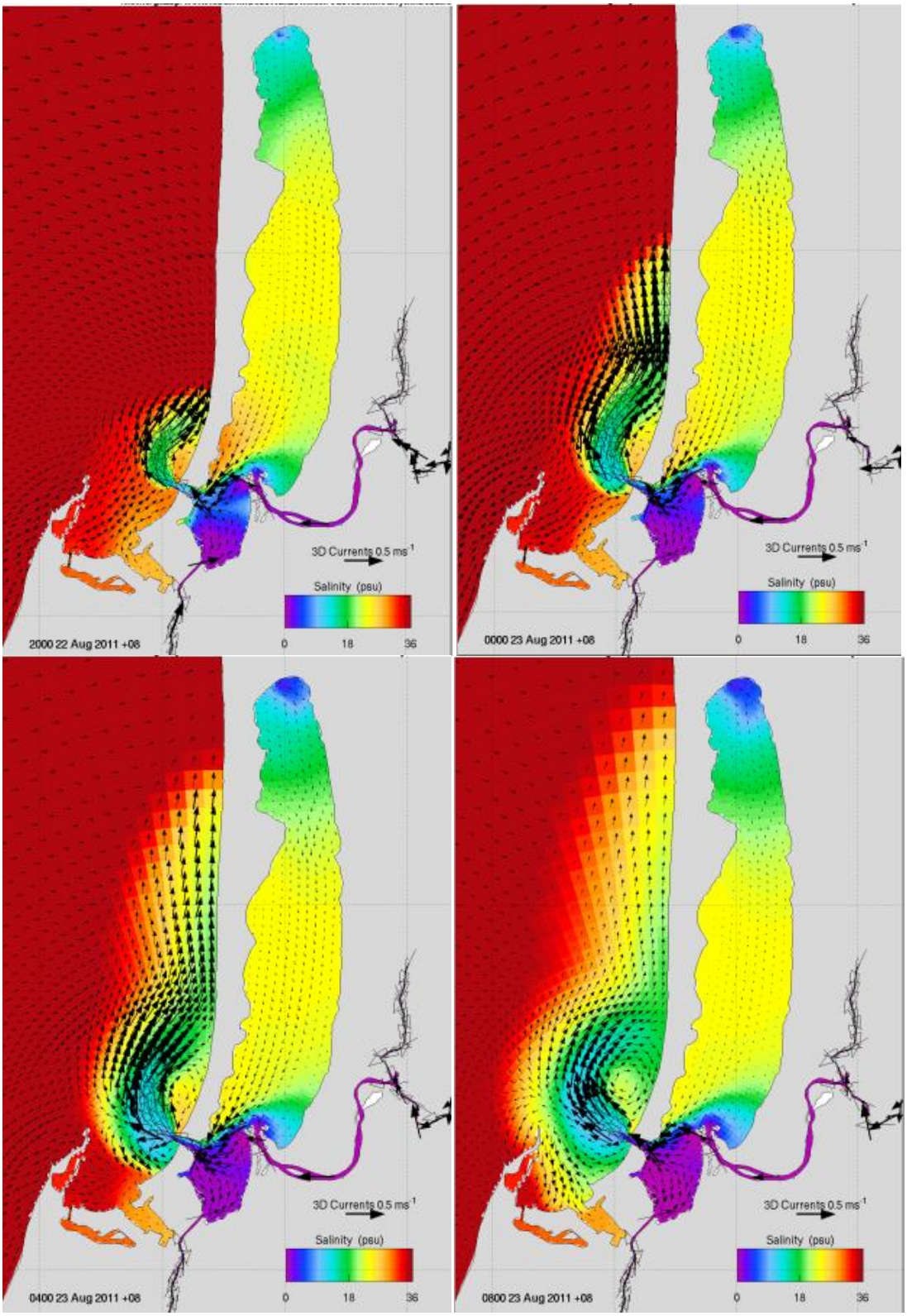

Figure 8.4.1 (cont'd). Near-surface salinity and velocity vectors during the flood event of August 2011. The images are snapshots every 4 hours, starting (top left) at 20:00 22 August 2011, finishing (bottom right) at 08:00 23 August 2011. Open vectors indicate current speed greater than 0.5 m s^{-1}. The salinity scale is from 0 (purple) to 36 (red).

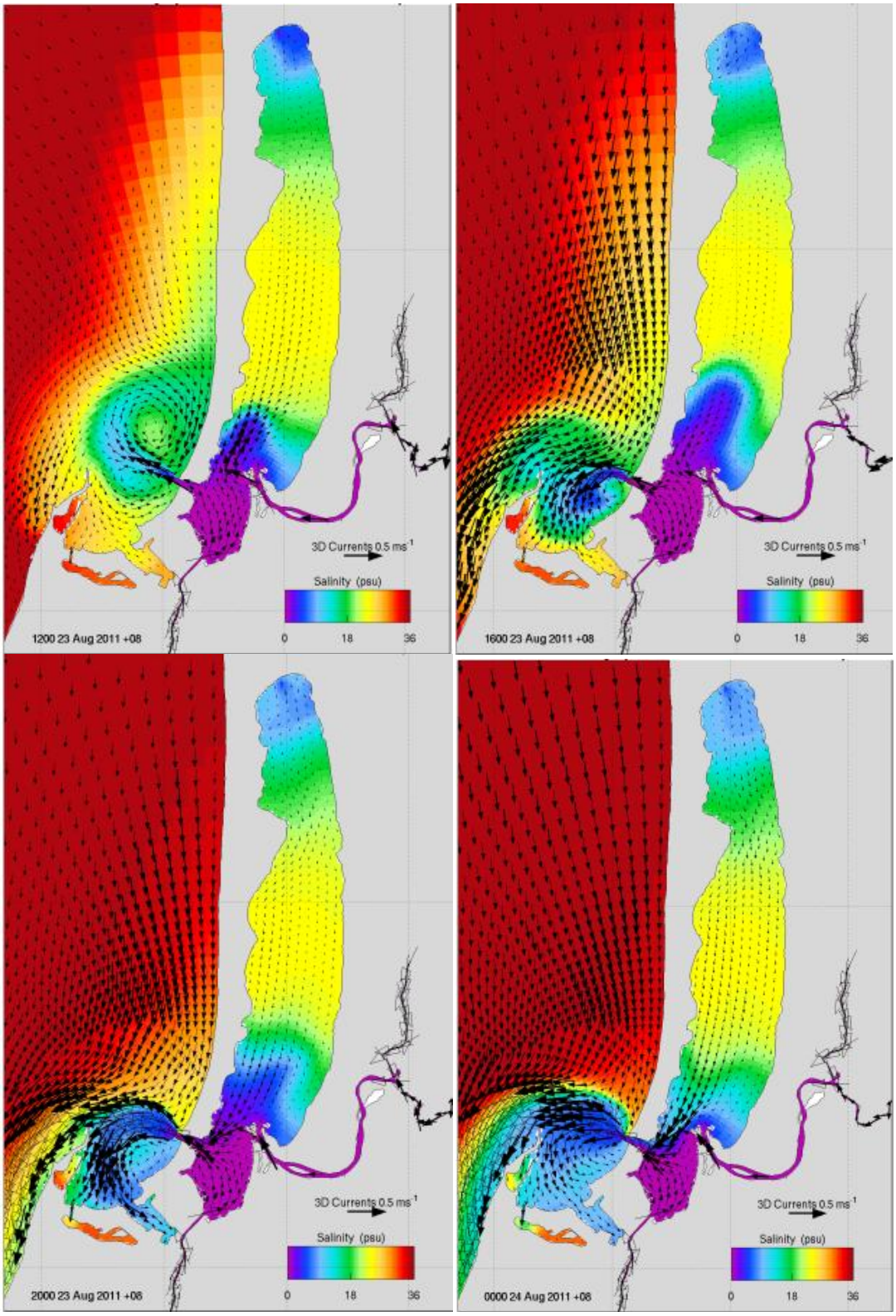

Figure 8.4.1 (cont'd). Near-surface salinity and velocity vectors during the flood event of August 2011. The images are snapshots every 4 hours, starting (top left) at 12:00 23 August 2011, finishing (bottom right) at 00:00 24 August 2011. Open vectors indicate current speed greater than 0.5 m s^{-1}. The salinity scale is from 0 (purple) to 36 (red).

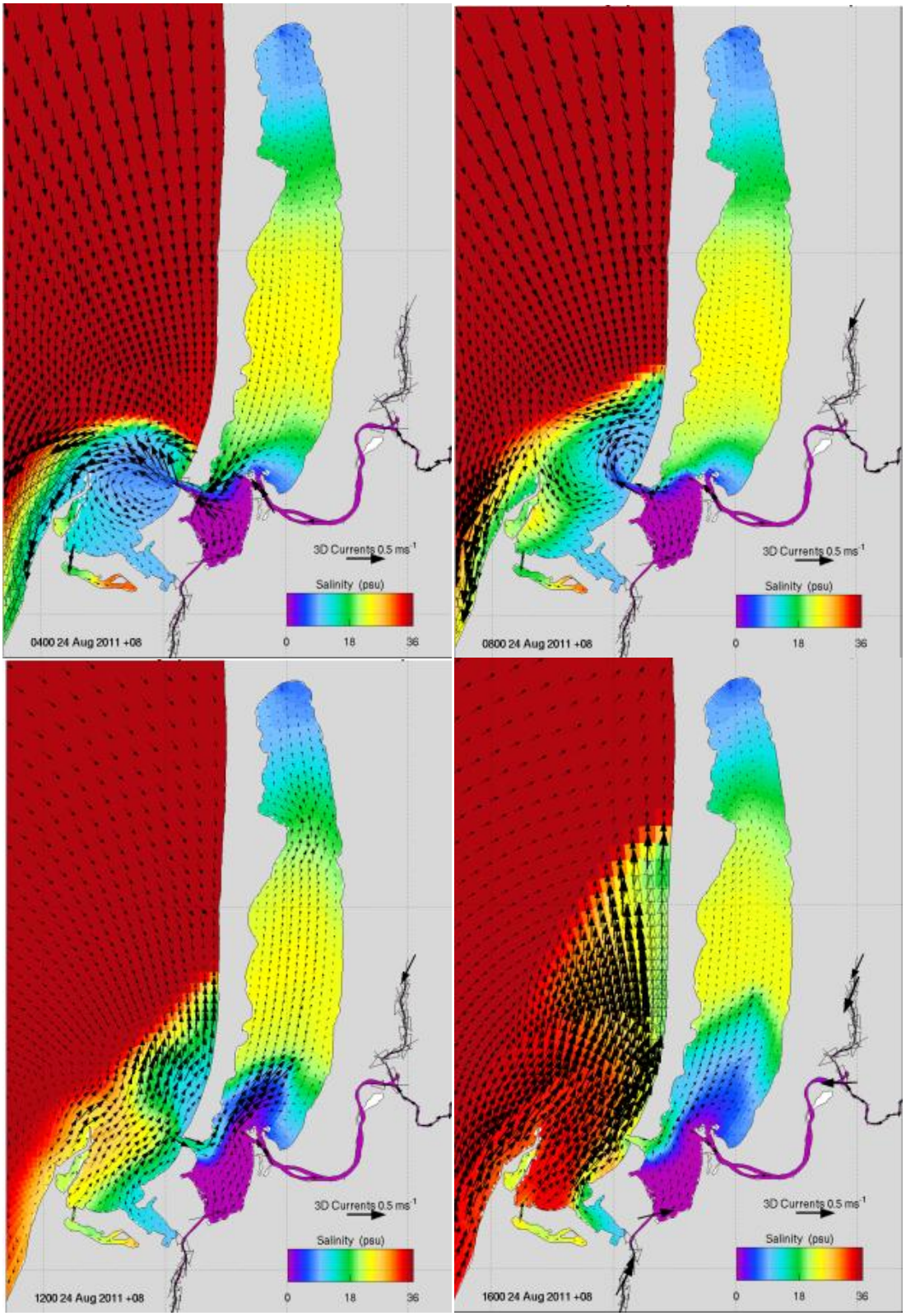

Figure 8.4.1 (cont'd). Near-surface salinity and velocity vectors during the flood event of August 2011. The images are snapshots every 4 hours, starting (top left) at 04:00 24 August 2011, finishing (bottom right) at 16:00 24 August 2011. Open vectors indicate current speed greater than 0.5 m s^{-1}. The salinity scale is from 0 (purple) to 36 (red).

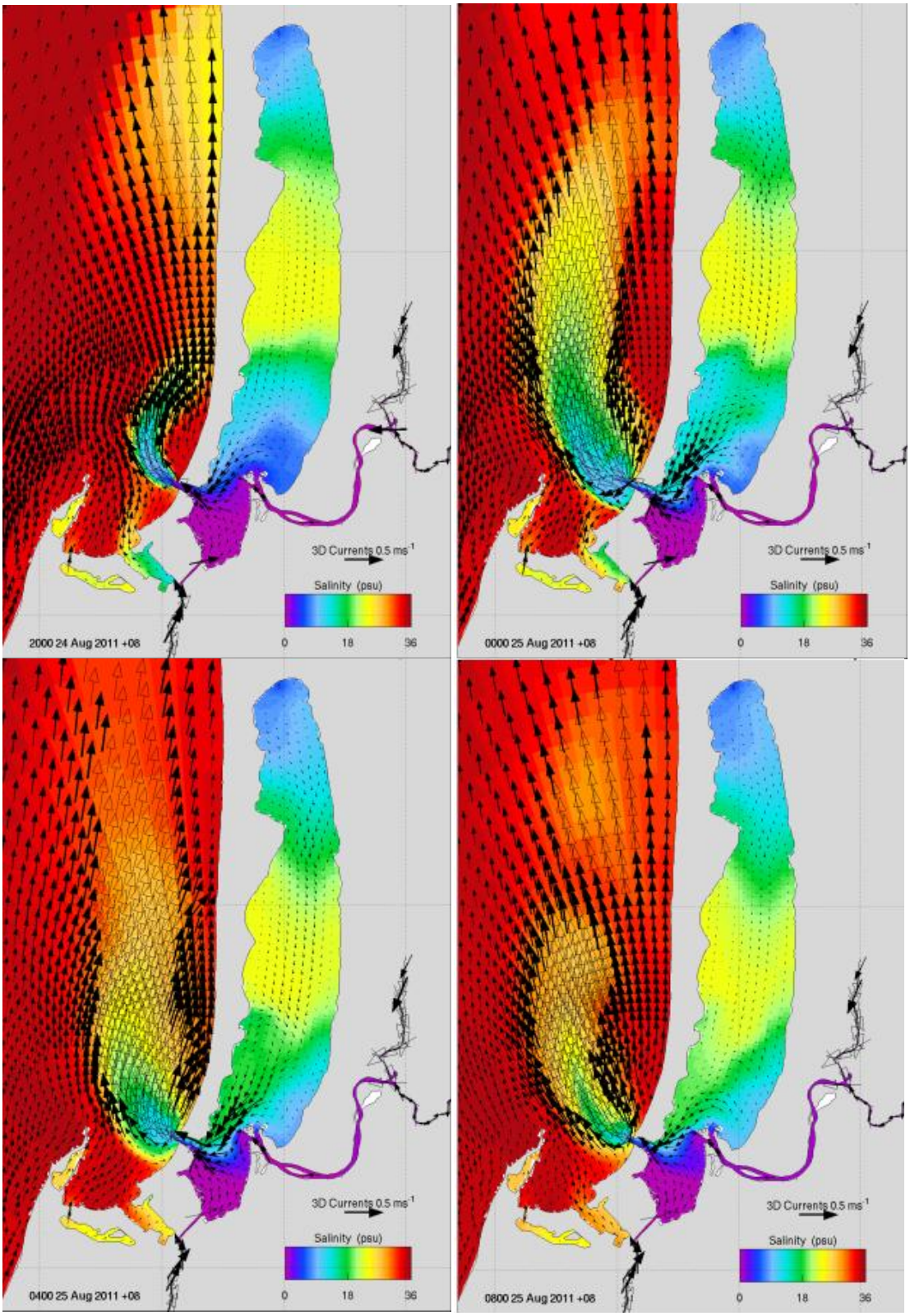

Figure 8.4.1 (cont'd). Near-surface salinity and velocity vectors during the flood event of August 2011. The images are snapshots every 4 hours, starting (top left) at 20:00 24 August 2011, finishing (bottom right) at 08:00 25 August 2011. Open vectors indicate current speed greater than 0.5 m s^{-1}. The salinity scale is from 0 (purple) to 36 (red).

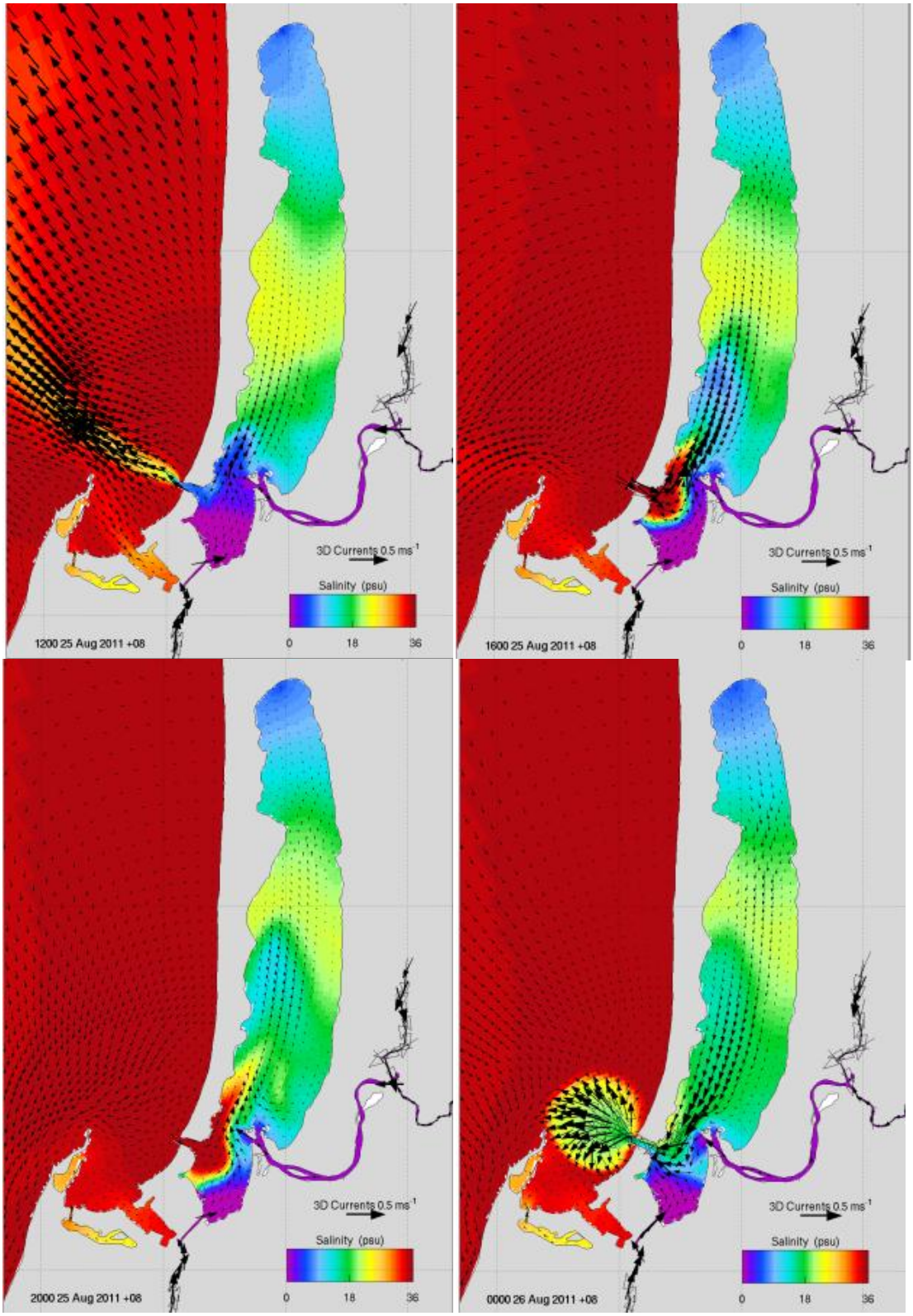

Figure 8.4.1 (cont'd). Near-surface salinity and velocity vectors during the flood event of August 2011. The images are snapshots every 4 hours, starting (top left) at 12:00 25 August 2011, finishing (bottom right) at 00:00 26 August 2011. Open vectors indicate current speed greater than 0.5 m s^{-1}. The salinity scale is from 0 (purple) to 36 (red).

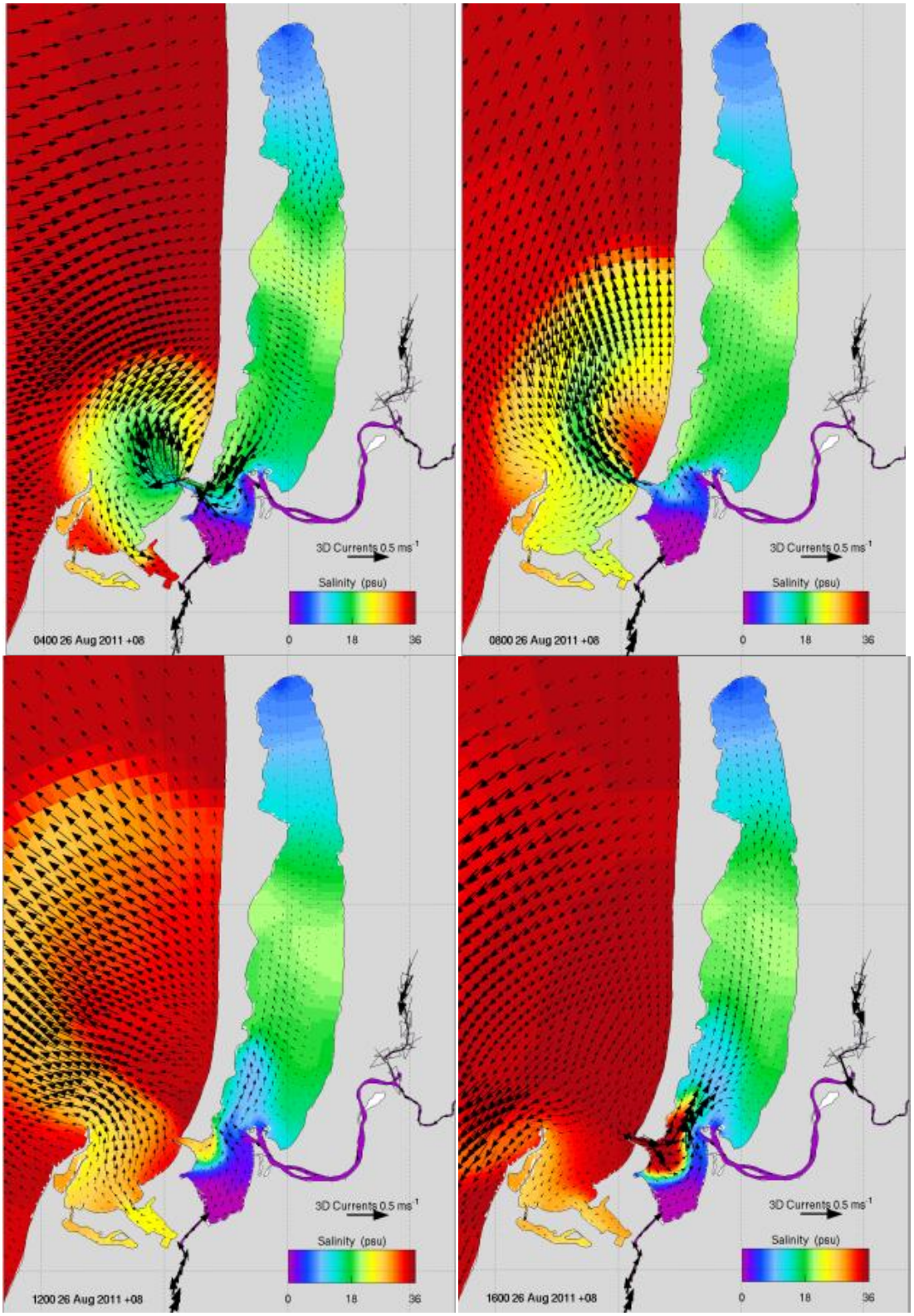

Figure 8.4.1 (cont'd). Near-surface salinity and velocity vectors during the flood event of August 2011. The images are snapshots every 4 hours, starting (top left) at 04:00 26 August 2011, finishing (bottom right) at 16:00 26 August 2011. Open vectors indicate current speed greater than 0.5 m s^{-1}. The salinity scale is from 0 (purple) to 36 (red).

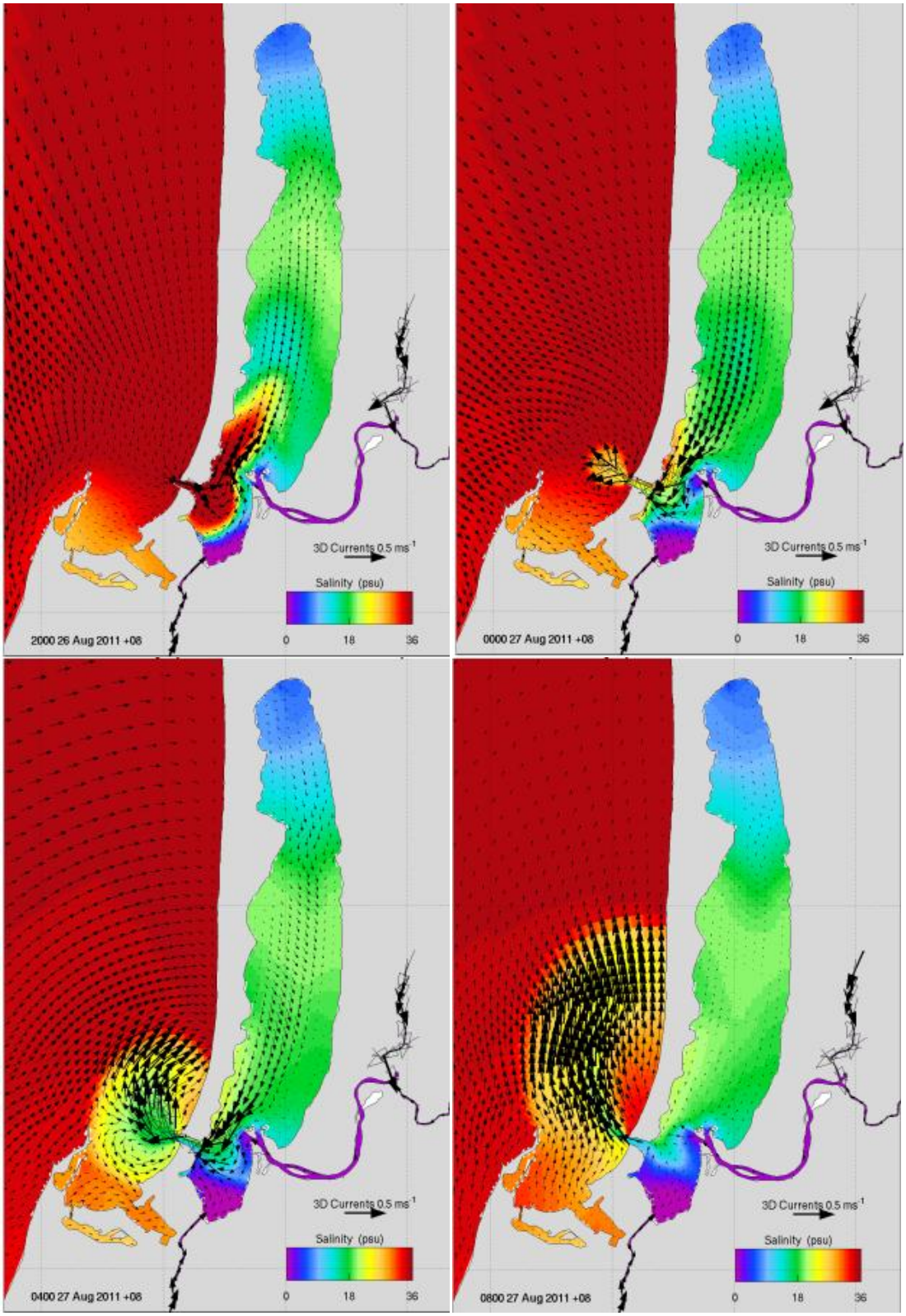

Figure 8.4.1 (cont'd). Near-surface salinity and velocity vectors during the flood event of August 2011. The images are snapshots every 4 hours, starting (top left) at 20:00 26 August 2011, finishing (bottom right) at 08:00 27 August 2011. Open vectors indicate current speed greater than 0.5 m s^{-1}. The salinity scale is from 0 (purple) to 36 (red).

8.5 Flushing Times

The flushing time of the main estuary basin was estimated from passive tracer simulations. Simulations were performed for each season, to quantify the difference in flushing rates under different atmospheric and oceanic forcing conditions. For each simulation, a numerical tracer distribution was initialised at the start of the season, and allowed to advect and diffuse with the prevailing current field. Tracer concentrations were initialised at 1 mg L^{-1} throughout the estuary (Figure 8.5.1) on 1 April 2011, 1 June 2011, 1 September 2011 and 1 December 2011 to simulate autumn, winter, spring and summer flushing respectively. (Note that the autumn simulation only lasted 60 days, from 1 April to 1 June, whereas the other seasonal simulations lasted 90 days). Everywhere else in the model domain (lower Collie, Brunswick and Preston Rivers, and the ocean), the tracer concentration was zero. By tracking the total mass of tracer remaining in the estuary over time, the flushing time of the estuary can be derived. The flushing time here is defined as the time, T_F, required for the tracer mass, M, in the estuary to fall to a factor e^{-1} (approximately 37%) of the initial mass M_0. The calculation of T_F assumes an exponential decrease in tracer mass, i.e.

$$\frac{M}{M_0} = e^{-t/T_F}$$

where t is time.

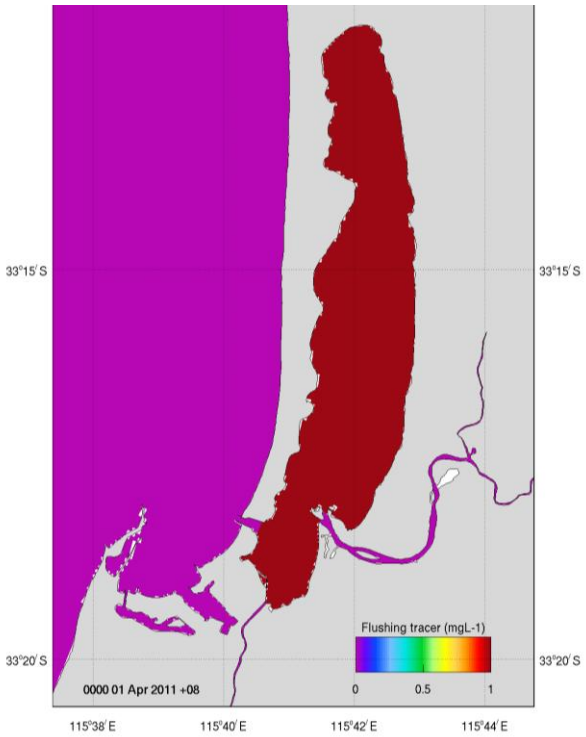

Figure 8.5.1. Initial tracer concentrations for the flushing time simulations. Concentrations were set to 1 mg L^{-1} (red) within the Leschenault Estuary and zero (purple) elsewhere.

The mass of tracer remaining in the estuary following each seasonal release is calculated as a proportion of the initial mass (Figure 8.5.2). Concentrations decreased approximately exponentially. Flushing of the estuary was quickest in spring (shortest flushing time) and slowest in autumn (longest flushing time). Nominal flushing times were 32, 19, 9 and 24 days for autumn, winter, spring and summer respectively.

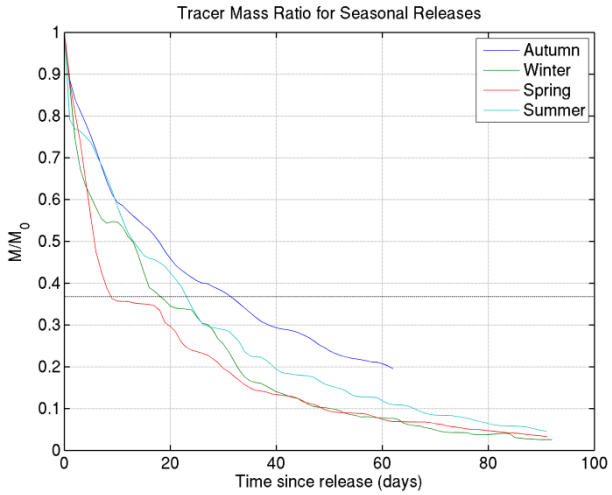

Figure 8.5.2. Time series of the relative tracer mass (M/M_0) for the four seasonal simulations of flushing. The horizontal dashed line marks the value of $M/M_0 = e^{-1} = 0.37$, from which the flushing time is derived.

It should be noted that flushing times are strongly dependent on conditions in the estuary at the time of release, particularly during the few days immediately following release of the tracer when concentrations fall most rapidly. For example, the release on 1 September 2011 (spring) followed soon after the strong river flood event in late August, and the estuary water was still very brackish (Figure 8.5.3a) leading to enhanced exchange with the ocean and export of estuary water. The spring tracer concentrations after 9 days (i.e. when $M/M_0 = e^{-1}$) show strongly variable concentrations along the estuary (Figure 8.5.3b). Near the southern river mouths, concentrations were low, but there remained a patch of high tracer concentration in the centre of the estuary. (Note also the plume of tracer exported into Geographe Bay). It is clear that at this time, exchange was relatively slow in the central and northern estuary. In contrast, tracer concentrations after 32 days of the autumn release (again, when $M/M_0 = e^{-1}$) varied more uniformly along the estuary, with lowest values at the southern end and highest values at the northern end (Figure 8.5.4b). Salinity values in the estuary were much higher (Figure 8.5.4a), as river flows during autumn were low. With low freshwater flows from the Parkfield Drain, flushing of the northern half of the estuary was relatively slow. After 60 days of the autumn release, 20% of the tracer mass remained in the estuary (Figure 8.5.2) and concentrations at the northern end were still 50% of the initial values (Figure 8.5.5).

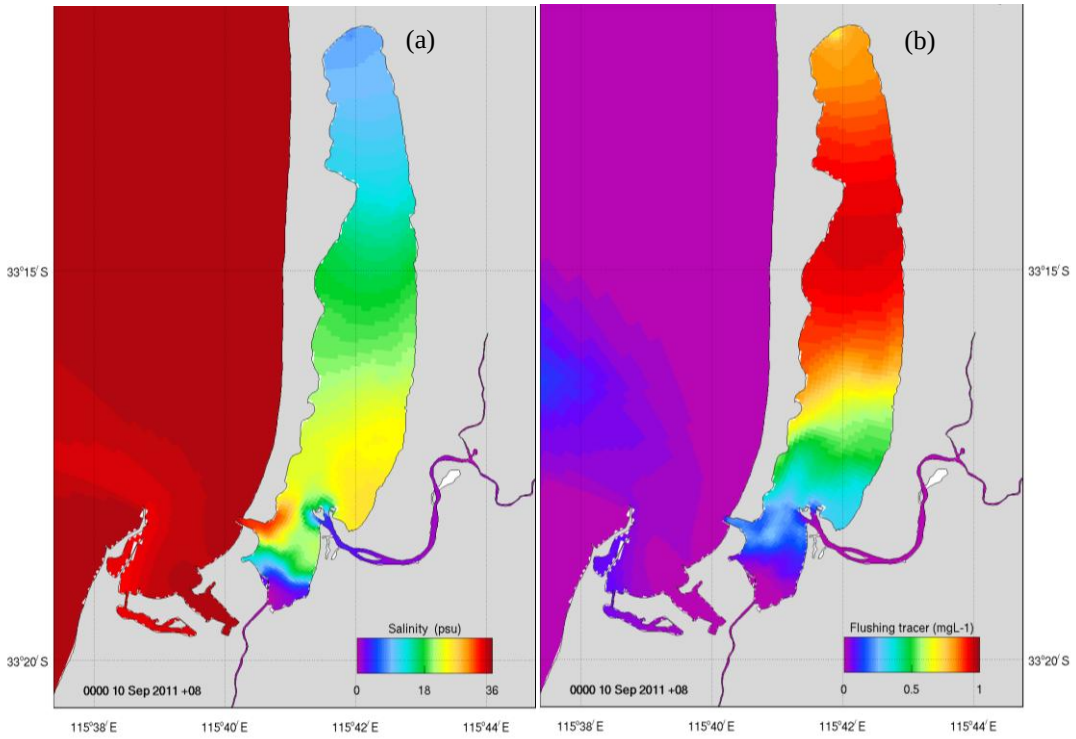

Figure 8.5.3. (a) Modelled surface salinity on 10 September 2011, (9 days after release) of the spring flushing tracer release. (b) Tracer concentrations on 10 September 2011 (9 days after release).

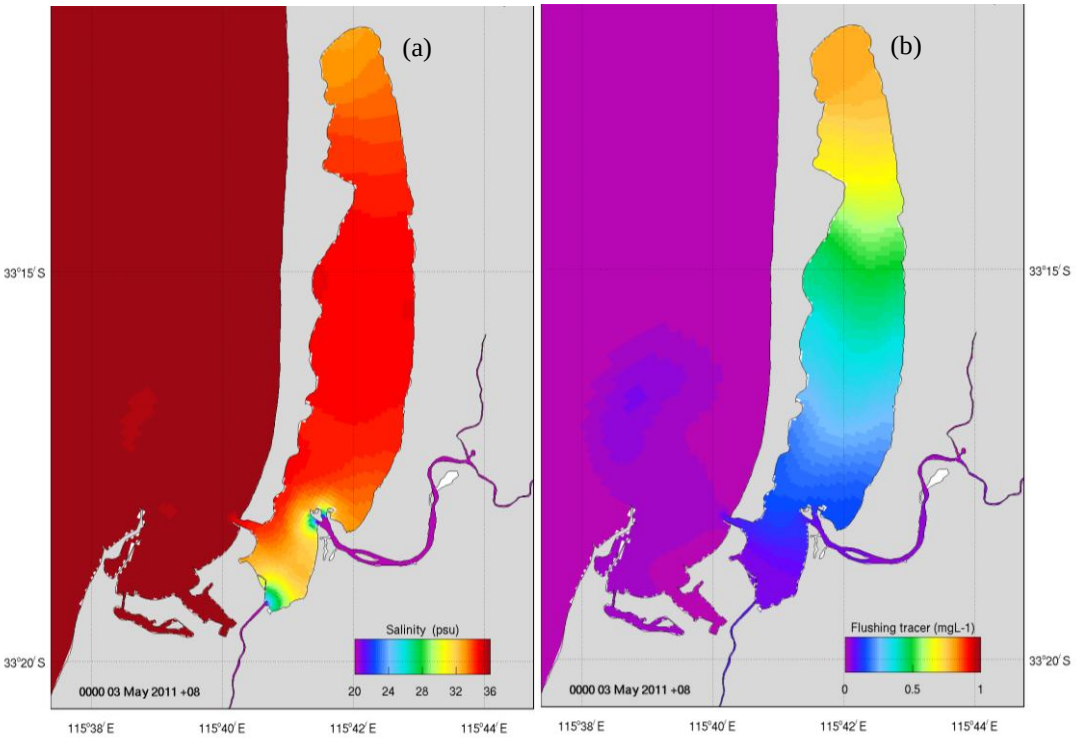

Figure 8.5.4. (a) Modelled surface salinity on 03 May 2011, (32 days after release) of the autumn flushing tracer release. (b) Tracer concentrations on 03 May 2011 (32 days after release).

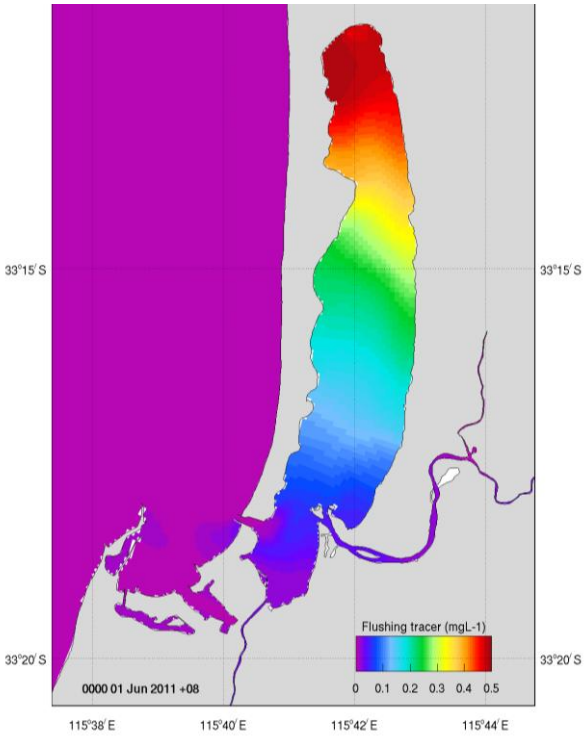

Figure 8.5.5. Modelled tracer concentrations on 01 June 2011, 60 days after release of the autumn flushing tracer simulation.

The results here illustrate the temporal variability in the flushing of the estuary, and also different flushing behaviours of the northern, central and southern basins.

8.6 Mixing Zones

In addition to the flushing time calculations using passive tracers described above, passive tracers were also released continuously from seven discrete sources (Figure 8.6.1) throughout the year-long simulation (April 2011 – April 2012). The source rate at each location was nominally 1 g s^{-1}, giving concentrations in units of mg L^{-1}, and the tracer was discharged at a depth of 0.5 m at each location. The subsequent advection and diffusion of the tracer from its source provides information on mixing zones and the area of influence of each source. The distributions of tracer at any given moment in time are not particularly informative; instead, a statistical analysis of the tracer distributions throughout the whole year-long simulation is presented.

Surface tracer concentrations for each source were separately output at one-hour intervals throughout the year, and post-processed to compute the 5^{th}, 50^{th} (median) and 95^{th} percentile concentration distributions. Only surface percentile distributions were calculated, but tracer concentrations did not vary significantly over the shallow depths of the Leschenault Estuary. The x^{th} percentile value at each location in the estuary means that the tracer concentration at that location

was less than that value for x% of the time. Thus 95th percentile values are higher than 5th percentile values. The results are presented in Figures 8.6.2 – 8.6.8. Note that the colour scales are different for most plots, to provide the best detail for individual plots.

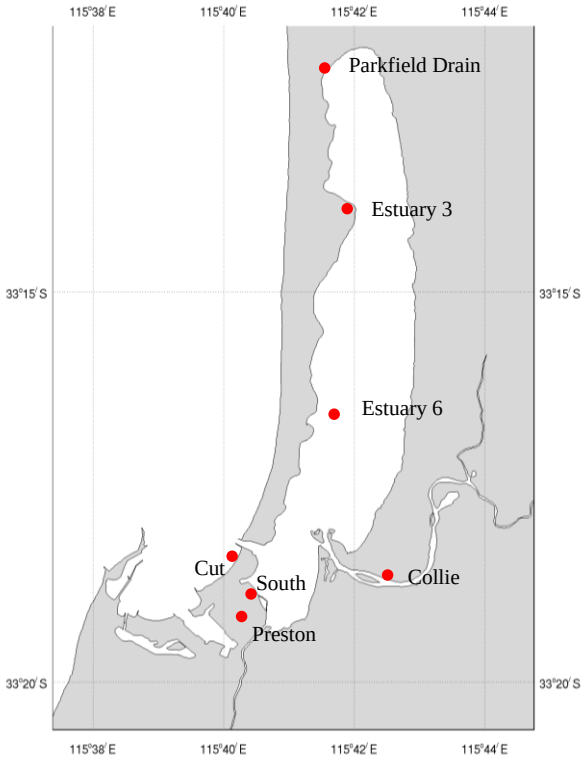

Figure 8.6.1. Locations of the continuous tracer releases.

The distributions illustrated above confirm that the Leschenault Estuary can be considered to consist of three distinct sub-areas. The northern part of the estuary, between the mouth of the Parkfield Drain and the Est 3 mooring, was predominantly influenced by the discharge from the Drain, with only gradual exchange with the central basin of the estuary to the south. That central basin, extending south from Est 3 to approximately a line orientated west from the Collie River mouth, shared little exchange of water with the southern basin. Water properties in the central basin were predominantly influenced by flows from the Cut and the Collie River. The southern basin was dominated by outflow from the Preston River, and exhibited minimal exchange with the central basin; water was exported from the southern basin directly through the Cut.

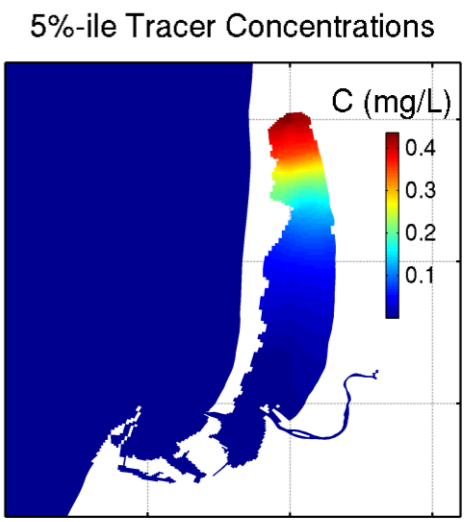

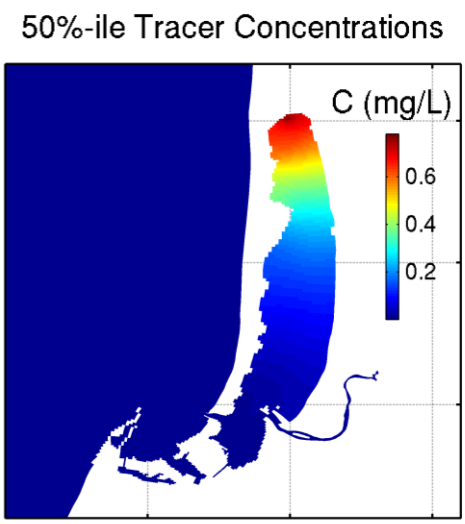

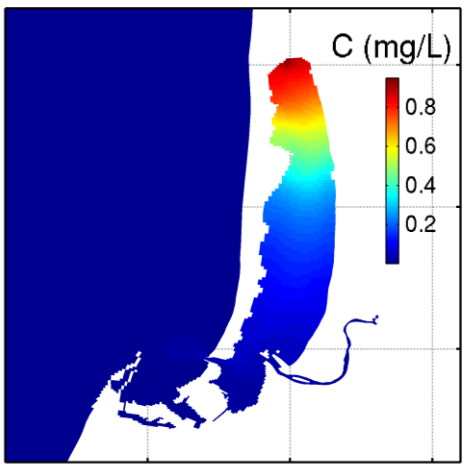

Figure 8.6.2. 5th (top), 50th (middle) and 95th (bottom) percentile distributions for a tracer release at the mouth of the Parkfield Drain.

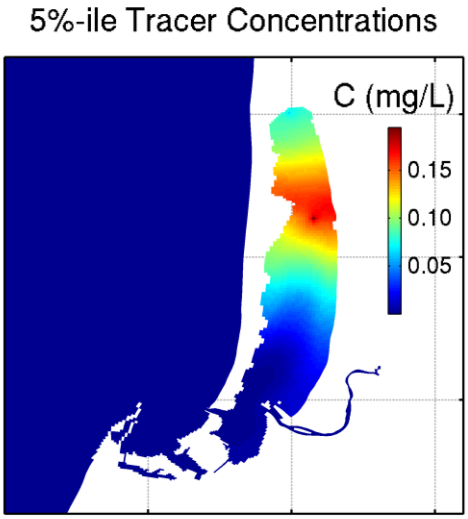

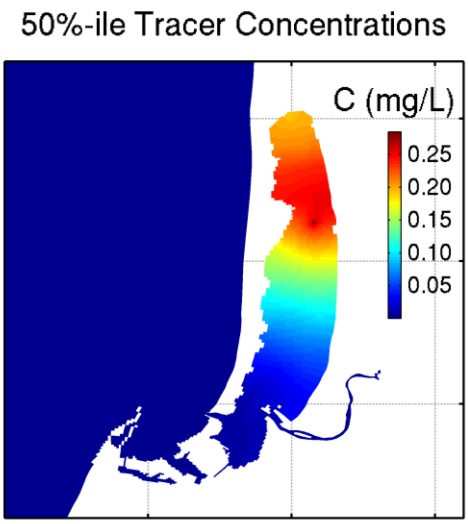

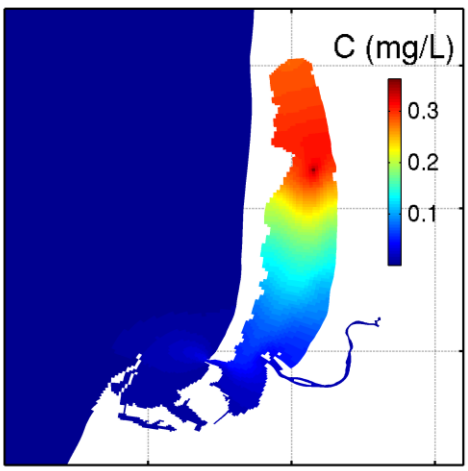

Figure 8.6.3. 5th (top), 50th (middle) and 95th (bottom) percentile distributions for a tracer release at the mooring location Estuary 3.

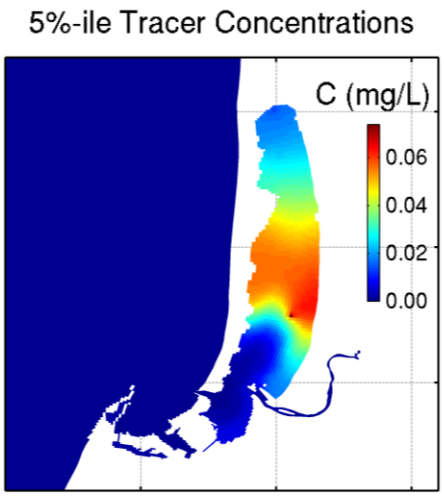

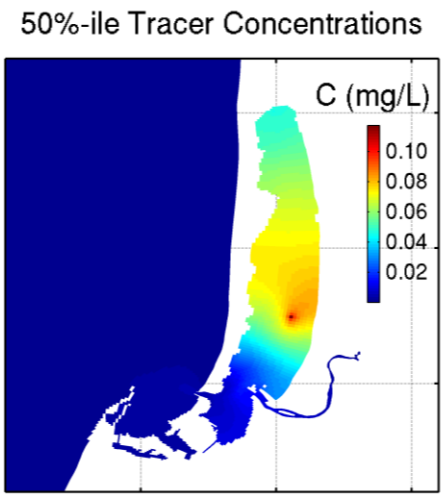

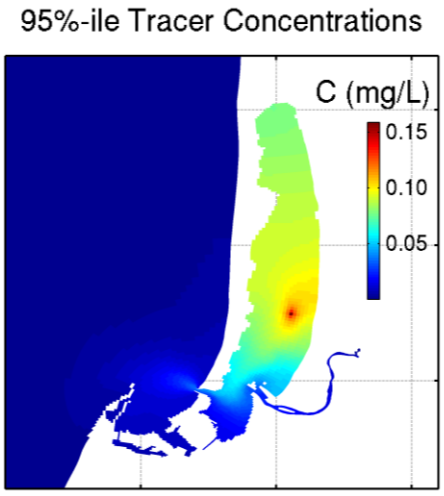

Figure 8.6.4. 5th (top), 50th (middle) and 95th (bottom) percentile distributions for a tracer release at the mooring location Estuary 6.

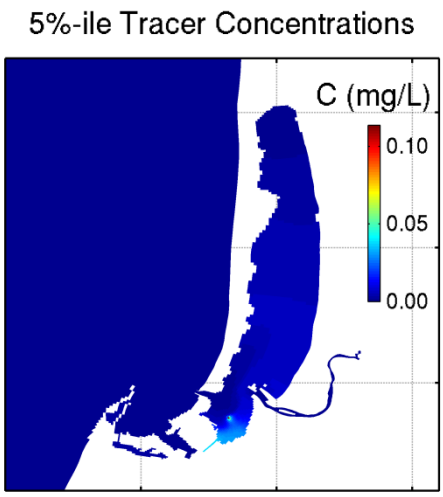

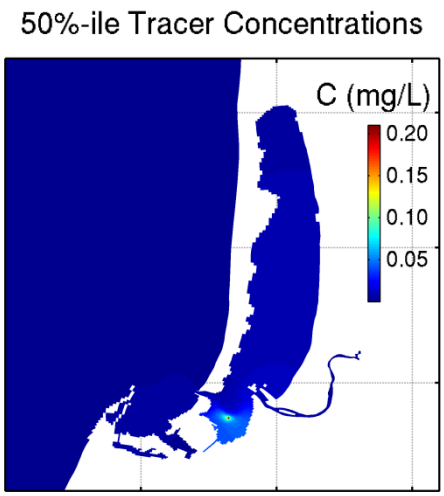

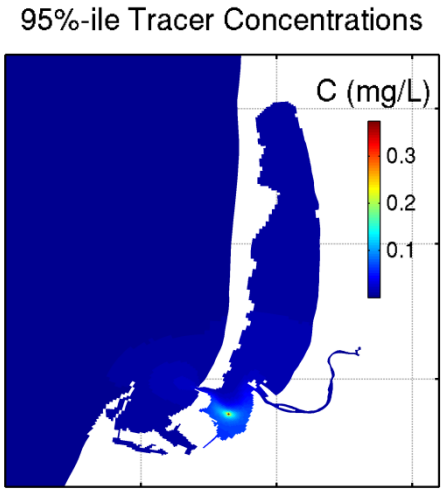

Figure 8.6.5. 5th (top), 50th (middle) and 95th (bottom) percentile distributions for a tracer release at the mooring location South.

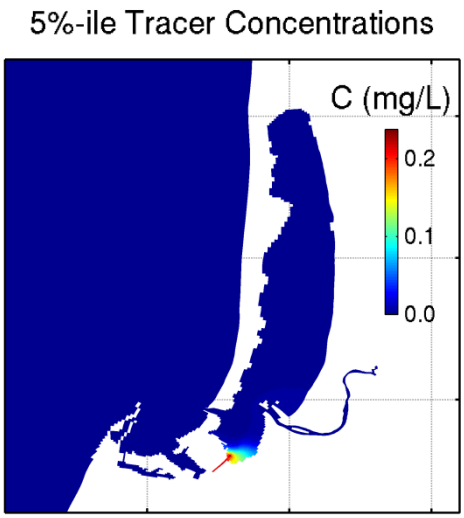

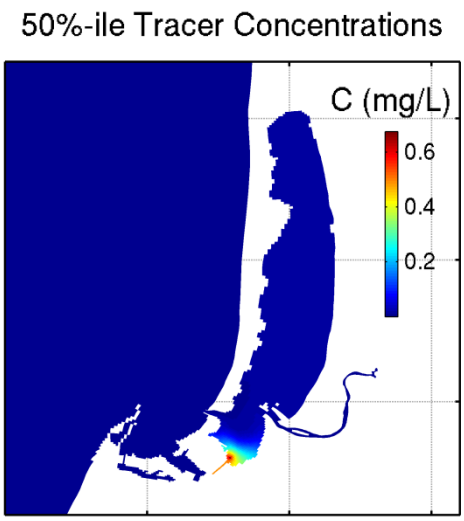

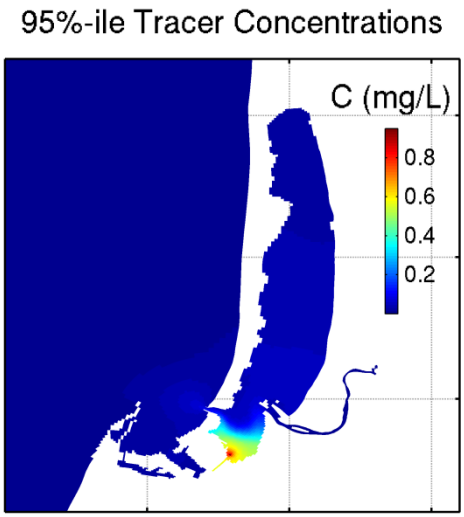

Figure 8.6.6. 5th (top), 50th (middle) and 95th (bottom) percentile distributions for a tracer release at the mouth of the Preston River.

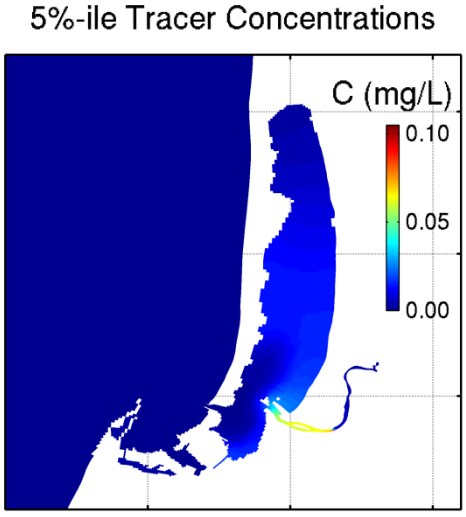

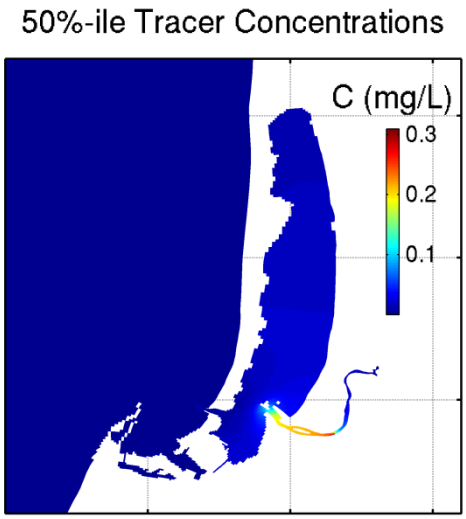

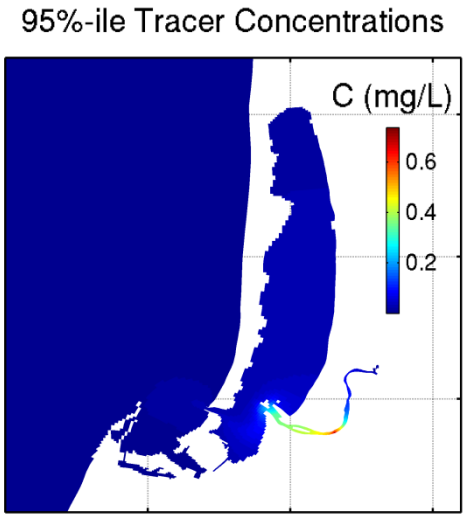

Figure 8.6.7. 5th (top), 50th (middle) and 95th (bottom) percentile distributions for a tracer release in the lower Collie River.

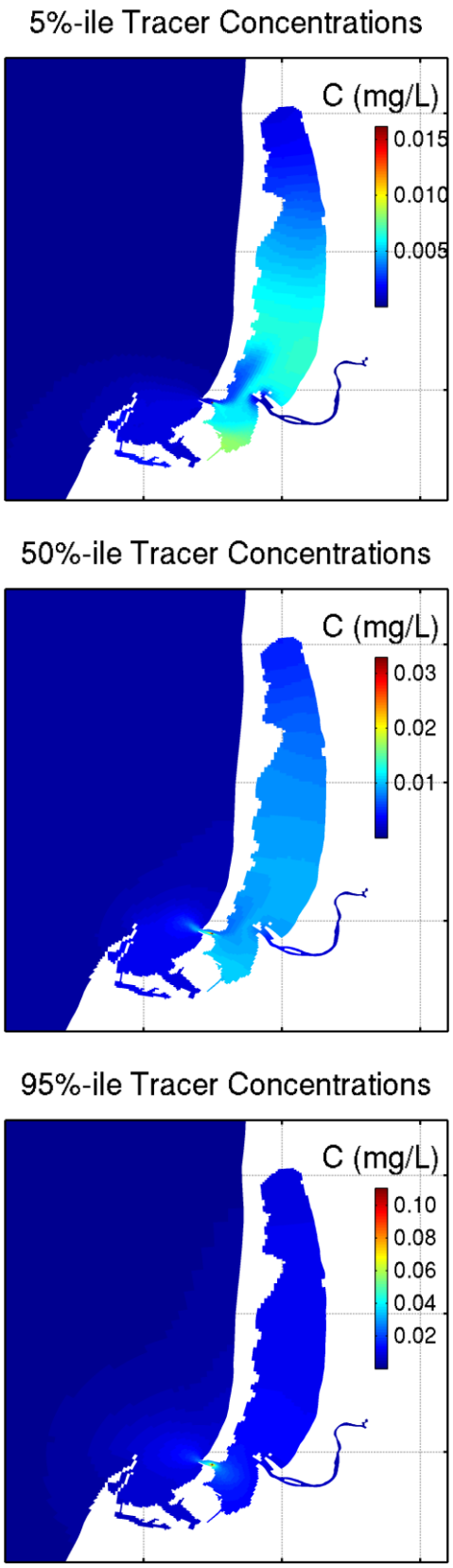

Figure 8.6.8. 5th (top), 50th (middle) and 95th (bottom) percentile distributions for a tracer release in the Cut.

The site with the best connectivity was the Collie River. Tracer from this source spread thoughout much of the central and southern Leschenault Estuary. Tracer from the Cut also dispersed over similar areas, though at lower concentrations than those from the Collie River. Maximum surface concentrations were confined to the immediate vicinity of the source for all releases. These were highest for the Parkfield Drain source, with maximum 95th percentile exceeding 0.8 mg L^{-1}. In contrast, the locations at Est 6 and the Cut were most dispersive, with maximum 95 percentiles of the order of 0.1 mg L^{-1}. Note that these distributions are specific to the period of April 2011 – March 2012, and changes in river flows and wind stress conditions may modify the distributions.

8.7 The Collie River Salt Wedge

The meeting of freshwater river flow from the Collie and Brunswick Rivers with saltwater from the Leschenault Estuary results in the formation of a strong salt wedge in the lower reaches of the Collie River. The location of the salt wedge is dependent on the magnitude of the river flow and the sea surface height in the estuary. The salinity interface between the salt wedge and the overlying freshwater in the Collie River was very sharp, and vertical diffusion of salt very low.

Vertical cross-sections of the salinity, temperature and vertical diffusivity in the Collie River were extracted from the model along the section shown in Figure 8.7.1. A typical snapshot of the salt wedge, from 02 July 2011 when river flows were moderate (gauged flow at Rose Road was about 2.5 m^3 s^{-1}) is shown in Figure 8.7.2. This snapshot follows a flood event, and the water in the river remained overwhelmingly fresh, with saline water beginning to penetrate up the Collie River underneath the overlying freshwater. In the Leschenault Estuary, the salinity was about 33 psu, with the surface front separating fresh and saline water at the mouth of the river extending about 0.5 km in length. Temperature gradients were weaker, with water in the Leschenault Estuary about 4 °C warmer than the river water.

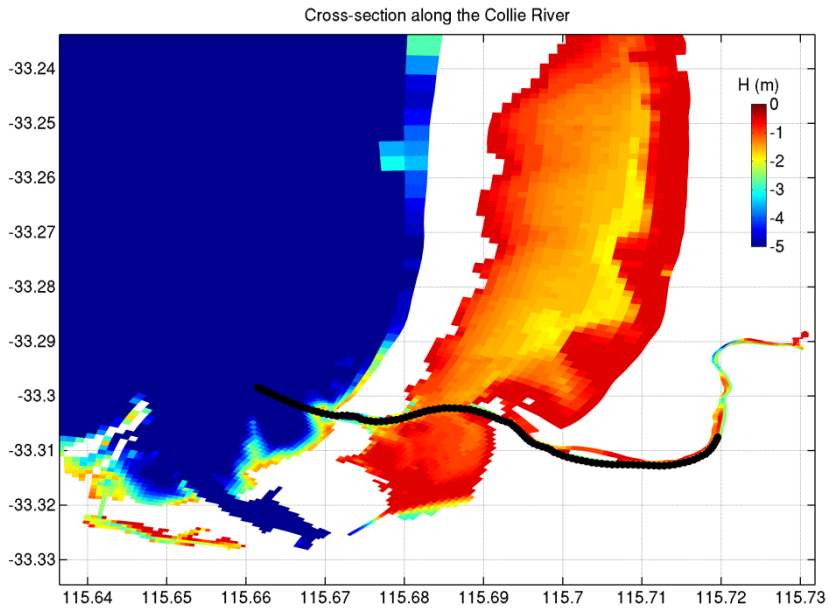

Figure 8.7.1. Locations of the data points (●) making up the cross-sections along the Collie River.

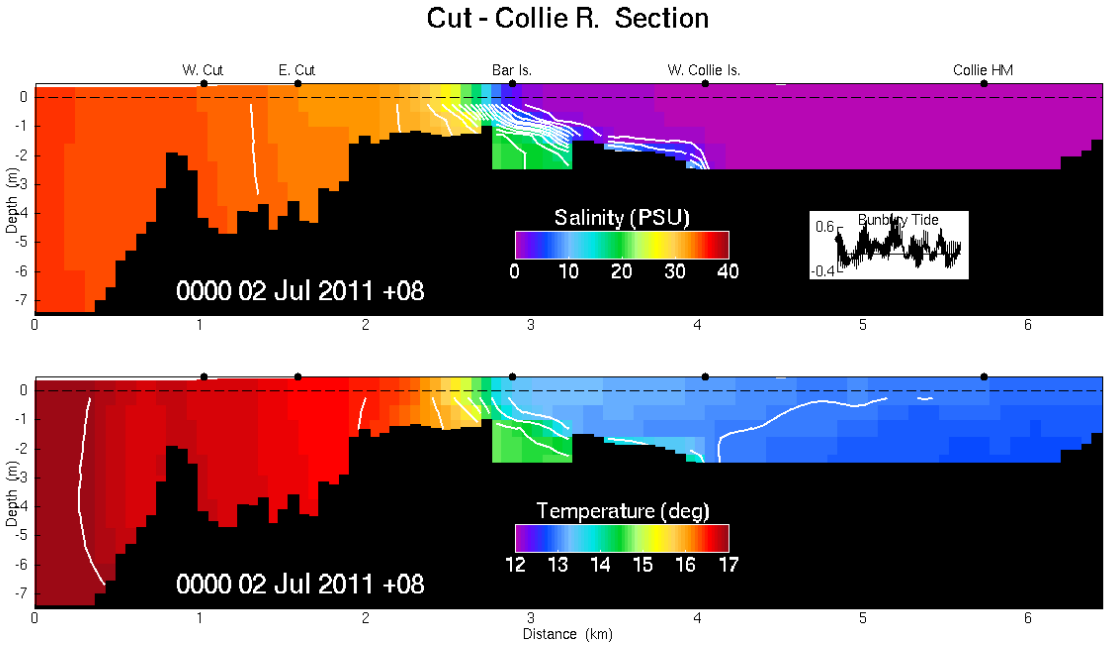

Figure 8.7.2. Cross-sections of salinity (top) and temperature (bottom) for the Collie River on 1 July 2011. River flow conditions were moderate.

Two weeks later, on 15 July 2011, the river flow had abated further (gauged flow at Rose Road was 0.3 $m^3 s^{-1}$), and the salt wedge had pushed further up the Collie River (Figure 8.7.3). Surface water in the lower reach of the river had a salinity of 5 – 10 psu; at the bottom, the modelled salinity was about 30 psu. Salinity in the Leschenault Estuary was about 34 psu. Temperature in the Collie River was also stratified, albeit more weakly than the salinity, with

cooler freshwater overlying warmer saltwater from the estuary. Simulation of the hydrodynamics of the Collie River was limited by the spatial resolution of the model, particularly in the vertical. The vertical grid spacing near the water surface was 0.5 m. Given that water depth in the Collie River is of the order 2.5 m, and with sea surface fluctuations of ±0.5 m, the water column is being resolved using 4 – 6 grid cells. Although this resolution is sufficient to reproduce the general features of the salt wedge, the salinity of the lower water column was being overly diluted, perhaps due to implicit vertical mixing in the model, as is evident in the time series of salinity at the bottom Collie River sensor location (Figure 7.2.6). Increasing the vertical resolution in the surface layers of the model would probably improve the simulation of the salt wedge properties, but would also significantly increase computational run times.

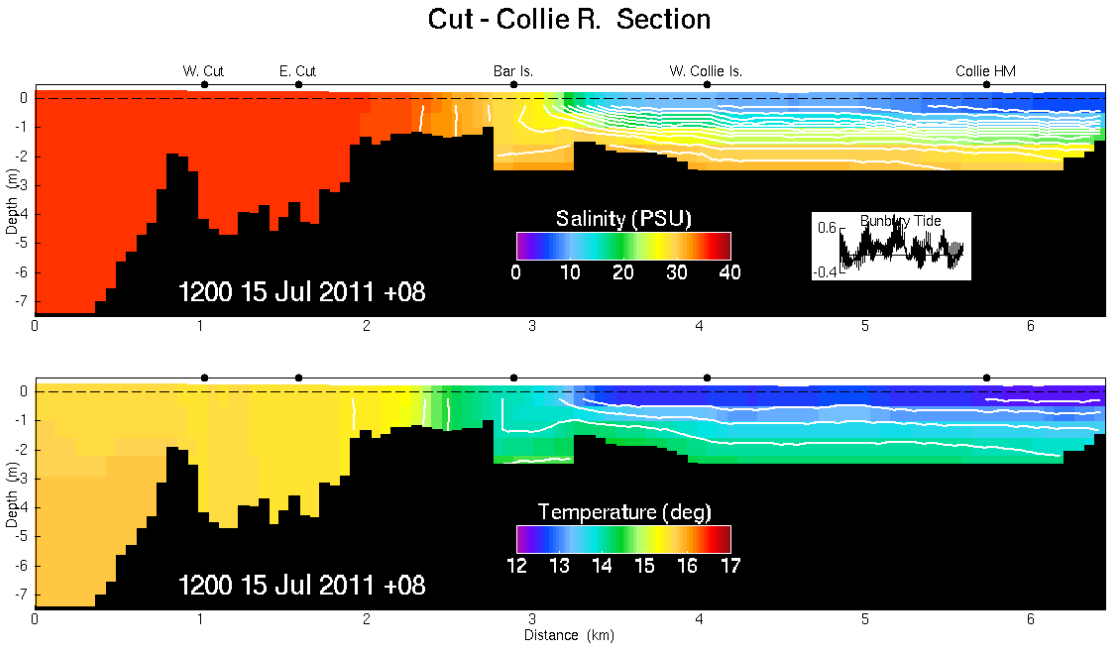

Figure 8.7.3. Cross-sections of salinity (top) and temperature (bottom) for the Collie River on 1 July 2011. River flow conditions were low

At times of high river flood, the salt wedge is pushed out beyond the mouth of the Collie River into the Leschenault Estuary. Cross-sections of temperature and salinity following the flood event of 22 – 25 August 2011 (Figure 8.7.4) illustrate the purging of saltwater from the river during high flow events. In the model simulation, freshwater extended across the surface of the estuary and through the Cut. A very sharp salinity gradient, from 0.5 – 1.5 m depth, separated the brackish surface plume from the coastal seawater. In the estuary, between the Cut and the bar at the mouth of the Collie River, salinity was less than 10 psu near the bed, and fresh at the surface. The river water had a uniform temperature of about 15°C, and overlay the warmer coastal water (Figure 8.7.4).

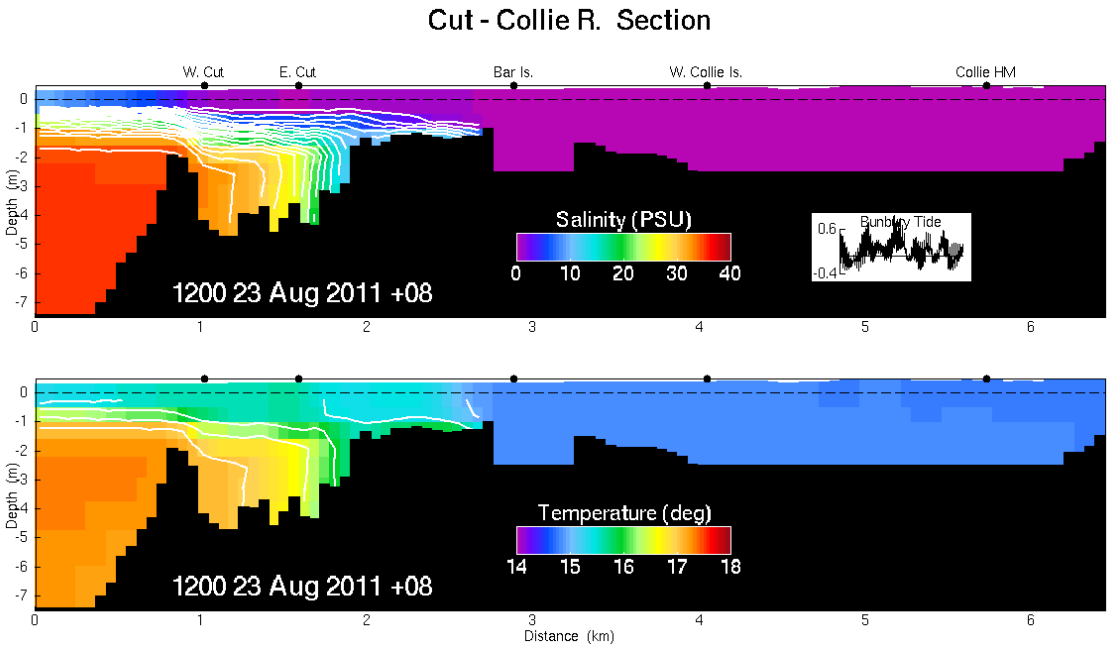

Figure 8.7.4. Cross-sections of salinity (top) and temperature (bottom) for the Collie River on 23 August 2011. River flow conditions were high.

During the dry summer, the salt wedge reached its maximum penetration up the Collie River. The cross-sections of temperature and salinity for 29 January 2012 are shown in Figure 8.7.5. At this time, the surface water in the lower Collie River was brackish, with salinity of 15 – 20 psu. The underlying saltwater had a salinity of 32 – 33 psu, with a sharp halocline separating it from the surface water. Observations showed that, during dry periods, the salt wedge penetrates far up the Collie River, beyond the Australind Bypass bridge. The model does reproduce salt penetration beyond the bridge, but to a lesser degree than observed. Modelled bottom salinities in the river channel during the summer were about 10 – 15 psu, rather than 30 psu as observed. This is again a function of the model resolution, which introduces more mixing in the water column than is evident from observations.

The cross-section temperature on 29 January 2012 was strongly stratified, with warm fresh water overlying the cooler estuary water. Outside the Cut, the coastal water temperature was cooler still (Figure 8.7.5).

Vertical turbulent diffusion in the Collie River during low flow conditions was weak. A cross-section of the vertical diffusivity (Kz) corresponding to the temperature and salinity sections in Figure 8.7.5 illustrates the variability in the strength of vertical mixing between the coastal ocean, Leschenault Estuary and the Collie River (Figure 8.7.6). Diffusivity in the Collie River was of the order 10^{-8} m^2 s^{-1}, the lower limit of diffusivity in the model. Small hotspots of mixing are apparent at the surface, probably due to sporadic moments of elevated current shear and weak localized stratification in the surface layer. Mixing was moderate outside the mouth of the river (Kz ~ 10^{-4} m^2 s^{-1}) and stronger around the western end of the Cut (Kz ~ 10^{-2} m^2 s^{-1}). In contrast, during the river flood event of 22 – 23 August 2011, mixing was strong (Kz ~ 10^{-3} – 10^{-2} m^2 s^{-1}) in the unstratified river water, and weaker in the strongly stratified waters in the

Cut and Koombana Bay. Thus the strength of mixing in the estuary can be seen to vary by several orders of magnitude, dependent on the stratification and current shear in the water column.

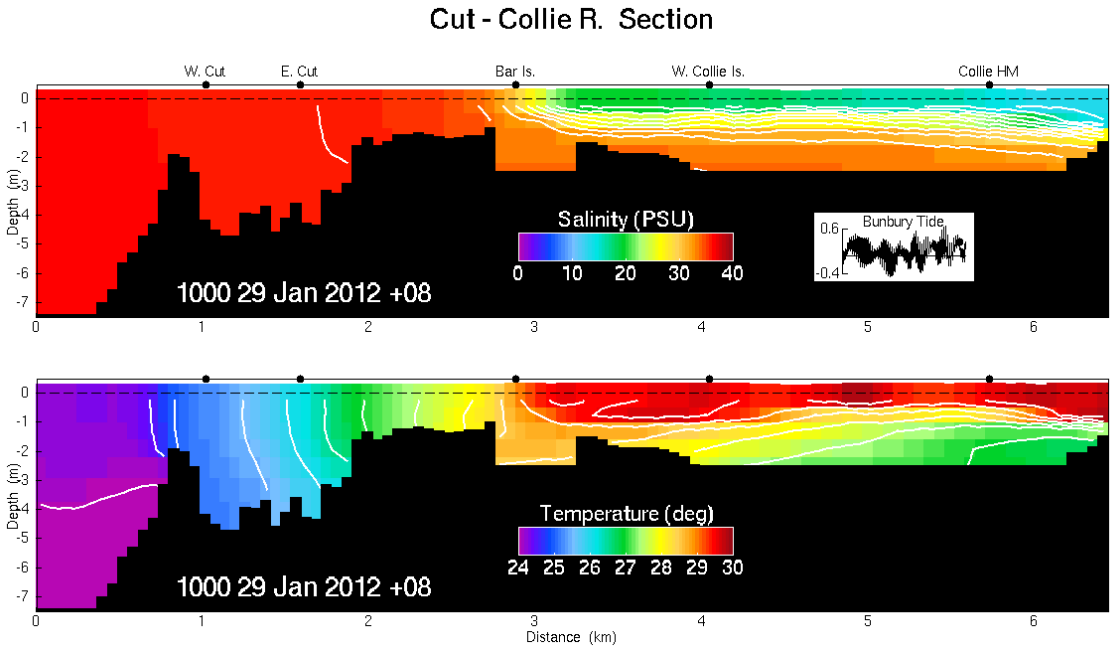

Figure 8.7.5. Cross-sections of salinity (top) and temperature (bottom) for the Collie River on 29 January 2012. River flow conditions were low.

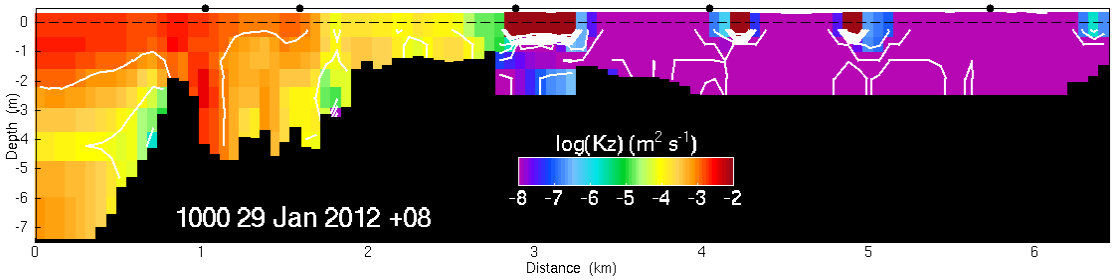

Figure 8.7.6. Cross-section of vertical diffusivity for the Collie River on 29 January 2012. Values of $log_{10}(Kz)$ are plotted. River flow conditions were low.

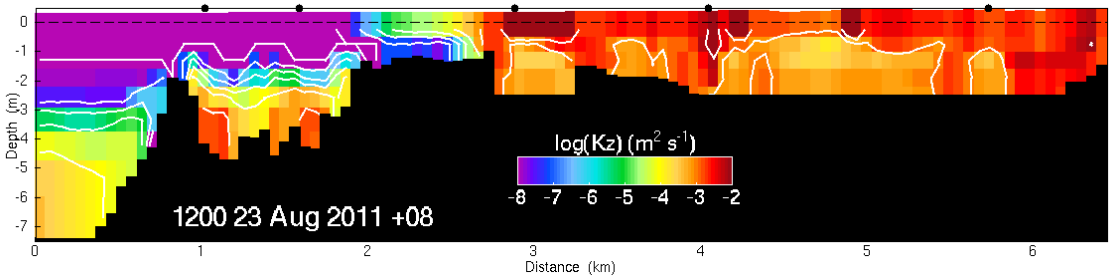

Figure 8.7.7. Cross-section of vertical diffusivity for the Collie River on 23 July 2011. Values of $log_{10}(Kz)$ are plotted. River flow conditions were high.

8.8 Future Projections

The simulation discussed so far in this report describes conditions in the Leschenault Estuary during April 2011 – March 2012. Climate change projections for Western Australia suggest that the region is likely to become warmer and drier over coming decades (www.climatechangeinaustralia.gov.au). For this report, we used projected climate changes for the year 2050. The potential effects of changing climate on the hydrography of the Leschenault Estuary were briefly examined by running the model under modified forcing conditions estimated from the climate projections. Key forcing variables, namely air temperature, daily rainfall, atmospheric humidity and ocean temperatures were modified from their 2011 – 12 values by fixed amounts, according to the climate projections. Wind speed and solar radiation were not projected to change. River flow data were also reduced by the same percentages as the rainfall projections i.e. 7.5% and 15%. The extent of warming and drying depends on global emissions scenarios, and the projected effects of three scenarios on the forcing variables are summarized in Table 8.8.1. Emissions scenarios are from the IPCC Special Report on Emission Scenarios: 'low emissions' corresponds to the B1 scenario, 'medium' is A1B and 'high' is A1FI. Note that the projected effects of each emissions scenario are given as a ranges of values; for the purposes of modelling the hydrodynamic effects on the Leschenault Estuary, the 50th percentile value was chosen for all variables.

	Low Emissions	Medium Emissions	High Emissions
Air Temperature	+1.00 °C	+1.25 °C	+1.75 °C
Rainfall	-7.5%	-15%	-15%
Humidity	-0.75%	-0.75%	-0.75%
Sea Surface Temperature	+0.8 °C	+1.25 °C	+1.25 °C

Table 8.8.1. Modifications applied to the 2011 – 12 model forcing to simulate potential future climate effects on the Leschenault Estuary. The values given for each emission scenario are the 50th percentile value.

The modifications detailed in Table 8.8.1 were applied uniformly to the forcing data used for the 2011 – 12 simulation. For example, for the 'Low Emissions' simulation, air temperatures for 2011 – 12 from the ACCESS model were increased by 1 °C for the entire 12 months, daily rainfall amounts were reduced by 7.5%, humidity was reduced by 0.75% and the ocean temperatures from OceanMaps were increased (at all depths) by 0.8 °C. Initial conditions for each simulation were revised, with water temperatures throughout the domain increased using the sea surface temperature adjustment in Table 8.8.1. Initial salinity values were not changed. The model was then spun-up from 17 March – 01 April as previously, and the 12-month simulation from 01 April repeated with the modified forcing.

Time series of temperature and salinity at the monitoring locations from the climate projections are shown in Figures 8.8.1 and 8.8.2 respectively. The 2011 – 12 model output and the observed data from 2011 – 12 are also shown for comparison. The greater changes were predicted in the temperature time series, with temperatures becoming increasingly warmer in the higher emissions scenarios. Predicted annual-mean temperatures were typically 1.5 °C warmer in the high emissions scenario than for the 2011 – 12 model run (Table 8.8.2), slightly greater than the increase in ocean temperatures.

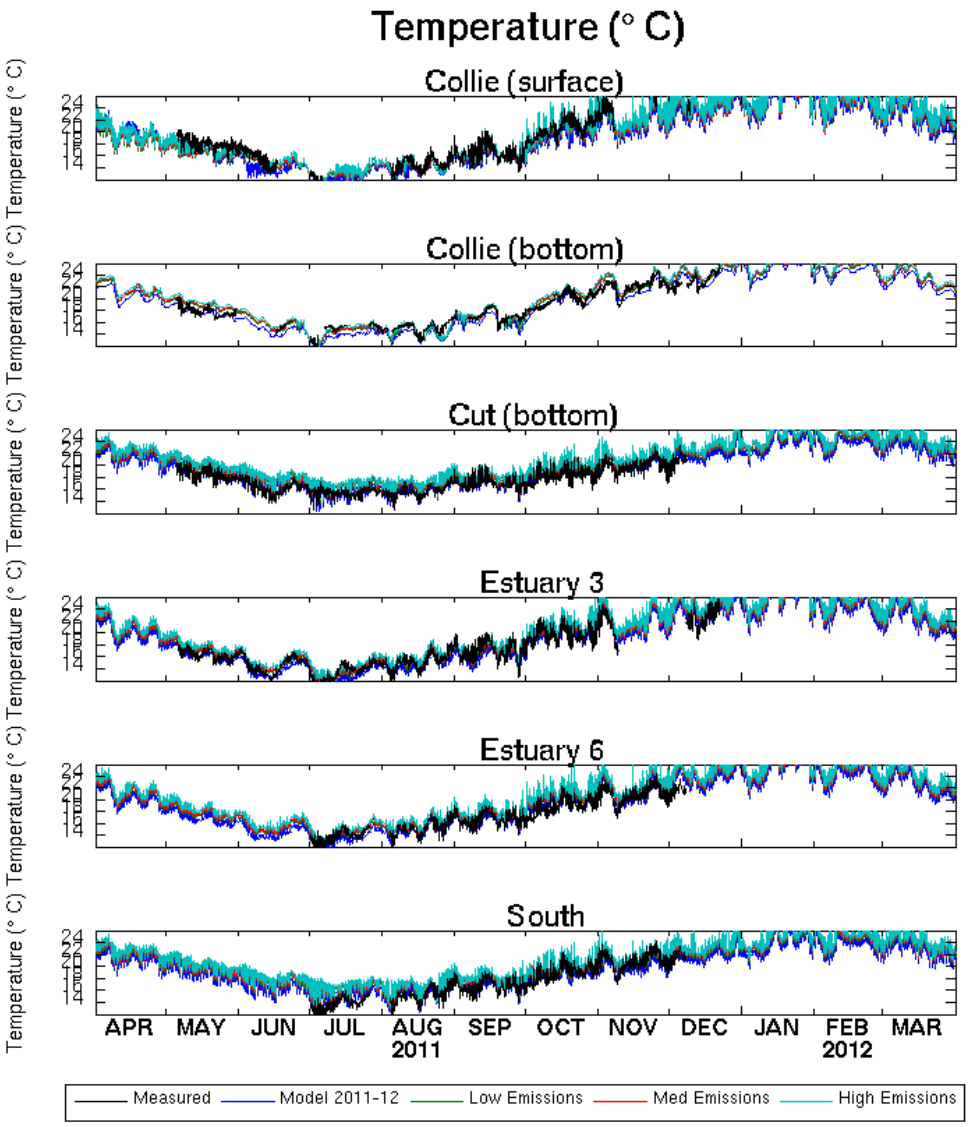

Figure 8.8.1. Time series of projected temperature at the six mooring locations for the three future scenarios. Time series for low, medium and high emissions scenarios are shown. The observed data from 2011 and the baseline model run for 2011 – 12 are also shown for comparison.

Projected changes to surface salinity in the Leschenault were most marked in the northern and central basins, with increases of 0.88 and 0.52 psu in the annual-mean salinity at Estuary 3 and Estuary 6 locations respectively (Table 8.8.3). Despite the reduced rainfall and river flows, the projected surface salinities were initially lower in the Collie River and at Estuary 3 and Estuary 6 sites. This was caused by a slight increase in stratification in the main estuary caused, in turn, by a reduction in the density of water leaving the Collie River due to elevated water temperatures in the river. The lighter density of the river water created stronger stratification in the estuary and a slightly reduced surface layer salinity.

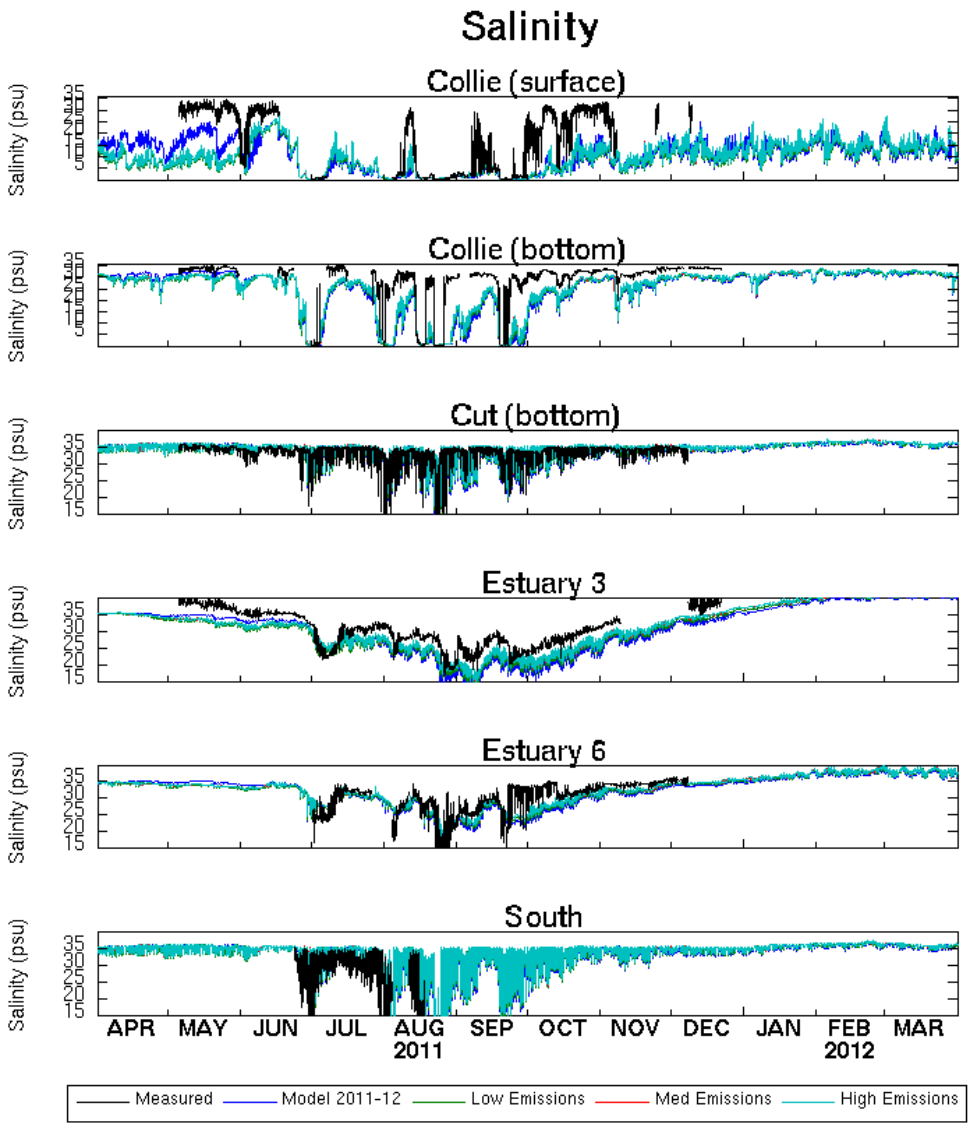

Figure 8.8.2. Time series of projected salinity at the six mooring locations for the three future scenarios. Time series for low, medium and high emissions scenarios are shown. The observed data from 2011 and the baseline model run for 2011 – 12 are also shown for comparison.

	Obs	2011 – 12	Low	Medium	High
Collie (surface)	*17.54*	19.20	19.72	19.92	20.21
Collie (bottom)	*18.43*	19.47	20.19	20.43	20.72
Cut (bottom)	*17.39*	19.69	20.50	20.80	21.06
Estuary 3	*16.77*	19.18	20.04	20.26	20.69
Estuary 6	*17.48*	19.47	20.32	20.54	20.94
South	*17.48*	19.68	20.49	20.78	21.05

Table 8.8.2. Projected annual-mean temperatures (°C) at the six mooring locations for the three future climate scenarios. Mean values for low, medium and high emissions scenarios are shown. The annual mean values of the 2011 – 12 model run are shown for comparison. The observed mean values from May – December 2011 are also shown, but do not comprise a full annual cycle and are therefore cooler.

	Obs	2011 – 12	Low	Medium	High
Collie (surface)	*17.58*	10.17	9.13	9.78	9.78
Collie (bottom)	*29.30*	24.42	24.55	24.98	24.99
Cut (bottom)	*32.98*	33.85	33.91	34.06	34.06
Estuary 3	*30.54*	30.81	31.08	31.65	31.69
Estuary 6	*30.12*	32.09	32.24	32.59	32.61
South	*27.67*	33.11	33.17	33.37	33.37

Table 8.8.3. Projected annual-mean salinities (psu) at the six mooring locations for the three future climate scenarios. Mean values for low, medium and high emissions scenarios are shown. The annual mean values of the 2011 – 12 model run are shown for comparison. The observed mean values from May – December 2011 are also shown, but do not comprise a full annual cycle.

Spatial maps of the projected changes in seasonal-mean surface temperature and salinity for 2050 relative to 2011 – 12 are presented in Figures 8.8.3 – 8.8.8. The values shown are differences from the values presented in Figures 8.3.2 and 8.3.4, and indicate the potential impacts of a warming, drying climate of the seasonal hydrography of the Leschenault Estuary. Differences in the seasonal-mean velocities were very small (less than 10^{-4} m s^{-1}), and the mean sea surface height and mean circulation fields have therefore not been plotted for the projections.

The projected winter-mean temperature for 2050 under a low emissions scenario was typically about 0.8 – 0.9 °C warmer than winter 2011 (Figure 8.8.3). The exception was the surface water in the Collie River which had a temperature very similar to the 2011 result; the

river water temperature was not modified for the projection since no information was available on projected river temperatures. In the main body of the Leschenault Estuary, the greatest increase in winter-mean temperature occurred in the central estuary; in the southern basin, temperature changes were less due to the strong riverine influence. Winter-mean salinity in the low-emissions scenario was slightly higher in the southern estuary, due to reduced rainfall and river flow. In the northern half of the estuary, the salinity did not change.

The summer-mean values of temperature were also about 0.8 °C greater than the 2011 – 12 summer values, but with less variability over the estuary. The change to summer-mean salinity increased steadily northward up the estuary, with a change of 0.1 psu near the Cut increasing to about 1 psu at the northern end. It is notable that the greatest changes to temperature occurred to winter values, and the greatest changes to salinity occurred in summer. This pattern was continued, and enhanced, in the medium and high emissions scenarios. In the high emissions scenario, projected winter-mean temperatures in the estuary were up to 1.6 °C higher in the northern and central estuary than in winter 2011. The increase was slightly less in summer, with projected increase of about 1.3 – 1.4 °C. The increased temperatures probably results from reduced winter cooling in the shallow water.

In contrast, the greatest projected changes to salinity occurred in summer. In the high emissions scenario, the summer-mean salinity in the northern basin of the estuary was 2 psu greater than summer 2011 – 12. The salinity change was less at the southern end of the estuary around the Cut, where unchanged oceanic water dominated. In winter, the increase in salinity was less, typically 0.2 – 1 psu.

As noted above, the projections exhibited little difference from the current simulations in terms of velocity fields. In order to confirm this, the tracer flushing simulations described in §8.5 were repeated for each emissions scenario. The time series of mass ratio under each scenario are shown in Figure 8.8.9. The projected rates of change in the tracer mass do not substantially differ from the tracer simulations for 2011 – 12 (Figure 8.5.2), implying that the projected changes in temperature and salinity will have only minor impacts on the estuary hydrodynamics. It should be noted, however, that the ecological implications of the projected changes to temperature and salinity may be more significant. It should also be remembered that these are rather simplistic projections of potential future climate impacts on the Leschenault Estuary, and could be made more rigorous by using a regional climate model to force the hydrodynamic model into the future.

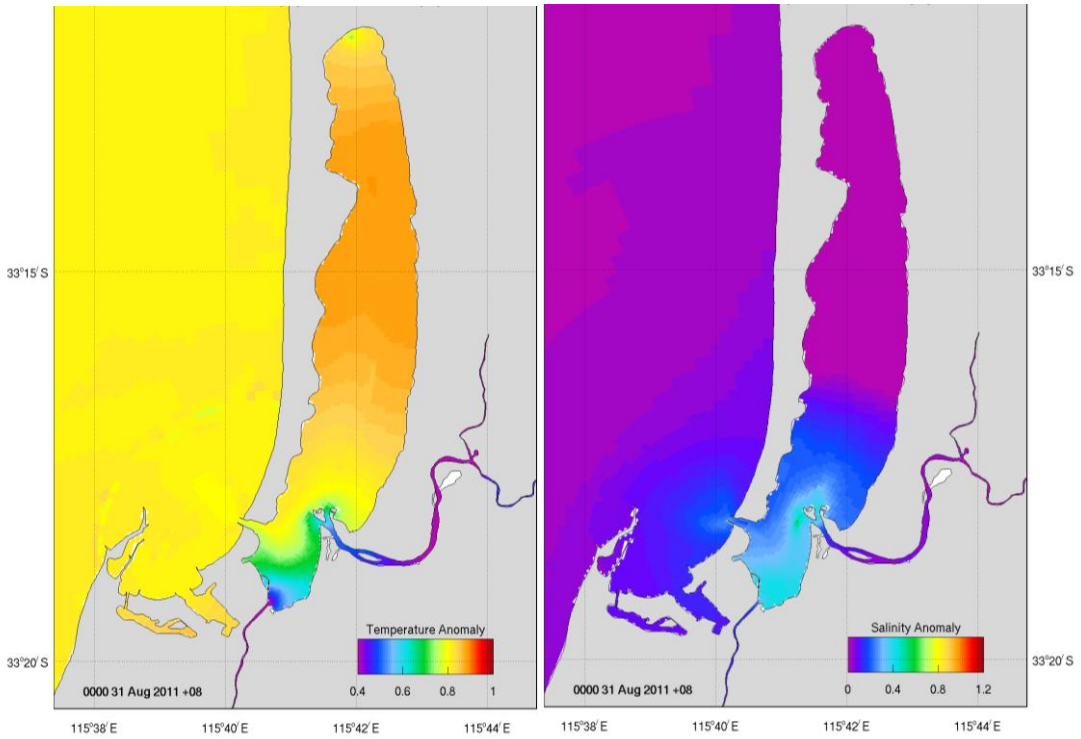

Figure 8.8.3. Modelled change ("anomaly") in the seasonal-mean surface temperature (left) and salinity (right) for "winter 2050" compared to winter 2011 under a low emissions scenario. The model results are averaged from 01 June – 31 August.

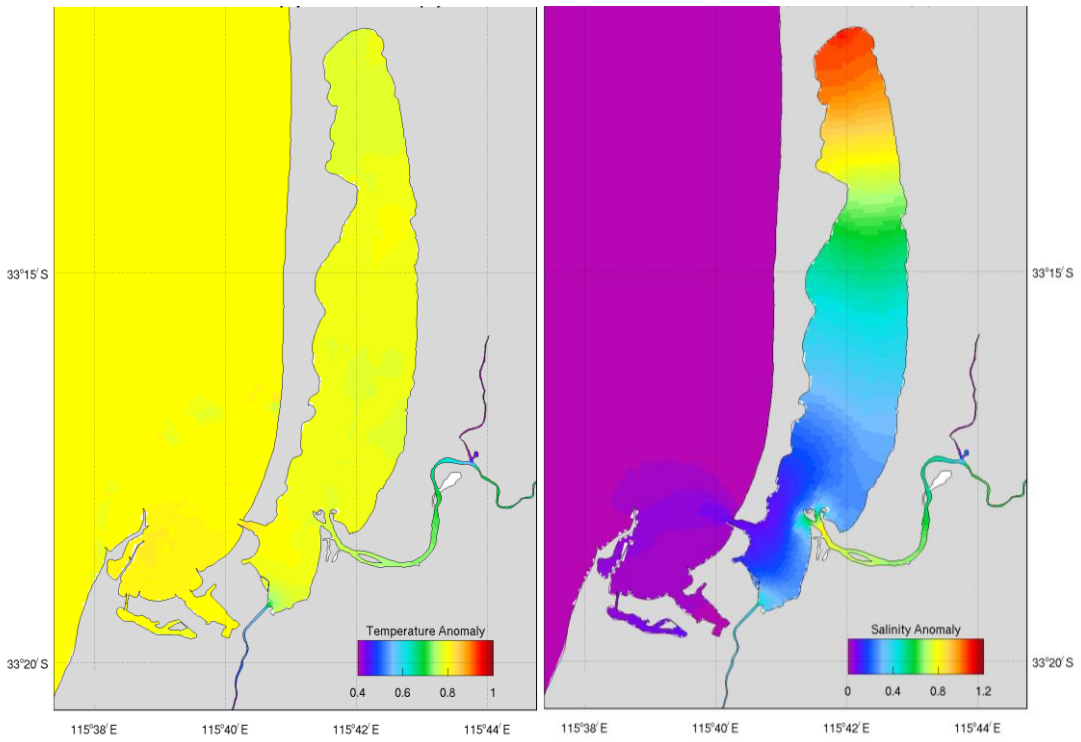

Figure 8.8.4. Modelled change ("anomaly") in the seasonal-mean surface temperature (left) and salinity (right) for "summer 2050" compared to summer 2011 – 12 under a low emissions scenario. The model results are averaged from 01 December – 29 February.

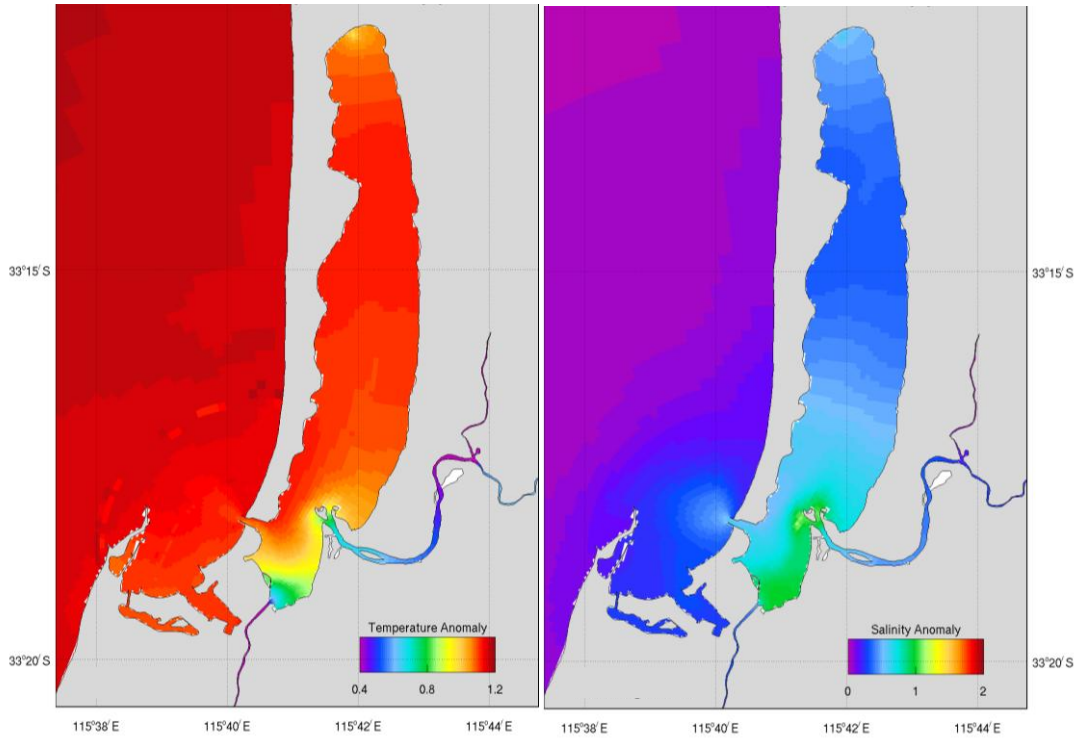

Figure 8.8.5. Modelled change ("anomaly") in the seasonal-mean surface temperature (left) and salinity (right) for "winter 2050" compared to summer 2011 – 12 under a medium emissions scenario. The model results are averaged from 01 June – 31 August.

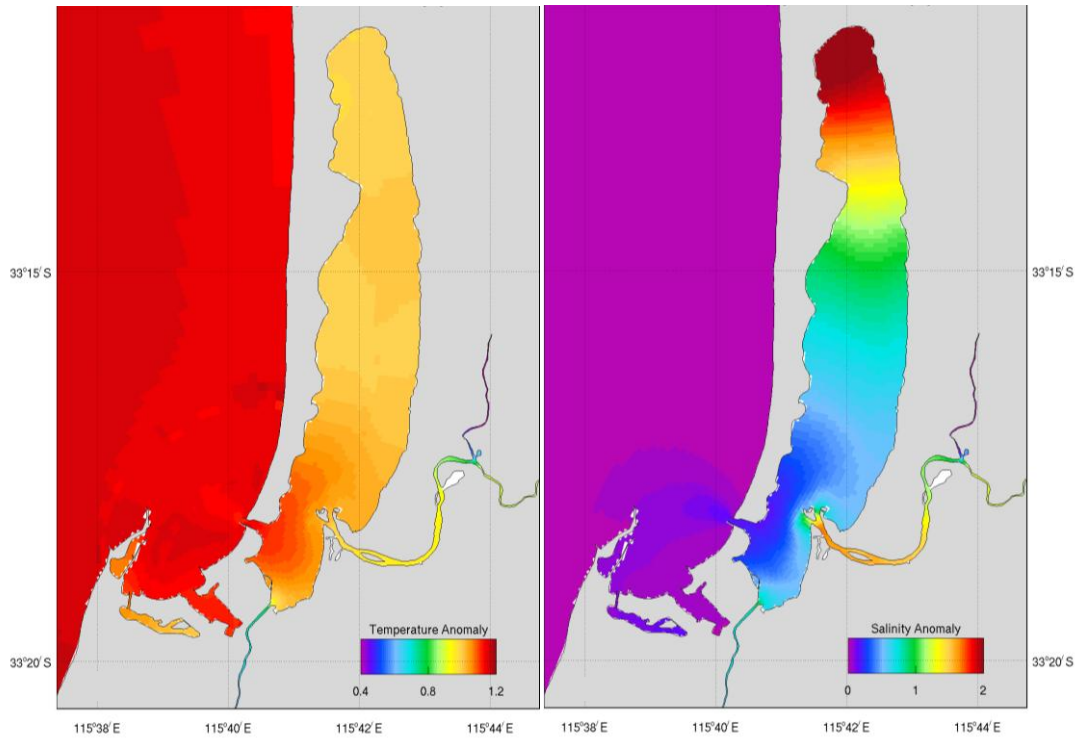

Figure 8.8.6. Modelled change ("anomaly") to seasonal-mean surface temperature (left) and salinity (right) for "summer 2050" from summer 2011 – 12 under a medium emissions scenario. The model results are averaged from 01 December – 29 February.

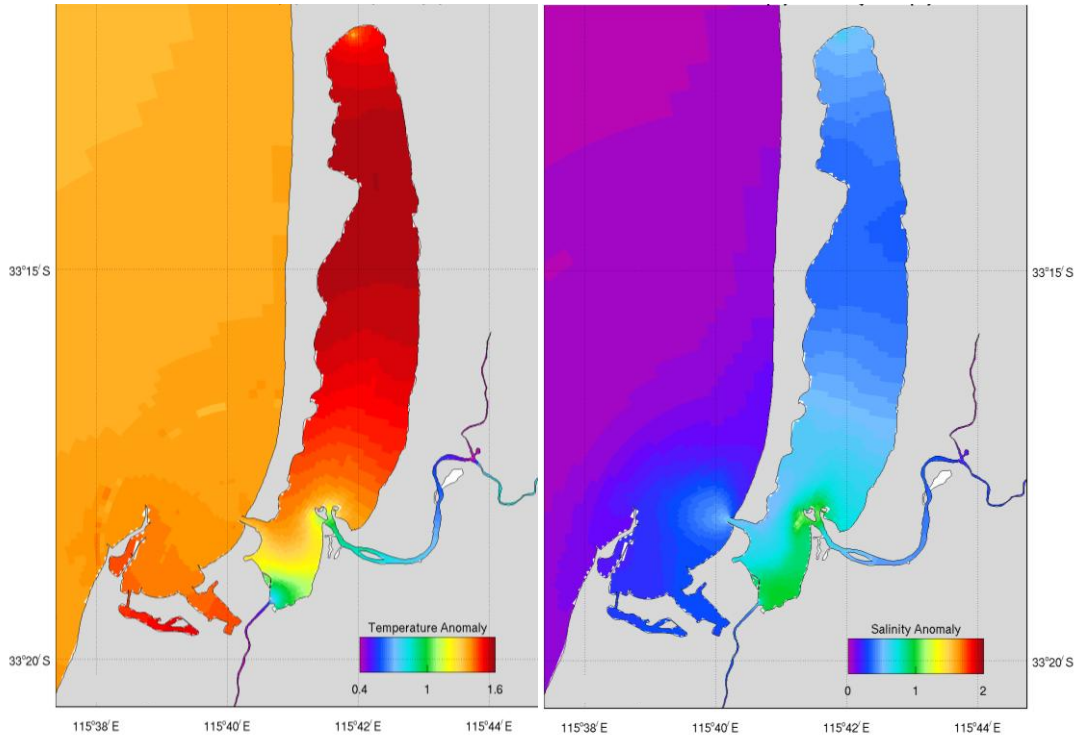

Figure 8.8.7. Modelled change ("anomaly") in the seasonal-mean surface temperature (left) and salinity (right) for "winter 2050" compared to summer 2011 – 12 under a high emissions scenario. The model results are averaged from 01 June – 31 August.

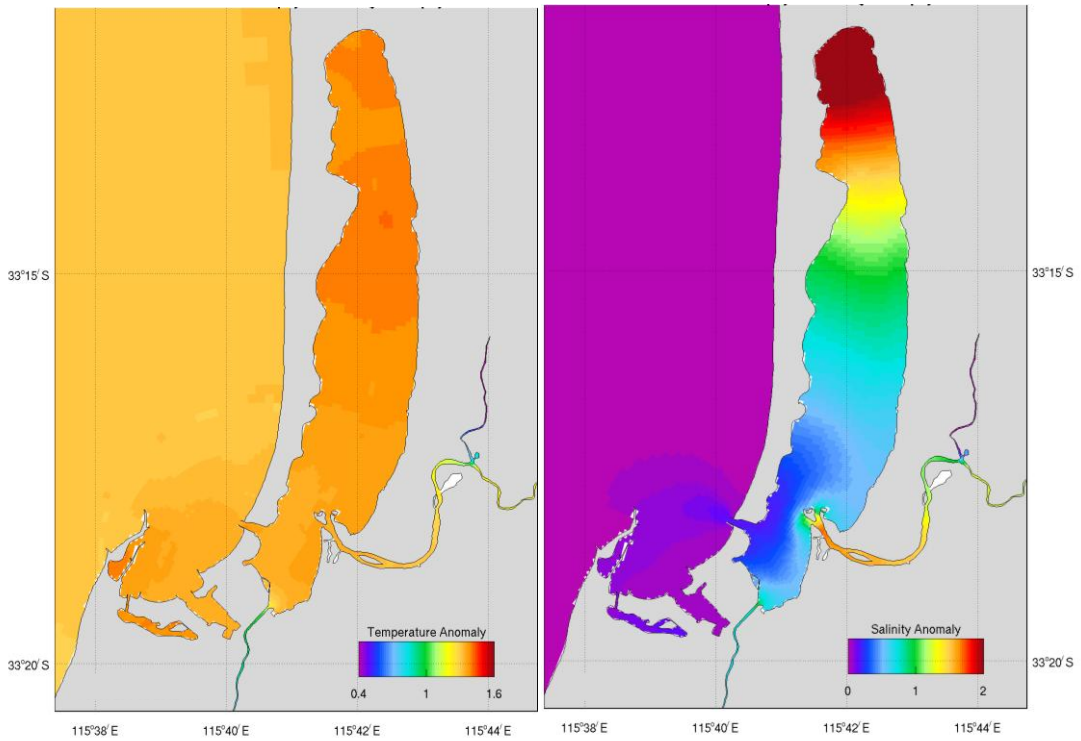

Figure 8.8.8. Modelled change ("anomaly") in the seasonal-mean surface temperature (left) and salinity (right) for "summer 2050" compared to summer 2011 – 12 under a high emissions scenario. The model results are averaged from 01 December – 29 February.

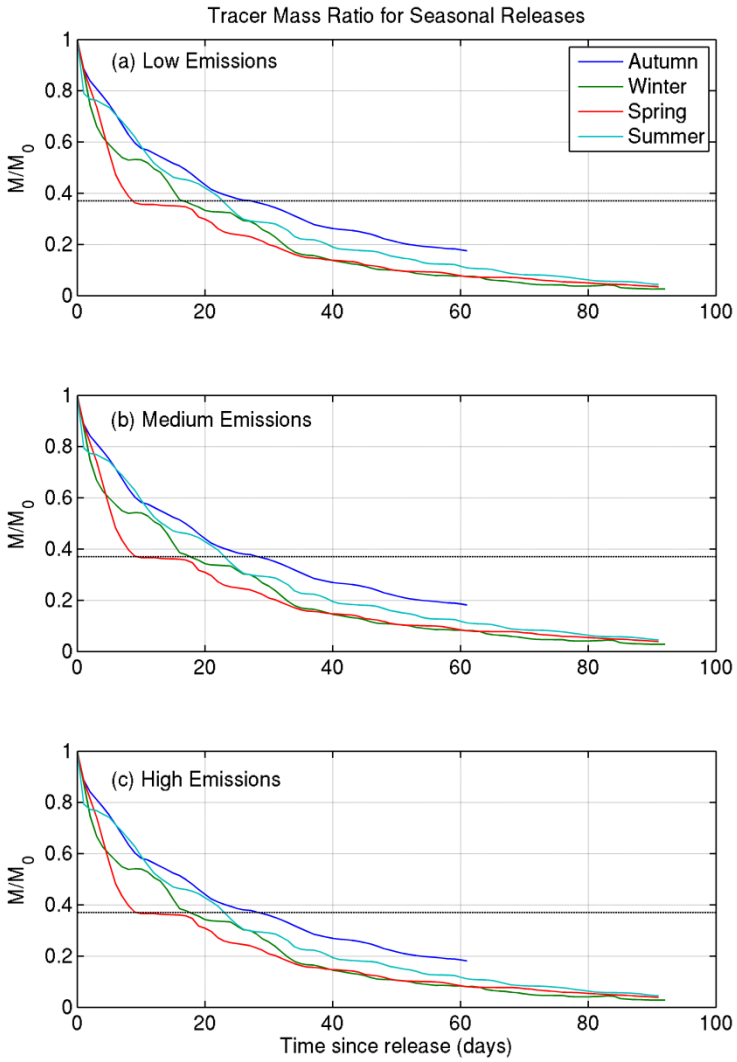

Figure 8.8.9. Projected time series of the relative tracer mass (M/M_0) from the seasonal simulations of flushing under future climate emissions scenarios: (a) low emissions, (b) medium emissions, (c) high emissions. The horizontal dashed line marks the value of $M/M_0 = e^{-1} = 0.37$.

9. Conclusions

A 3D primitive equation model was applied to the Leschenault Estuary to examine the hydrodynamics of the region. The estuary was modelled using a curvilinear grid, with high resolution focused on the estuary, its entrance and inflowing rivers. Model forcing included tides, low-frequency sea level fluctuations, wind stress, surface heat and salt fluxes, river flow and oceanic temperature and salinity. The model was run for a 12-month period from April 2011 – March 2012, and calibrated against temperature and salinity time series data collected at five locations in the estuary.

The model proved sensitive to the prescription of heat and salt fluxes through the ocean surface, in particular to the values of transmission and attenuation of the shortwave radiation. The method of specifying latent and sensible bulk fluxes also proved important, particularly to the summer salinity solutions. Due to the shallow nature of the estuary, and its restricted exchange with the adjacent ocean, modelled temperature was particularly sensitive to this atmospheric forcing, with marked differences from the oceanic temperatures during summer and winter. Modelled salinity in the estuary was also notably modified from ocean values, fresher in winter due to high river flows and saltier in summer due to strong evaporation.

No data were available to force the offshore boundaries of the model. Instead, low-frequency (non-tidal) fluctuations in sea level, velocitiy, temperature and salinity were taken from operational model output for the Australasian region and combined with a global tide model. The model boundary condition was then inversely scaled to provide a satisfactory comparison with observed sea level at Bunbury. Boundary values of temperature and salinity were not adjusted, since the uncertainty in the prescribed ocean values is small relative to the variability of the modelled temperature and salinity in the estuary. Furthermore, the ocean boundary forcing has little impact on the circulation in the estuary, which responds more strongly to tides, river flows and atmospheric forcing. The approach is justified by the excellent agreement between observed and modelled temperature achieved. The comparison between observed and modelled salinity is also good throughout most of the estuary; the weakest agreement occurs in the Collie River, where limited spatial resolution coincides with complex salt wedge dynamics. Nevertheless, the model reproduced the fundamental aspects of salt wedge dynamics in the Collie River. Higher spatial resolution in the model, and improved digital bathymetry would help improve the simulations. Improvement in this area may be achieved by two-way nesting a high resolution Collie River model into the Leschenault Estuary model; however, the reduced run times necessary for a high resolution model will remain the limiting factor for overall run-time, hence model throughput may be compromised.

Instantaneous currents in the Leschenault Estuary are dominated by tidal forcing, particularly in the southern basin around the entrance channel. In the Cut, tidally-driven velocities exceed 1.5 m s^{-1} at times. The narrow Cut channel exerts control on the estuary-ocean exchange, and chokes the tide inside the estuary relative to the external tide, reducing the amplitude of the surface oscillation. The shallow water depths in the estuary also lead to a slow progression of the tide northwards and eastwards from the Cut; observations of sea surface height in the estuary would be useful to verify the tidal propagation speed. Water entering through the Cut during flood tide is largely diverted northward into the central estuary; a secondary current generates an anti-clockwise circulation in the southern basin. During ebb tides, the circulation is reversed, with southward flow in the northern and central basins, and a clockwise flow in the southern basin. Away from the entrance channel, tidal currents quickly

become weaker. Around the mouths of the major river channels, such as the Preston and Collie Rivers, currents due to the river flow may overpower tidal currents and become uni-directional during periods of high river flow.

The residual (net) circulation, presented here as seasonally-averaged velocities, exhibited a classical estuarine circulation during winter 2011, and an inverse estuarine circulation during summer 2011 – 12. The winter-mean surface circulation in the estuary was seaward, forced by elevated freshwater inputs into the estuary, with current speeds of the order of 1 cm s^{-1} in the main body of the estuary; in the southern basin, current speeds were stronger, typically 3 – 4 cm s^{-1}, driven by the freshwater discharge from the Collie and Preston Rivers. The bottom layer winter-mean currents in the main estuary were landward and of the same strength as the near-surface velocities. During summer, high evaporation in the shallow northern estuary combined with low river discharge, led to an inverse circulation pattern in the central and northern estuary, with landward mean surface currents and seaward mean currents at depth. Summer-mean current strengths were slightly stronger than the winter-mean values, with values of about 2 cm s^{-1}. In the southern basin, the circulation pattern was less structured, but appeared generally seaward at the surface, driven by the weak river flows and not affected by high evaporation.

High river flow events, such as occurred during August 2011, have major impacts on the dynamics of the southern basin of the Leschenault Estuary, but only moderately impact the northern and central estuary. During the August 2011 event, the southern basin was filled with fresh river water, which was gradually ejected from the estuary through the Cut, emerging as a buoyant plume into Geographe Bay with velocities exceeding 0.5 m s^{-1}. The plume was diverted along the coast by the prevailing circulation on the shelf. In the northern and central estuary, water salinity was progressively diluted during the flow event, caused by freshwater input through the Parkfield Drain and through mixing with water from the southern basin. The freshening of the northern and central basins was gradual however, indicating how isolated the two basins are from the southern basin.

The division of the Leschenault Estuary into three distinct basins is emphasized by the tracer simulations carried out during the study. Both the whole estuary tracer experiment and the point source simulations illustrated the differing characteristics of the northern, central and southern regions of the estuary. Tidal currents in the northern estuary are weak, and the dynamics are strongly influenced by the freshwater discharge from the Parkfield Drain. However, the exchange and dispersion of tracer in the region was slow. In the central region, no river discharges are present, and dynamics are controlled by weak tidally-driven mixing with the northern and southern basins. As seen during the river flood of August 2011, evolution of water properties is generally slow, even during extreme events. At the Estuary 3 location, some freshening was observed and modelled during the August 2011 flood, but the

response was relatively muted compared to the rest of the estuary. The southern basin of the estuary is clearly the most dynamic, with the Cut exchanging water with the adjacent ocean and the Collie and Preston Rivers discharging into the basin. Tidal oscillations in water properties were strongly evident in the basin time series ('South Estuary' location) as were changes in response to river flow. The flushing of the southern basin is much more rapid than that of the northern or central basins. Although the flushing time of the whole basin was estimated to vary from 9 – 32 days in the four simulations performed here, the tracer lost from the system in these simulations was predominantly from the southern basin; tracer concentrations remained comparatively high in the northern and central basins.

The dynamics of the Collie River are dominated by the salt wedge in the lower reaches of the river. The model results illustrate some of the variability in the position and strength of the interface between the fresh and salt water. During high flow events, the salt water may be purged completely from the river, and the freshwater extend across the surface of the southern Leschenault Estuary into the Cut. At other times, salt water may penetrate far upstream in the bottom layer of the river. As noted above, however, due to resolution issues the performance of the model is weakest in the Collie River, and a more accurate simulation of the Collie River dynamics may require a much higher resolution model of the river alone.

Some tentative simulations of the potential impacts of projected climate change on the Leschenault Estuary were made. In the warmer drier climate expected for 2050, the Leschenault is predicted to also be warmer and saltier than at present. The impacts on the dynamics of the estuary are currently small, but the ecological implications of the higher temperatures and increased salt content may be greater. The strength of the predicted impacts increases with higher emissions scenarios.

References

ANZECC (2000). Australian and New Zealand Guidelines for fresh and marine water quality. Australia and New Zealand Environment and Conservation Council & Agriculture and Resource Management Council of Australia and New Zealand. http://www.environment.gov.au/water/publications/quality/nwqms-introduction-4a.html

Blanc, T.V. (1985) Variation of bulk-derived surface flux, stability, and roughness results due to the use of different transfer coefficient schemes. *J. Phys. Oceanogr.*, **15**, 650-669.

Blumberg, A.F. and Herring, J., (1987) Circulation modelling using orthogonal curvilinear coordinates, **in** *Three-Dimensional Models of marine and Estuarine Dynamics*, eds. Nihoul, J.C.J and Jamart, B.M., Elsevier.

Cartwright, D.E. and R.D. Ray (1990) Oceanic tides from Geosat altimetry. *J. Geophys. Res.,* 95 (C3), 3069-3090.

DoW (2007) The Leschenault Estuarine System, South-Western Australia. Condition Statement and Recommendations for Management. Department of Water, Government of Western Australia, June 2007, 180 pp.

Herzfeld, M. (2005) SHOC, sparse hydrodynamic ocean code, scientific manual. CSIRO Marine and Atmospheric Research, 149 pp.

Herzfeld, M. (2009) The role of numerical implementation on open boundary behaviour in limited area ocean models. *Ocean Modelling*, **27**, 18-32.

Herzfeld, M. and J.R. Andrewartha (2011) A simple, stable and accurate Dirichlet open boundary condition for ocean model downscaling. *Ocean Modelling*, 43-44, 1-21.

Herzfeld, M. and J.R. Waring (2012) SHOC, sparse hydrodynamic ocean code, user manual. CSIRO Marine and Atmospheric Research, 161 pp.

Kondo, J. (1975) Air-sea bulk transfer coefficients in diabatic conditions. *Boundary-Layer Meteorology*, **9**, 91-112.

Large, W.G. and S. Pond (1981) Open ocean momentum flux measurements in moderate to strong winds. *J. Phys. Oceanogr.,* **11**, 324-336.

Mellor, G.L. and T. Yamada (1982) Development of a turbulence closure model for geophysical fluid problems. *Rev. Geophysics and Space Phys.*, **20(4)**, 851-875.

O'Callaghan, J., C. Pattiaratchi and D. Hamilton (2007). The response of circulation and salinity in a micro-tidal estuary to sub-tidal oscillations in coastal sea surface elevation. *Cont. Shelf Res.*, 27, 1947-1965.

Oke, P. R., G.B. Brassington, D.A. Griffin and A. Schiller (2008). The Bluelink ocean data assimilation system (BODAS). *Ocean Modelling*, *21*(1-2), 46-70.

Pugh, D.T. (1987) Tides, Surges, and Mean Sea-Level. John Wiley Sons Inc, 486 pp.

Simpson, J.J. and T.D. Dickey (1981) The relationship between downward irradiance and upper ocean structure. *Journal of Physical Oceanography*, **11**, 309 - 323.

Smagorinsky, J. (1963) General circulation experiments with the primitive equations, I. The basic experiment. *Mon. Wea. Rev.*, **91**, 99 – 164.

Umlauf, L., H. Burchard and K. Hutter (2003) Extending the k-ω turbulence model towards oceanic applications. *Ocean Modelling*, **5**, 195-218.

Van Leer, B. (1979). Towards the ultimate conservative difference scheme. V: a second order sequel to Godanov's method. *J. Comput. Phys.*, 32, 101-136.

Walker, S.J. and J.R. Waring (1998) A multiple grid, 3-dimensional, non-linear, variable-density hydrodynamic model with curvilinear horizontal coordinates and level (*z*) vertical coordinates, CSIRO Marine Research, Report OMR-118/120.

Warner, J.C., C.R. Sherwood, H.G. Arango and R.P. Signell (2005) Performance of four turbulence closure models implemented using a generic length scale method. *Ocean Modelling*, **8**, 81-113.

Willmott, C.J., S.G. Ackleson, R.E. Davis, J.J. Feddema, K.M. Klink, D.R. Legates, J. O'Donnell, and C.M. Rowe (1985). Statistics for evaluation and comparison of models, *J. Geophys. Res.*, *90* (C5), 8995-9005.